VILNIUS UNIVERSITY

CENTER FOR PHYSICAL SCIENCES AND TECHNOLOGY

DOVILĖ ANDERSON

HYDROGEN BONDED CAVITY AND POLYMERIC NANOTUBULAR ASSEMBLIES FROM SMALL BICYCLIC MONOMERS

Doctoral Dissertation

Physical sciences, chemistry (03P)

Vilnius, 2016

The research has been carried out at Vilnius University during the years 2011 – 2015.

Scientific supervisors:

Assoc. Prof. dr. Edvinas Orentas (Vilnius University, physical sciences, chemistry - 03P). October 24, 2012 – September 30, 2015

Prof. habil. dr. Eugenijus Butkus (Vilnius University, physical sciences, chemistry - 03P). October 01, 2011 – October 23, 2012

1 CONTENTS

1 List of Abbreviations 4

2 Acknowledgements 6

3 Outline and Objective of the Thesis 7

4 Complex decameric H-bonded capsule 10

4.1 Introduction to design principles of H-bonded self-assembled systems 10

4.1.1 Association constant 14

4.1.2 H-bonded nanotubes 16

4.1.3 H-bonded cavity assemblies and discreet structures 22

4.2 NMR characterization of the H-bonded decameric capsule 25

4.2.1 Introduction 25

4.2.2 Aggregation in carbon disulfide 26

4.2.3 Tautomeric forms 30

4.2.4 Connectivity of the units 33

4.2.5 Final H-bonding pattern elucidation 34

4.3 Host-guest chemistry with C_{60} 39

4.3.1 Stoichiometry determination of host guest complex 40

4.3.2 Molecular dynamic simulations 41

5 Organic nanotubes from bis-Ic monomers based on 9-azabicylo[3.3.1]nonane and bicyclo[3.3.1]nonane frameworks 43

5.1 Introduction to 9-azabicyclo[3.3.1]nonane derivatives 43

5.1.1 Synthetic routes to 9-azabicyclo[3.3.1]nonane derivatives 44

5.1.2 Preparation of enantiomerically pure of 9-azabicyclo[3.3.1]nonane derivatives 47

5.1.3 Enzymatic enantiomer resolution methods 48

5.2 Introduction to H-bonded supramolecular polymers 51

5.2.1 Design principles and driving forces for the formation of high DP H-bonded polymers 52

5.2.2 Bulk properties of H-bonded polymers 55

5.2.3 Hierarchical supramolecular polymers 57

5.3 Enantiomer separation of 9-benzyl-9-azabicyclo[3.3.1]nonane-2,6-diol 59

5.4 Synthesis of bis-Ic derivatives based on 9-azabicyclo[3.3.1]nonane as new supramolecular synthons 63

5.5 Supramolecular tubular polymers obtained from new bis-Ic monomers 64

5.5.1 Molecular modeling 69

5.5.2 Solid state NMR 71

5.6 Bis-UPy type quadrupole H-bonding synthons 74

6 Octameric tube from C_1 symmetric monomer: guest induced rearrangement and self-sorting behavior 81

6.1 Introduction to molecular self-sorting 81

6.2 Synthesis of the UPy-Ic monomer and characterization of the octameric tube 87
6.3 Guest induced rearrangement 90
6.4 Complexation induced self-sorting of structurally similar compounds 94
7 Conclusions of the thesis 100
8 Experimental part 102
9 Publications 122
10 References 123

1 LIST OF ABBREVIATIONS

1,2-CBD	1,2-dichlorobenzene
1,5-COD	1,5-cyclooctadiene
2D	Two dimensional
3D	Three dimensional
A	Acceptor
AFM	Atomic force microscopy
Boc	Tert-butyloxycarbonyl
C	Cytosine
CA	Cyanuric acid
CDI	Carbonyl diimidazole
CE	Cotton effect
COSY	Correlation spectroscopy
CRL	Lipase from *Candida Rugosa*
D	Donor
DCM	Dichloromethane
DMF	Dimethylformamide
DMSO	Dimethylsulfoxide
DNA	Deoxyribonucleic acid
DOSY	Diffusion-ordered spectroscopy
DP	Degree of polymerization
DPPA	Diphenylphosphoryl azide
HMPA	Hexamethylphosphoramide
DSC	Differential scanning calorimetry
ee	Enantiomeric excess
FTIR	Fourier transform infrared spectroscopy
G	Guanine
GC-MS	Gas chromatography mass spectroscopy
GPC	Gel permeation chromatography
H-bonding	Hydrogen bonding
HMBC	Heteronuclear multiple bond coherence
HMQC	Heteronuclear multiple quantum coherence
HPLC	High performance liquid chromatography
HRMS	High resolution mass spectrometry
Ic	Isocytosine
LC	Liquid crystal
LiHMDS	Lithium hexamethyldisilazane
M	Melamine
MAS	Magnetic angle spinning
MD	Molecular dynamics
MM	Molecular mechanics
mp	Melting point
Napy	2,7-diamido-1,8-naphthyridine
NMR	Nuclear magnetic resonance
NOE	Nuclear Overhouser effect

OPV	Oligo(p-phenylenevinylene)
PCL	Lipase from *Pseudomonas cepasia*
RBF	Round bottom flask
ROESY	Rotating frame nuclear Overhauser effect spectroscopy
rt	Room temperature
SEC	Size exclusion chromatography
SS NMR	Solid state nuclear magnetic resonance spectroscopy
STM	Scanning tunneling microscopy
T	Thymine
TEA	Triethylamine
TEMPO	2,2,6,6-tetramethyl-piperidin-1-yl)oxyl
TFA	Trifluoroacetic acid
TFAA	Trifluoroacetic acid anhydride
TGA	Thermogravimetric analysis
TLC	Thin layer chromatography
U	Uracil
UPy	2-Ureido-4[*1H*]-pyrimidinone
VT NMR	Variable temperature nuclear magnetic resonance spectroscopy

2 ACKNOWLEDGEMENTS

First I would like to thank my supervisor Prof. Eugenijus Butkus. Who invited me to study at Vilnius University and guided me through the first years of my PhD studies. He also offered me the opportunity to go study an internship at Lund University. Also many special thanks goes to Dr. Edvinas Orentas, who often shared his brilliant research ideas and supported me in every aspect of my research and studies. I would like to thank to Prof. Kenneth Wärnmark, who provided me an opportunity to join their team at Kemicentrum. His kind supervision during my intern periods and access to the laboratory and research facilities were invaluable. I would like to thank my lab mate Dr. Sami Dawaigher for the many stimulating discussions, and for all the fun times we had in the lab. I am grateful to Lukas Taujenis for his assistance with mass spectrometry and nice chats over lunch. I would like to thank Dr. Sigitas Stončius for his help and advice during the complicated part of my thesis project. Last but certainly not least I am deeply grateful to Dr. Karl-Erik Bergquist for being a great help and friend during my years of studies within this field.

3 OUTLINE AND OBJECTIVE OF THE THESIS

Nature works through well-coordinated ensemble of noncovalent interactions. Synthetic supramolecular systems are the first stopover on the way into deeper understanding and insight into how complex biological systems are organized and functioning. H-bonding is one of the most abundant noncovalent interactions used to build multicomponent supramolecular systems. To meet energetic demands and to pay entropic cost for spontaneous formation of thermodynamic aggregate elaborated covalent synthesis is often performed. The ultimate goal of scientific activities dealing with nanosized objects and technology, whether they are of biological importance or intended for electronic, photonic or other applications, is creation of new molecules and their assemblies able to perform the anticipated specific function. To create complex systems one must consider employing not only noncovalent interactions but also cooperative and multivalence interplay between the respective components. Just as in biological molecular machinery, extravagant molecular structures incorporating necessary functional fragments become desirable rather than avoidable in creating novel synthons. Tubular shape organic objects with adjustable pore size and well defined inner and outer surfaces offers tunable variables for novel functional materials. Many general strategies for establishing aggregation propagation in 1D direction are known, yet comprehensive knowledge in achieving tubular structures is lacking. One of the most explored strategy for obtaining nanotubes with tunable diameter is stacking of macrocycles. However, to obtain macrocycle building blocks require considerable synthetic efforts. In principle, employing properly designed monomers having angular shape and complementary hydrogen bonding (H-bonding) sites, tubular polymeric assemblies could be spontaneously obtained in solution.

The main objective of this work is the construction of tubular polymers and cyclic cavity objects utilizing supramolecular approach i.e. self-assembly of small building blocks. Bicyclo[3.3.1]nonane and 9-azabicyclo[3.3.1]nonane framework has been utilized as the shaping unit that imparts L shape to the structure of the monomers. Isocytosine (Ic) H-bonding motif is capable of adopting two tautomeric forms (*1H* and *3H*) and hence participating in several different binding modes (*vice versa*).

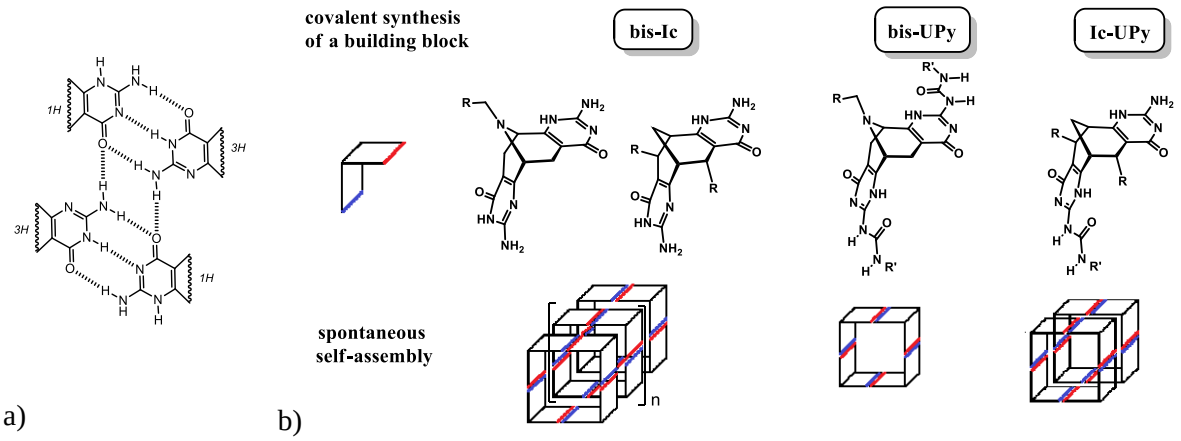

Figure 1. a) H-bonding pattern in tubular polymers formed from bis-Ic monomers; b) General strategies used to assemble different topology H-bonded objects: tubular polymers, tetrameric cycles and short tube.

Tautoleptic aggregation of the bis-Ic monomers into tetramers results in establishment of orthogonal H-bonding between tetramers and subsequent polymer formation (Fig. 1a). The aggregation of bis-Ic monomers depend on the size of the solubilizing chains. Bis-Ic monomer with large 3,5-bis(decyloxy)benzyl chains near H-bonding sites could not form supramolecular polymers, but resulted in the formation of a complicated capsule (Chapter 4). Therefore, bis-Ic monomers with decyl chains and bis-Ic monomers based on 9-azabicyclo[3.3.1]nonane were proposed (Chapter 5). New bis-ureidopyrimidinone (bis-UPy) monomers were also proposed, that are expected to form self-assembled tetrameric cycles (Fig. 1b).

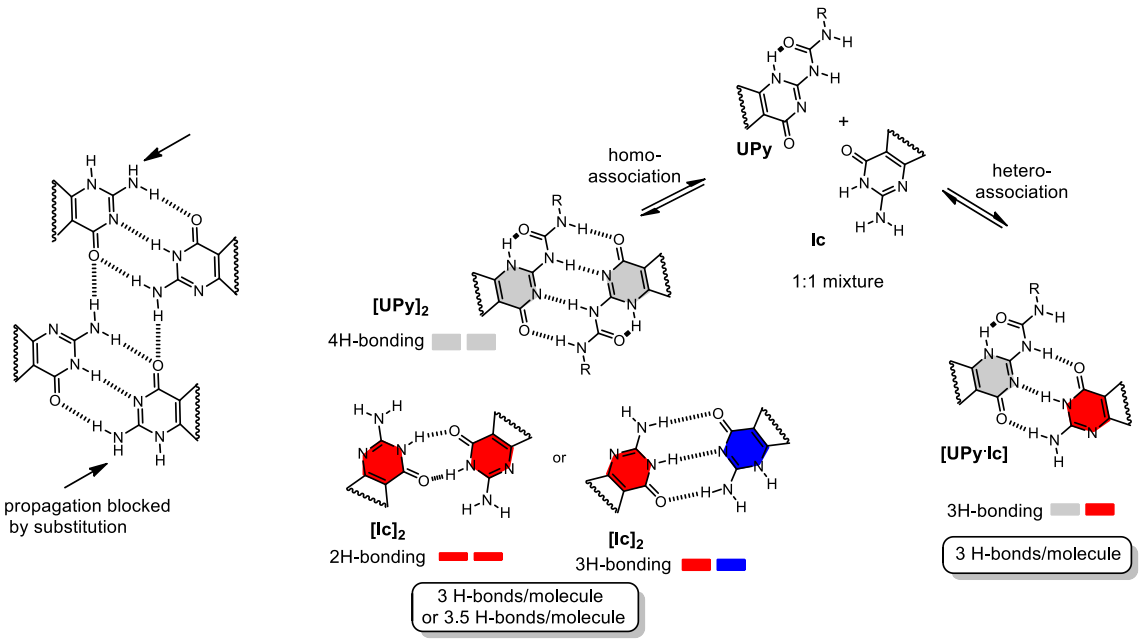

Figure 2. a) H-bonding of the bis-Ic monomers; b) Different scenarios for Ic and UPy motifs association.

Having established the orthogonal H-bonding in perpendicular direction which connects the tetramers, it was interesting to explore the situation where short tubes could be obtained from two assembled tetramers. Such limited stacking of cyclic tetramers could be realized by designing asymmetric monomer having Ic and UPy motifs incorporated into one monomer, where UPy motif will block further tetramer stacking (Fig. 2a). It is known, that hetero-association will prevail over homo-association if higher number of H-bonding is established in the final structure even if association constants are higher for homo-association events. Two scenarios are possible for binding of Ic and UPy motifs: Ic-UPy hetero-association via 3H-bonding or Ic-Ic and UPy-UPy homo-association through 2H-/3H-bonding and 4H-bonding, respectively (Fig. 2b). In the simplest case when only these H-bonding modes are operating (no orthogonal binding), homo-association could be expected due to larger number of H-bonding formed per molecule. In addition, by utilizing additional orthogonal H-bonding of Ic motif, larger total number of H-bonding will be established in the final assembly – the proposed octameric tube.

To test this idea and to see whether tetramers would form by the virtue of homo-association between UPy-UPy/Ic-Ic or hetero-association between Ic-UPy motifs, structure of C_1 symmetric Ic-UPy monomer was proposed (Chapter 6).

To achieve the proposed objectives several targets were formulated:

- Using modern NMR techniques to determine supramolecular structure of a complicated decameric capsule, assembled from bis-Ic monomers, decorated with bulky 3,5-bis(decyloxy)benzyl chains;
- Investigate host-guest chemistry of the obtained capsule and C_{60} molecule;
- Separate 9-benzyl-9-azabicyclo[3.3.1]nonane-2,6-diol enantiomers;
- Synthesize new enantiopure bis-Ic monomers based on bicyclo[3.3.1]nonane and 9-azabicyclo[3.3.1]nonane with less bulky chains;
- Investigate the obtained tubular polymers;
- Synthesize bis-UPy monomers and investigate their aggregation in nonpolar solvents;
- Synthesize Ic-UPy monomer which would assemble into octameric tube;
- Investigate its C_{60} complexation and C_{60} induced self-sorting in the presence of structurally similar bis-UPy monomers.

4 COMPLEX DECAMERIC H-BONDED CAPSULE

4.1 INTRODUCTION TO DESIGN PRINCIPLES OF H-BONDED SELF-ASSEMBLED SYSTEMS

The factors affecting the stability[1] of complex supramolecular systems based on H-bonded arrays such as attractive secondary interactions, preorganization[2a, 2b] and cooperativity[3, 4] are well understood yet the synthesis and precise control over multicomponent assemblies still remains challenging. In the past few decades crystal engineering has focused on developing of repetitive 2D and 3D networks with different topologies.[5] New area of surface supramolecular chemistry has now begun to explore 2D extended structures and their binding to surface events.[6] The majority of the discrete H-bonded assemblies are two-dimensional or layered while construction of discreet three-dimensional aggregates were less explored and remained limited to dimeric and trimeric capsule-like architectures.[7] Chirality directed self-assembly was first suggested by Lehn, where he proposed different aggregation profiles in crystal for racemic (Fig. 3a) and enantiopure (Fig. 3b) bicyclic bislactam compound capable of self-association through 2H-bonding.[8] Although the suggested bislactam failed to produce entirely hydrogen bond directed entities in crystal (due to weak 2H-bonding), this concept based on purely geometrical considerations was valid and somewhat different but distinct crystal packing geometries were obtained for racemic and enantiopure forms.

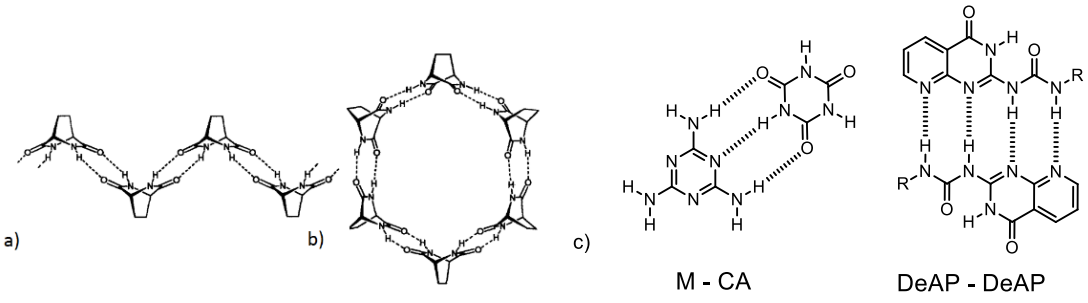

Figure 3. The effect of the chirality to the outcome of self-assembly. a) The expected assembly of the racemic bislactam; b) The expected assembly of the enantiopure bislactam; c) Hydrogen bond modules melanine – cyanuric adic (M - C) and DeAP – DeAP.

3H-, 4H- or even 6H- hydrogen bond arrays can be incorporated into heterocyclic rings with ease. It was found [3] that the strength of such arrays depends on secondary electrostatic interactions which in turn can be either repulsive (as in the alternating D and A pair ADA-DAD) or attractive (as in the pair AAA – DDD). In case of favorable

arrangement and in the absence of other interfering factors the binding constants of such arrays can reach up to 10^7 M^{-1} in $CHCl_3$ (Fig. 4).[9]

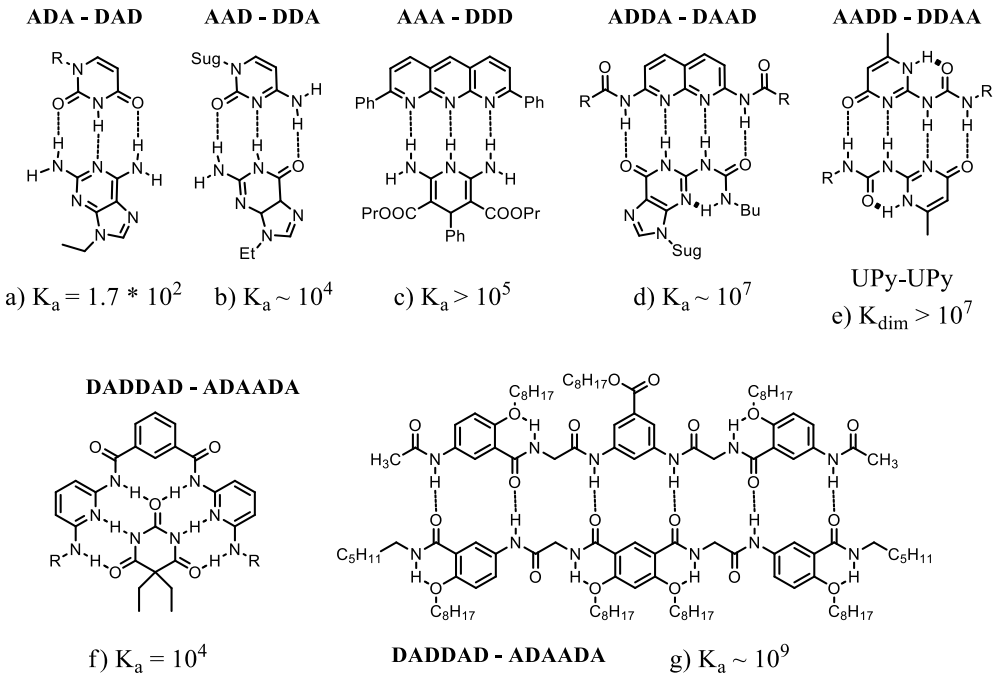

Figure 4. Most widely used hydrogen bond arrays and their association constants (M^{-1}) in $CHCl_3$.

The nature of solvent and its effect on hydrogen bond strengths is critical. It is well known that nonpolar noncompetitive solvents lacking H-bonded donor and acceptor sites will strengthen hydrogen bond and favor association. Therefore, solvents such as chloroform, toluene, benzene and dichloromethane are used most often. Multiple H-bonded arrays are usually incorporated into heterocyclic rings (Fig. 4) such as melamine (M), cyanuric acid (CA) (Fig. 3c), ureidopyrimidinone (UPy), isocytosine, DeAP (Fig. 3c) , nucleic bases etc.[10] the presence of different tautomeric forms could be used in advantage or in contrary might introduce difficulties if they are not complementary and present simultaneously. Tautomerisation of otherwise intrinsically non-self-complementary 3H-bonding array in isocytosine (2-amino-4(*1H*)-pyrimidone) leads to formation of a dimer via AAD – DDA H-bonding mode. In water, unsubstituted isocytosine exists as a mixture of the two tautomers *1H* and *3H* and crystalizes as 3H-bonded self-dimers (Fig. 5a).[11] In ethanol and diethyl ether the *3H* tautomer is predominant.[12] Quite different aggregation profile is observed for 6-substituted isocytosines. 6-Ethyl and 6-Phenyl isocytosines crystalizes in 2D networks by using urea-type bifurcated hydrogen bonds between AD-DA dimers (Fig. 5b).[13] Isocytosine ring fused with imidazole (Fig. 5c) is found in guanidine base (G)

where it adopts *3H* tautomeric form and pairs via 3H-bonding with cytosine. Two more arrangements are possible if the association via 2H-bonding array AD-DA between *3H-3H* and *1H-1H* tautomers is taken into account (Fig. 6). In the gas phase however, isocytosine exists in its lactim form (Fig. 5d) as was shown by experimental and theoretical studies.[14]

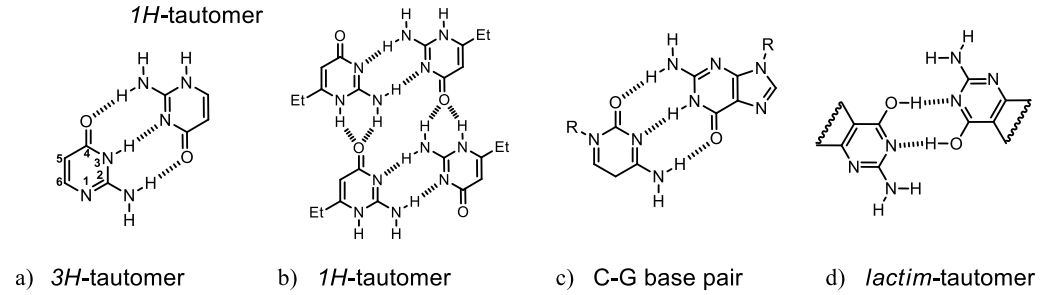

Figure 5. a) Tautomeric forms and self-dimerization of isocytosine; b) Aggregation of 6-substituted isocytosine in solid state; c) Cytosine-Guanidine base pair; d) Lactim form of isocytosine.

In this light, isocytosine (Ic) ring is a versatile building block which offers several aggregation profiles with the possibility to build extended structures (Fig. 6). Ic motif has been incorporated into simple supramolecular structures although deeper understanding what governs its tautomer's distribution is missing.[15] [16]

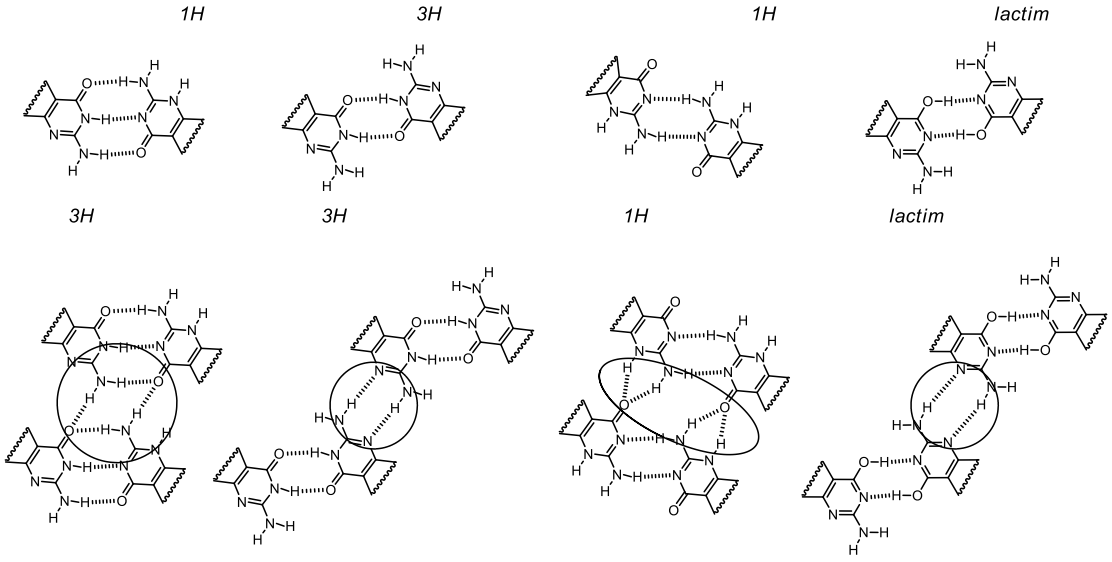

Figure 6. Possible H-bonding patterns involving different isocytosine tautomeric forms and their possible orthogonal H-bonding (marked with circles).

Chelate cooperativity. Supramolecular systems are usually constructed from monomeric units that have multiple binding sites from which bidendate synthons are employed most often. The molecules of this type may assemble into linear oligomers or form cyclic

structures. Linear chain oligomers are usually obtained as polydisperse aggregates while cyclic structures are well-defined. Formation of closed cyclic structures will depend on the size and shape of the monomer, or generally speaking on the spacer incorporated between the two binding sites, and the mutual interaction of these binding sites. Chelate effect in cyclisation event of two bidendate synthons is understood taking into account the first binding event as intermolecular and the second binding as intramolecular. A recent study[17] compares the effects of symmetry of hydrogen bond array (i.e. ADD or DDA vs ADA) on chelate cooperativity, expressed as *effective molarity EM*. EM is the ratio between K_a of the intramolecular event over K_a of corresponding to the intermolecular event with values $K_{a\ intra}/K_{a\ inter} > 1$ indicating the preference towards formation of cyclic structures i.e. intramolecular association. In favorable situations for cycle formation, $K_{a\ inter}$ and EM should be both large, where $K_{a\ inter}$ indicates strong binding and EM means that the cycle formation is favorable over linear structures. Indeed, significant influence of the symmetry of 3H-bonding arrays on association constant was found. Formation of cyclic square-shaped assemblies from bidendate monomers featuring nucleic bases connected through a π conjungated bridge capable of rotation along its axis was investigated (Fig. 7). It was shown, that A and U association in the reverse Watson-Crick manner creates additional possibilities to engage binding modes through 120 º angle which do not yield intended tetramer, but results in formation of oligomers (Fig. 7b and 7d). In this way additional degrees of freedom are introduced into the system which causes decrease of tetramerization constant by three orders of magnitude. Contrary, the GC pair which has DDA-AAD arrangement is not complementary after rotation along the axis, that is, DDA is not complementary DAA. In this case only 90 º angle association mode is possible which leads to the formation of cyclic aggregate to much higher extent (Fig. 7a and 7c).

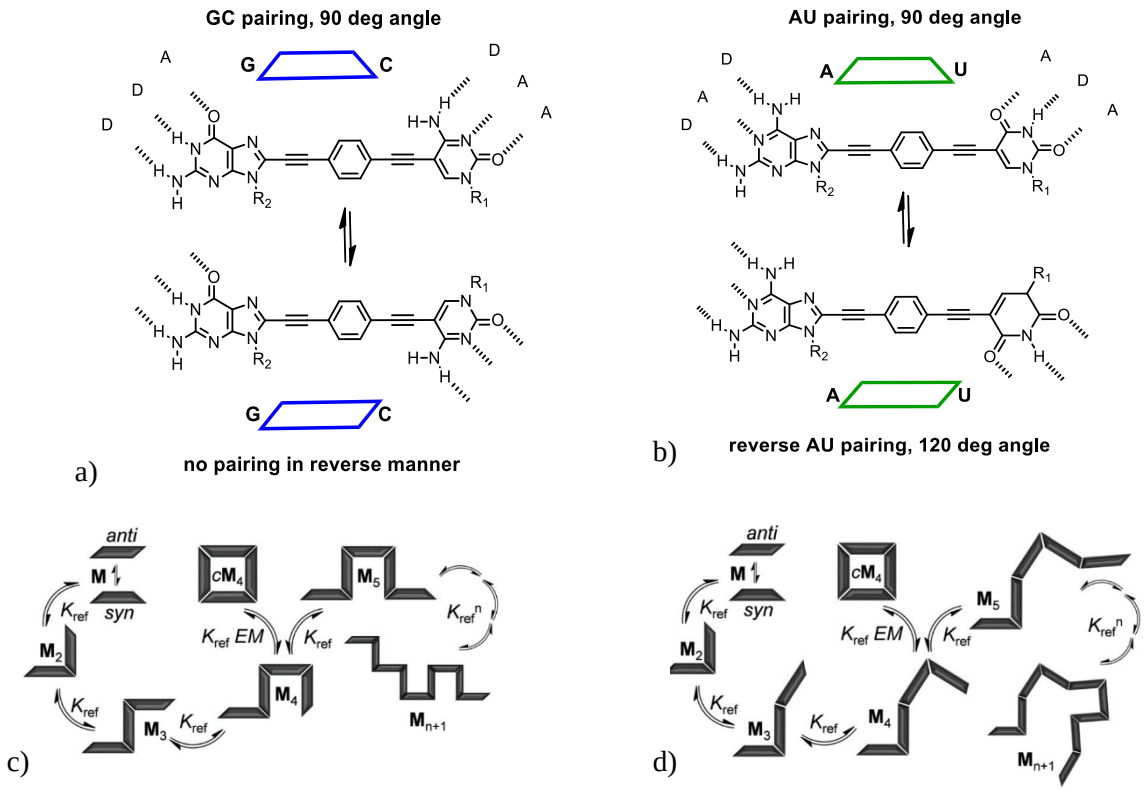

Figure 7. Molecular structure of the bidendate ligands: a) GC; b) AU; c) Situation for GC Watson-Crick pair (ADD – DAA); c) Situation for AU Watson-Crick pairing (DAD - ADA) which has equal possibility to form reverse AU Watson-Crick pair (DAD – ADA).

The important message as the authors conclude is that although the ADA 3H-bonding array arrangement binds most strongly to its complementary partner DAD due to minimum secondary repulsive interactions, such symmetrical arrangement in some particular cases might cause unwanted additional self-complementary conformations. In such situations the overall effect can be detrimental for the formation of desired species.

4.1.1 ASSOCIATION CONSTANT

The ultimate measure which quantifies the overall strength of reversible interactions in a supramolecular system of interest is the association constant K_a which is defined as ratio of equilibrium concentrations of products to reagents. For a simple host-guest system H + G ↔ HG, association constant is equal K_a = [HG]/[H][G]. Large positive values indicate favorable binding of host and guest. Often to determine K_a is primary aim in characterizing supramolecular system yet not always feasible. For host guest interactions the binding constant express how good the guest is for a particular host and *vice versa*. While it is

relatively straightforward to determine K_a in the systems of two binding partners in 1 : 1 stoichiometry, it becomes more complicated to fit the data for multicomponent or especially to cooperative systems. Depending on what type of functional groups are present in the molecular structure and binding strength of the system of interest, titration experiments using different techniques are employed. UV, ^{1}H NMR or fluorescence spectroscopy are used most often, although now isothermal calorimetric titration finds frequent applications.[18] For example, NMR can be used to determine relatively small K_a up to 10^5 M^{-1}. In a simplest case, incremented amounts of a guest is added to the solution of a host and a physical property which changes upon binding is monitored. The acquired data is then fitted to an existing binding model. Several widely accepted models for calculating K_a exist: *dimerization model*, noncooperative multicomponent *equal K model (EK)* and *cooperative equal K model (coEK)*.[19]

$$A + A \overset{K_2}{\rightleftharpoons} A_2 + A \overset{K_3}{\rightleftharpoons} A_3 + A \overset{K_4}{\rightleftharpoons} \ldots \overset{K_i}{\rightleftharpoons} A_i$$

a) dimerization model: $K_{dim} = K_2$; $K_3, K_4, \ldots K_i = 0$
b) equal K model: $K_E = K_1 = K_2 = K_3 = \ldots = K_i$
c) cooperative EK model: $K_E = K_2/\rho = K_3 = K_4 = \ldots = K_i$
where $\rho = K_2/K_E$

In the simplest dimerization case, $K_a = [\text{dimer}]/[\text{monomer}]^2$. For multiple species equal K model is usually applied which assumes that binding of the successive monomer is not affected by binding of the previous monomer and K_a of every stepwise process as well the overall binding constant K_E holds the same (b). This model is extensively applied in the most cases of multicomponent assembly and indefinite stacking of the same monomers. The third and the most complicated model to assess is the cooperative binding fashion (c). Following simple definition, positive (or negative) cooperative self-assembly systems after binding the first guest increases (or decreases) the binding strength of the second and every following guest are described by the cooperative coEK model. In other words, K_a of the first binding (dimerization) is different from all subsequent bindings $K_2 \neq K_3 \neq K_4 \ldots \neq K_i$, but $K_3 = K_4 \ldots = K_i$. If a system expresses positive cooperativity (factor $\rho < 1$, then $K_2 < K_E$) formation of a dimer from monomers is more energetically demanding than attaching monomer molecule to a stack. In the case of dimerization, the entropy is lost by two monomer molecules, as both of them lose substantial degree of freedom. Attaching

one monomer to a stack is less entropically disfavored. If $\rho = 1$, the noncooperative EK model is obtained. Straightforward application of this model was criticized by Ercolani[20] where he established an alternative approach to determine whether cooperativity is actually operating in a system by considering first binding as intermolecular and the successive binding events as intramolecular. Cooperative model is extremely case dependent (homotropic or heterotropic systems, allosteric or chelate cooperative cases) and requires deeper mathematical evaluation, especially when intermediate species are hard to detect and the determination of microscopic constants K_2, K_3 etc. is challenging. [21] For highly cooperative systems intermediate state is never observed, two state behavior is dominating in virtually all cases.[22] To conclude, cooperativity is the concept of two or more noncovalent (intermolecular or intramolecular) interactions operating in one system and more importantly, affecting each other's binding. It is very often met in natural systems but rather rare in synthetic supramolecular systems, as commented by Ercolani. Concepts established in self-assembly and crystal engineering fields, briefly introduced in this section, have led to many sophisticated H-bonded multicomponent systems like hexameric rosettes[23], G-quartets[24], cyclic structures,[25] self-assembled capsules[7] [26], organic nanotubes[27] etc. Such thermodynamic assemblies express different physicochemical behavior compared to their components alone. The next step to take is to think of highly interactive and responsive systems, i.e. to move from stable noncovalent materials to dynamic systems.[28]

4.1.2 H-BONDED NANOTUBES

In biological systems limited hollow space provided by enzymes or transmembrane transporters mechanisms allows specific substrate binding. Well known example is a transmembrane protein aquaporin which selectively allows water molecules transport, but blocks the way for other small molecules.[29] Another intriguing phenomenon is transmembrane ion channels which in their pores are able to discriminate between different ions with excellent selectivity. Assemblies containing cylindrical functionalized inner space e.g. chiral pocket, provide a chemical environment for highly specific reactions. H-bonded tubular structures draw much attention due to their potential applications such as sensing, specific guest inclusion and separation and consequently,

catalysis, transmembrane transport[30], biomimetic orthopedic materials [31] and drug delivery.[32] Several strategies for construction of organic nanotubes are known, which could be roughly subdivided into covalent and supramolecular approaches. Helices from linear oligomers held together by internal hydrogen bonds e.g. helices in protein secondary structure or synthetic foldamers, is an example of covalent nanotube. More advantageous situation is when a tube forms from small identical monomers of which self-organization is driven by noncovalent forces. Careful design of monomeric units with their inherent geometrical features leads to controlled spatial arrangement and propagation to one direction. Tubular structures can be achieved by combining building blocks in many different geometrical ways and with different degree of covalent synthesis employed,[32], [33] from which most successful are helices, stacks of macrocycles, hierarchical aggregation of rosettes and few others.

Stacked macrocycles

Tubes from stacked cyclic peptides of even number of alternating D- and L- amino acids represent large body of organic nanotubes. In such an arrangement the peptide backbone is virtually flat and is able to bind to the next cyclic peptide in a fashion very much similar to β sheet. α, β and γ amino acids or their combinations can be used for cyclic polypetide synthesis arranging them in such way that carbonyl groups point up and down in alternating order (Fig. 8). Peptide nanotubes offer access to control over inner diameter and interior and exterior hydrophobicity by controlling number and selection of amino acids in a cyclic peptide. They are promising candidates for nanomedicine applications[34], for example, nanotubes with hydrophobic outer walls can be inserted into membranes and used for selective transport of small molecules.

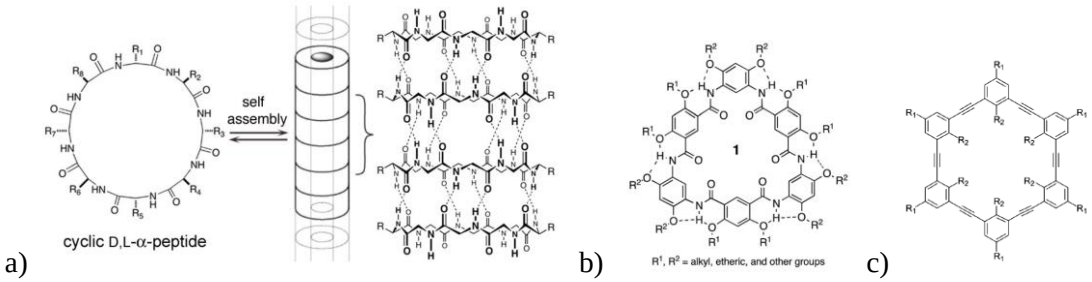

a) b) c)

Figure 8. a) Ghadiri's cyclic peptide nanotube; b) General structure of aromatic oligoamide macrocycle; c) Generalized molecular structure of shape persistent macrocycle

Related to the cyclic peptide stacks are rigid aromatic oligoamide macrocycles (Fig. 8b)[35] that produce strongly assembled tubes in nonpolar solvents and hexagonal stacks in solid state. Tubular stacks from shape persistent macrocycles (Fig. 8c)[36] aimed to overcome limitations associated with fixed pore size of carbon nanotubes (CNT) and at the same time make use of unique properties of hydrophobic nanopores inherent to CNT. They consist of rigid planar conjungated scaffold with fixed positions available for substitution. Arene-arene and solvophobic interactions led to face to face stacking of aromatic planes which give rise to a variety of porous assemblies.

Discotic stacks

Into this category of organic nanotubes falls in various hierarchical assemblies formed by virtue of orthogonal noncovalent interactions i.e. H-bonding holds together disc shaped assemblies which then stack in face-to-face fashion driven by π – π interactions and solvophobic repulsions. Most prominent examples are stacked rosettes from melamine (M) and cyanuric acid (CA), guanine and cytosine (G∧C) containing modules and G-quartets stacks. Formation of this type of stacked discs shares fundamental self-organization features of nucleic bases – the discs are formed upon multiple H-bonding between heteroaromatic partners which then stack in aqueous or organic media.

CA and M recognition motifs introduced by Whitesides are known to provide 2D networks when mixed in equimolar amounts. Whitesides et al recognized that some extent of preorganization is necessary to obtain discrete cyclic structures in favor of 2D network. 3 melanine units were connected by a flexible linker which after mixing with CA resulted in six membered rosettes held by 18 H-bonds (Fig. 9a)[37]. To form rosette nanotubes different approach was utilized: bis-M and bis-CA monomers with different length linkers were employed which resulted in high molecular weight polymers in solution and fibrous morphologies after evaporating the solvent (Fig. 9b).[38] Similar strategy has been employed by others to construct related bis-M/bisCA nanotubes. [39a, 39b]

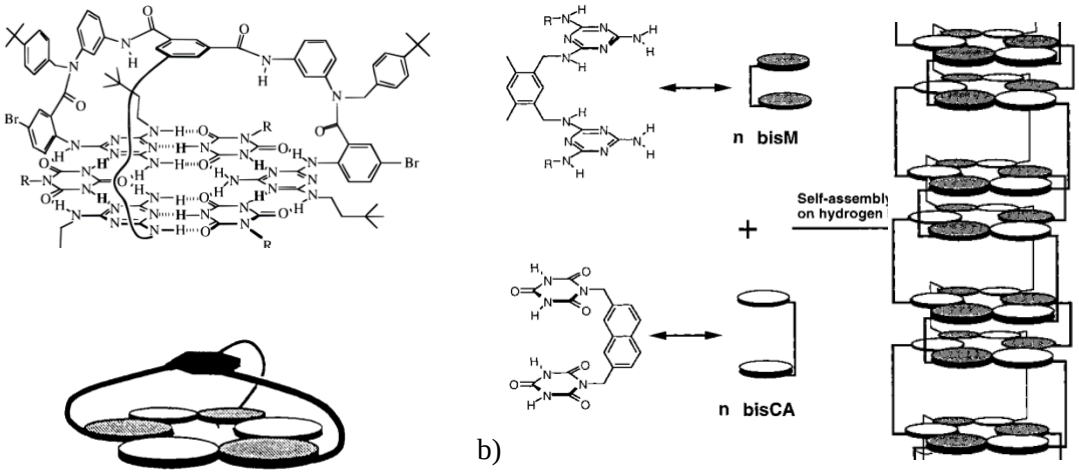

Figure 9. Whitesides strategies towards a) rosettes[37] and b) rosette nanotubes in organic solvents.[38]

Fenniri's fused guanidine – cytosine module G∧C is known to undergo hierarchical self-assembly driven by hydrophobic effects in water.[40] Six membered macrocycle rosettes are formed by the virtue of 18 H-bonds. The resulting disc shaped aggregate is substantially more hydrophobic which leads to stacking into columnar structures (Fig. 10). Electrostatic interactions between amino acid side chains also contribute to the stacking. The outside walls of the so build tube can be decorated with various substituents, although stability was found to be dependent on the size and electronic properties of the substituents.[41] Inner diameter of GC stacks is about 1.1 nm and the outer diameter about 3.2 nm. The G∧C module decorated with crown ether on the side chain express interesting temperature dependence: the rosettes forms longer stacks when temperature is raised.[42] This case constitutes a rare example of entropy driven assembly in artificial systems. The authors postulate, that upon increase of temperature water molecules which are closest to the hydrophobic surface of the tubes end, are released to bulk water and so new rosette stacks can be connected.

G-quartets are long recognized supramolecular building blocks based on guanosine monophosphate (G) identified in DNA[24]. Guanosine and related compounds such as folic acid derivatives[43] contains Watson-Crick H-bond interface and Hoogsteen interface which are complementary partners to each other and are positioned at 90 º angle thus able to form tetrameric rosettes (Fig. 11a). In alkaline pH and in the presence of Na^+ or K^+ , G-quartets sandwich ions and form stacked structures.

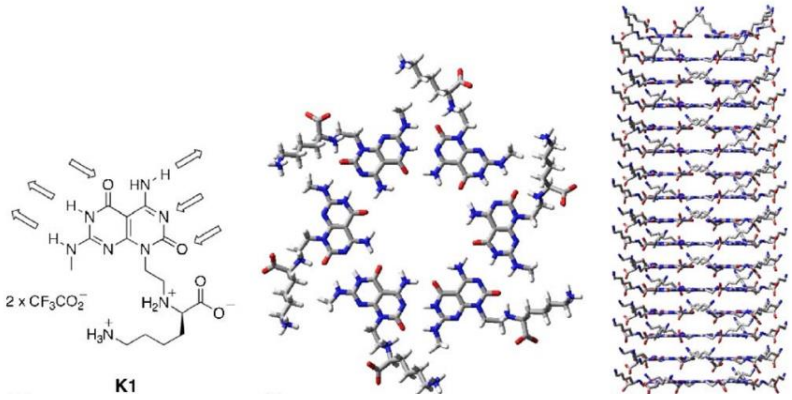

Figure 10. Fenniri's rosette nanotube assembled from fused G∧C module.

Lipophilic G analog (Fig. 11b) which have long chains on ribose unit reported by Gottarelli and Spada, assemble into ribbon chains in organic media.[44] In this case, cation templating was found to be necessary for the formation of G-quartets. In contact with alkaline aqueous K^+ solution, these building blocks extract K^+ ions and produce stable octameric G-quartet sandwiches which by increasing K^+ concentration stacks into columnar structures due to solvophobic interactions.[45]

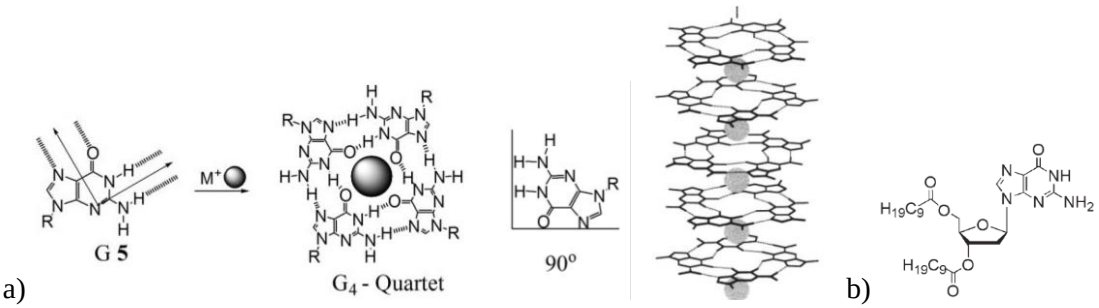

Figure 11. a) General structure and assembly fashion of G-quartet; b) Lipophilic G derivative.

Miscellaneous

Bent aromatic receptor with hydrophilic tail in the presence of phenylphenol self-assembles into tubular structure (Fig. 12).[46] This example is a manifestation of the importance of shape and size match to achieve desired aggregation. Although the monomer lacks any directional binding sites, it is able to form ordered superstructure in aqueous media driven by amphiphilic effects. Upon addition of guest, the assembled fibril is able to rearrange into a polymeric tube. The rearrangement triggered by pyridine complexation with phenylphenol via H-bonding, which imposes steric crowding and causes tube to "inflate".

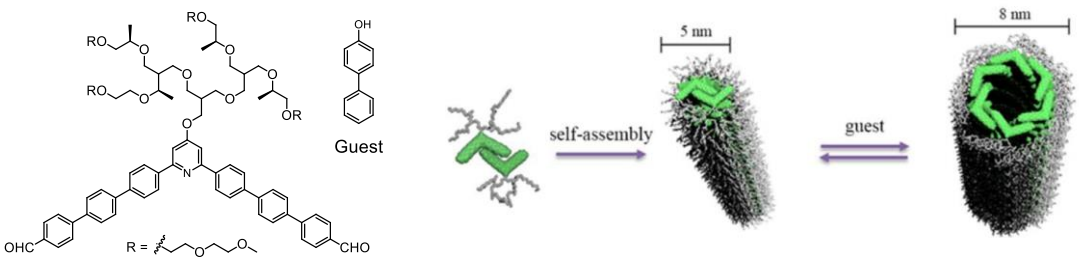

Figure 12. Tube formation from aromatic bend amphiphilic molecule.[46]

In recent years novel rational design towards peptide-based organic nanotubes has been devised.[47] In this approach coiled coils (bundles of α-peptides helices) are utilized for hierarchical assembly into fibers and nanotubes (Fig. 13).

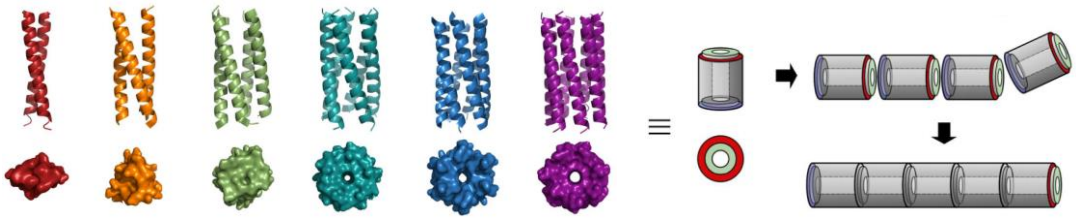

Figure 13. Coiled coils used as building blocks. Taken from ref [47]

Conticello et al. have reported 29 residue peptide assembly into very well defined bundles which are able to form extended tubular structures.[48] It was demonstrated, that replacing some of the amino acids in the sequence with other amino acids have crucial effect on assembly outcome. When the four arginine amino acid residues in the amino acid sequence are changed to lysines, tubes of different morphology and considerably larger diameter are obtained (Fig. 14).

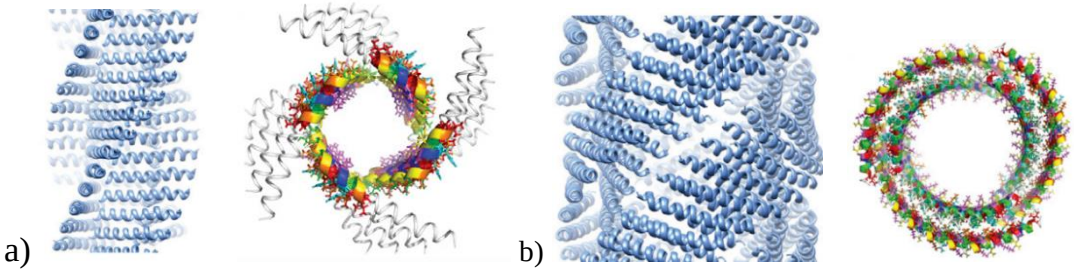

Figure 14. Coiled coil based nanostructured tubular assemblies from two different sequences.[48]

The findings presented by authors widens implications on peptide based nanostructure constructs and also stresses the challenge in supramolecular design due to quaternary structure lability at protein-protein interfaces.

Research endeavor in constructing organic nanotubes and other objects is foreseen as very promising for future technological developments in various novel fields. However, from its dawn couple of decades ago till now it stayed at fundamental research stage where main focus is kept on creating and characterizing new nanosized objects with defined nanostructures whereas their practical applications remain scarce most likely due to the lack of efficient and scalable methodologies.

4.1.3 H-BONDED CAVITY ASSEMBLIES AND DISCREET STRUCTURES

Just as organic nanotubes provide limited space inside their open end interiors, molecular capsules are attractive for creation of even smaller spaces inside their walls. Molecular cavity assemblies and capsules were studied intensively during recent years because of their potential use for molecular reactors, catalysis, encapsulation and molecular recognition concepts. Another attractive feature is chiral pockets that self-assembled capsules can provide: concept highly exploited in nature.[49] Capsule designs are directed towards generation of curvature or bowl shaped monomeric units which can dimerize via noncovalent interactions. Inside them, the inner space of few hundreds $Å^3$ can be utilized for one or few guests inclusion. In such way, a number of covalently preorganised macrocylic structures e.g. calixarenes or resorcinarenes form homodimeric structures connected via multiple hydrogen bonds, resulting in cavity compounds of different sizes (Fig. 15)[50].

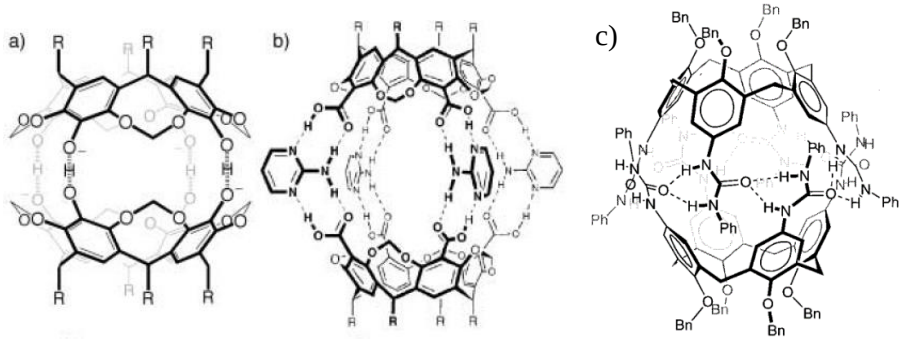

Figure 15. Homodimeric capsules based on: a) Resorcin[4]arene building blocks;[51] b) Resorcin[4]arene tetracarboxylic acid and 2-aminopyrimidine;[52] c) Tetraurea-substituted calix[4]arene.[53]

Capsules of similar design, held together by large number of H-bonding in nonpolar solvents are perfect hosts for small molecule aromatic guests. The capsule in Fig. 15a lacks a well-defined H-bond pattern but forms when monomer is partially deprotonated - ionic hydrogen bonds are formed. Most of H-bonded cavity assemblies are only stable in nonpolar media. Surprisingly, conventional H-bonding capsule was reported to form in water (Fig. 16a). [54] Monomers that are decorated with water soluble side groups were reported to dimerize in water through hydrogen bonds due to perfectly matching shape. These assemblies were found to have selectivity for hydrophobic guests according to their size.

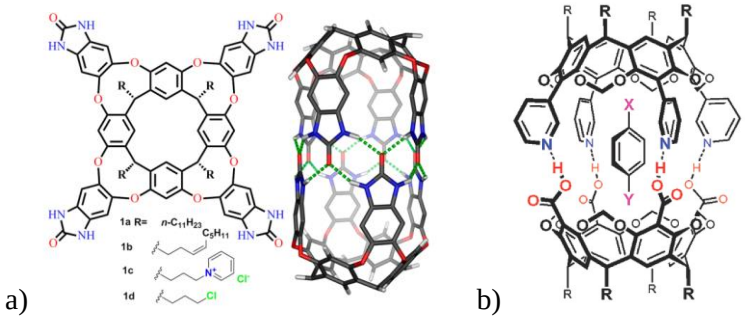

Figure 16. a) H-bonded capsule in water;[54] b) Guest induced formation of heterodimeric capsule.[55]

Often, the formation of capsule is triggered or templated by the complexation of suitable guest for the empty cavity to be energetically unfavorable.[56] [57] [58] Therefore, the behavior of the cavity assemblies can be largely influenced and controlled to some extent by solvophobic effects and guest nucleation. As in the case of heterodimeric capsule in Fig. 16b, mixing equimolar amounts of the two components in $CDCl_3$ gave mixture of undefined assemblies as indicated by proton NMR, which upon addition of 1,4-disubstituted benzene guest assembled into well-defined heterodimeric complex.[55] Two hemispheres connected through four carboxylic acid-pyridine H-bonding provide different electronic environments for encapsulated guest: inherently symmetrical guest becomes electronically nonsymmetrical as evident from its proton resonances in ^1H NMR spectrum.

Rebek's et al. famous dimeric capsule was an early prototype of H-bonded capsules.[59] Due to the binding fashion of the two glycouril monomers, it was playfully called "tennis ball" (Fig. 17a). The discovery of this assembly led to the development of various structurally similar capsules with different spacers between glycouril fragments and hence adjustable volume and shape of the cavities.[60] The concept was extended to achiral

asymmetric glucouril monomers which assemble into chiral capsule.[61] This asymmetric capsule (Fig. 17b) has four additional H-bonding provided by phenolic groups which give rise to decreased exchange rate as compared to other glycouril based capsules. Fast guest inclusion and slow capsule exchange impose chiral memory effect: after chiral guest is included, capsule adopts one of diastereomeric assemblies which will persist for prolonged time after the guest is removed. When chiral guest is exchanged with achiral, homodimeric capsules stay in their diastereomeric distribution state for few hours until slowly re-equilibrates to statistical distribution of the two diastereomeric states. The memory effect is the result of slow dimerization exchange rate as compared to guest inclusion rate.

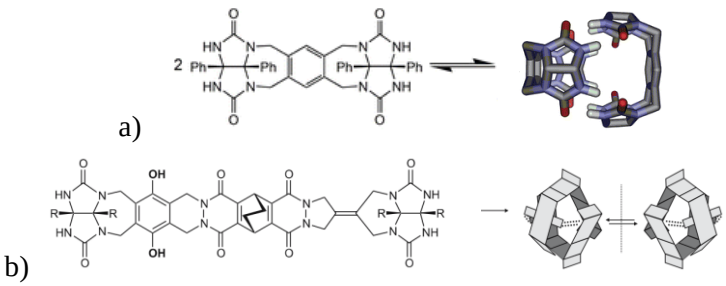

Figure 17. a) Homodimeric capsule based on glycouril fragments; b) Chiral capsule expressing enantioselective recognition properties and chiral memory effect.[61]

Hexameric H-bonded capsules having remarkably large cavity has been devised from monomers depicted in Fig. 18. It was found, that small amount of water present in $CDCl_3$ facilitates the assembly of **1a**, but hampers the assembly of **2a**. Eight water molecules are included into hydrogen bond network. Self-sorting into homoaggregates only occurs if small amount of water is added.

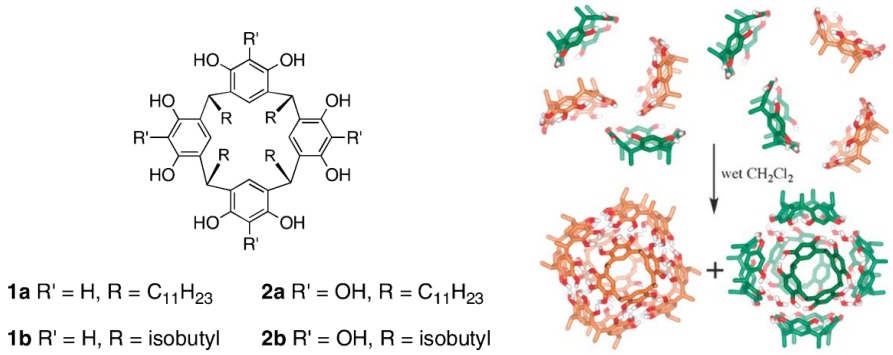

Figure 18. Hexameric capsules in nonpolar solvents from resorcin[4]arene **1** (green) and pyrogallol[4]arene **2** (orange) and their self-sorting.[62] Stable hexameric capsules **1b** and **2b** in acetone/water mixture.[63]

Guest exchange occurs through partial or complete dissociation of original capsule within time periods of up to few hours required to reach new equilibrium state. Good match in size and shape is essential for encapsulation upon which new physical properties of guest may arise.[64] To facilitate small molecule encapsulation solvents with large molecular size can be employed which do not compete for binding. The water present in organic solvent sample can be detrimental for stability of H-bonded capsules or essential as in the latter example.

4.2 NMR CHARACTERIZATION OF THE H-BONDED DECAMERIC CAPSULE

4.2.1 INTRODUCTION

The synthesis of compound **2** and its self-assembly into tetrameric rings in chloroform solution was reported by our group earlier.[65] To ensure unambiguous formation of cyclic structures over linear assemblies the compound **2** was used in its enantiomerically pure form. The enantiopure **2** was synthesized from (+)-bicyclo[3.3.1]nonane-2,6-dione precursor available after enzymatic resolution using baker's yeast for sweet dough.[66] Large solubilizing chains were introduced into the structure of monomer **2** to provide necessary solubility in nonpolar solvents. New aggregation fashion through association induced tautomerism was coined as tautoleptic aggregation. A single monomer **2** incorporates two isocytosine rings capable of tautomerism, embodied on the bicyclo[3.3.1]nonane framework. In the case of **2** in $CHCl_3$ solution heteroleptic aggregation was taking place when two different tautomeric forms resides on the same molecule (Fig. 19c).

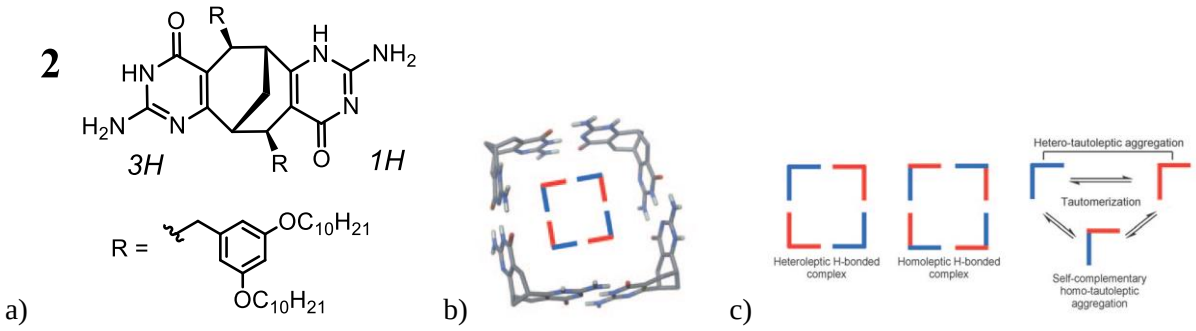

Figure 19. a) Molecular structure of C_2-symmetric monomer **2**; b) Self-assembled tetramer $\mathbf{2_4}$ in $CDCl_3$; c) Schematic representation of tautoleptic aggregation concept from ref[65].

The existence of both tautomeric forms was clearly evident from its proton NMR spectrum which also implies symmetrical arrangement of monomeric units. Using various analytical methods such as diffusion NMR and vapor pressure osmometry (VPO) the cyclic aggregate was found to be composed of four monomers (Fig. 19b). We noticed that in ^{1}H NMR spectrum at high concentrations (>10 mM) in $CDCl_3$ additional set of resonances starts to appear. This drawn our attention to investigate this system further in different media. The unique self-assembly of **2** in carbon disulfide is presented in this part of the work.

^{1}H NMR spectra in various nonpolar solvents (Fig. 20) revealed the formation of tetrameric aggregates in chlorinated solvents ($CDCl_3$, 1,1,2,2-tetrachloroethane and CCl_4). In other solvents such as in benzene-d_6, toluene-d_8 and CD_2Cl_2 the observed NH resonance patterns indicated more complicated structure or possible stacking of tetrameric rings.

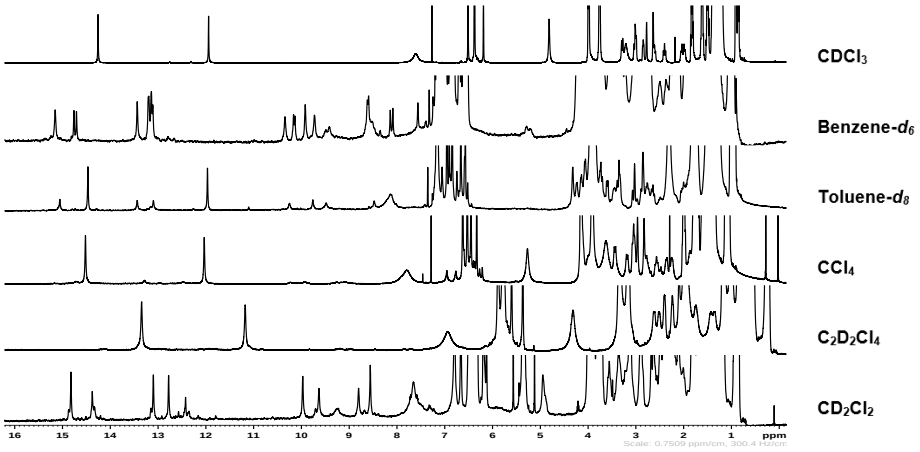

Figure 20. ^{1}H NMR spectra of **2** in various nonpolar solvents.

4.2.2 AGGREGATION IN CARBON DISULFIDE

Similar resonance pattern to the one observed in CD_2Cl_2 was obtained in carbon disulfide (Fig. 20). The very well resolved proton spectrum contained complicated NH resonance pattern of 5 NH signals and two sharp NH_2 signals in the downfield region together with several broad NH_2 signals which clearly indicates reduced symmetry as compared to tetramer $\mathbf{2_4}$ and probably higher number of monomeric units involved in the assembly. Racemic **2** in CS_2 gave distinct resonance pattern (Fig. 21b) indicating a different symmetric supramolecular entity which was not further investigated.

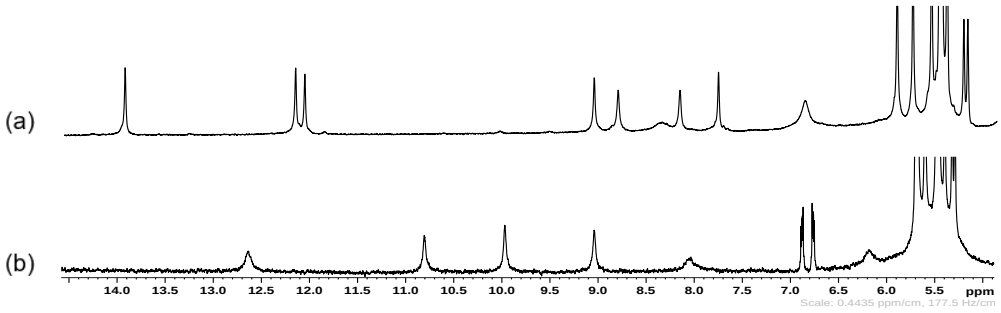

Figure 21. Expanded ^{1}H NMR spectra of **2** in CS_2. a) Enantiopure **2**; b) Racemic **2**.

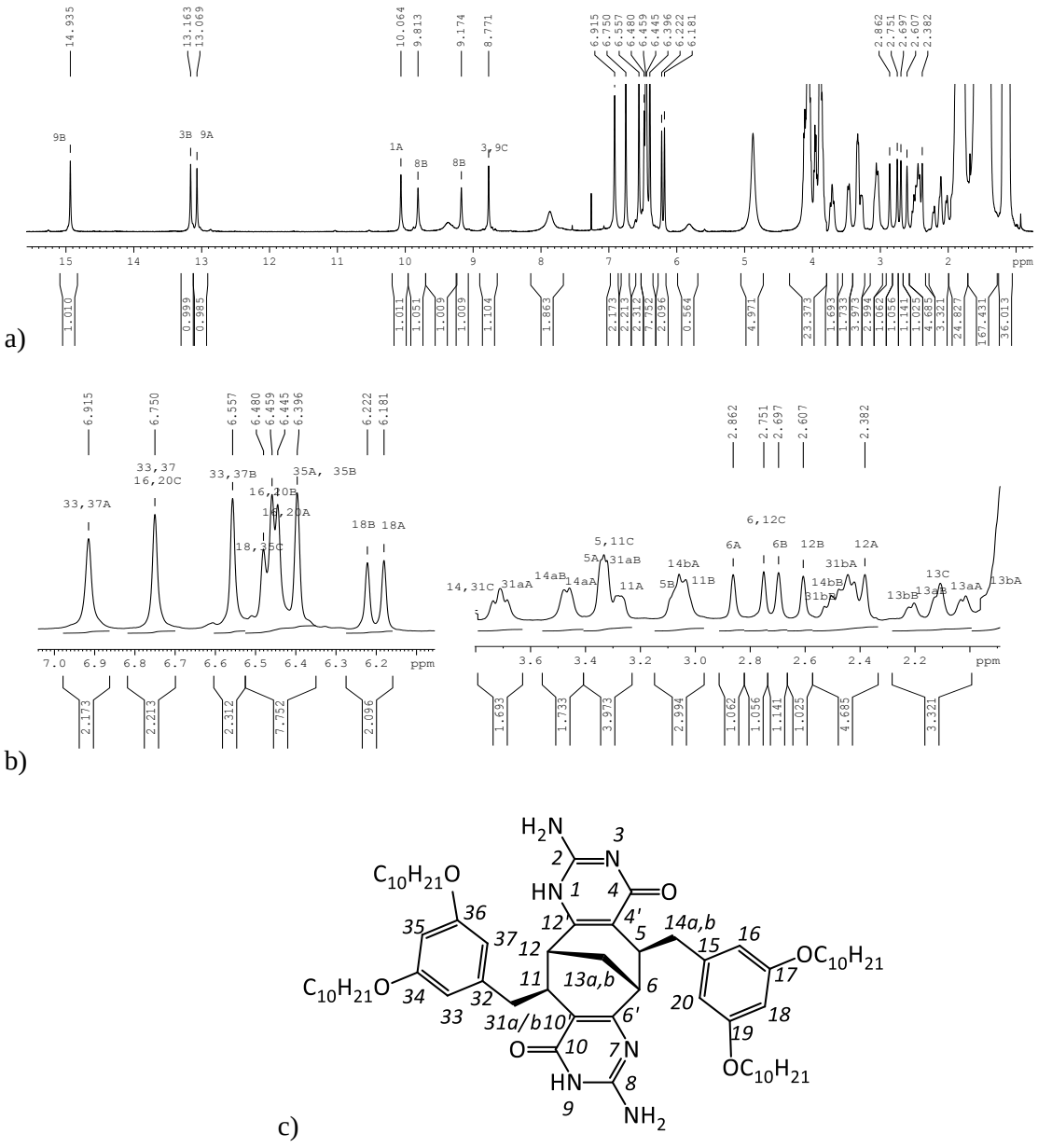

Figure 22. a) ^{1}H NMR spectrum of **2** in CS_2 with the assignment information of NH signals. Letters A, B and C label atoms belonging to monomeric units **A**, **B** and **C**; b) Extended aromatic and aliphatic regions with the assignment information; c) Molecular formula of **2** and atom labeling.

The lactim form of isocytosine (Ic) which could self-associate via 2H-bonding was ruled out after ^{1}H - ^{15}N HMQC experiment which confirmed that all hydrogens in the downfield region are residing on nitrogen atoms. It also allowed to differentiate between hydrogens belonging to NH_2 groups and aromatic nitrogen atoms. Protons having chemical shift 8.2 ppm and 8.8 ppm are located on the same nitrogen atom, which also indicated that rotation of this particular amino group is restricted due involvement of both protons in strong H-bonding. (Fig. 23)

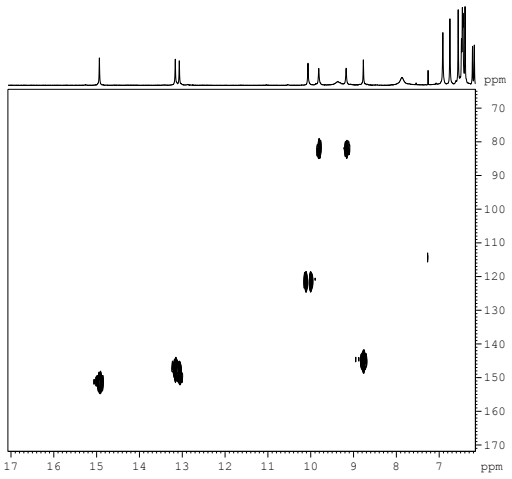

Figure 23. ^{1}H - ^{15}N HMQC spectrum of **2** in CS_2.

The COSY spectrum revealed 5 analogous scalar coupling patterns (Fig. 24a). Starting the analysis with the diagnostic bridgehead protons labeled by numbers 6/12 (2.87, 2.76, 2.71, 2.62 and 2.39 ppm), five analogous sets of peaks were found (correlations to the benzylic protons 14a, 14b/31a, 31b and to the bicyclic skeleton protons 5/11 and 13a/b).

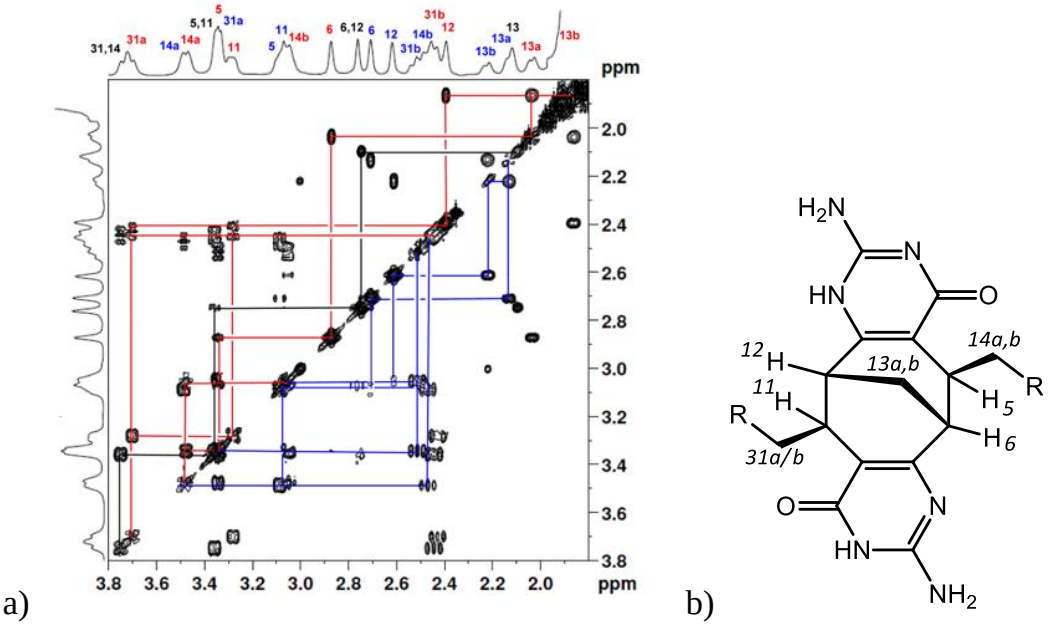

Figure 24. a) The upfield region of the COSY spectrum (red – unit A, blue – unit B, black – unit C); b) Molecular structure of **2**.

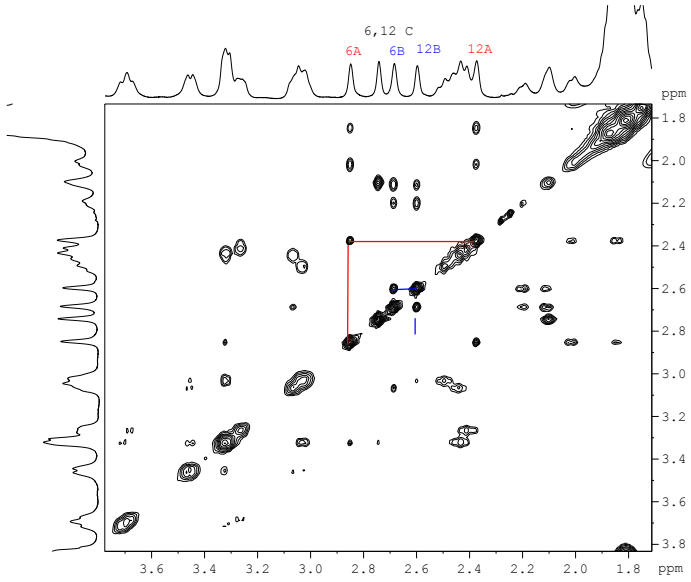

Figure 25. The upfield region of the TOCSY spectrum (red – unit A, blue – unit B).

TOCSY spectrum (Fig. 25) allowed to connect two pairs of protons 6 and 12 on the opposite side of the molecule: proton signal at 2.87 ppm (6A) gives correlation to the signal at 2.39 ppm (12A); signal at 2.71 ppm (6B) correlates to the signal at 2.39 ppm (12B). The signal at 2.76 ppm corresponds to overlapping protons 6 and 12 in unit **C**. Hence, three forms of monomers can be identified. For convenience slightly different monomers were labeled **A**, **B** and **C**, more explicitly, two C_1 symmetrical units **A** and **B** (that gives separate signals for the protons on the opposite side of the molecule, 6 and 12)

and one C_2 symmetrical unit **C** (that gives one peak for the protons 6/12). Assuming the integrals are 1 : 1 : 1 : 1 : 1, the units **A**, **B** and **C** exist in ratio 2 : 2 : 1, respectively.

DOSY NMR confirmed that units **A**, **B** and **C** belong to a single supramolecular species – all proton resonances correlates to the same diffusion coefficient of $3.1*10^{-10}$ m^2s^{-1} (Fig. 26a). DOSY experiment of **2** in the mixture of $CDCl_3$ and CS_2 showed the tetramer $\mathbf{2_4}$ and the unknown aggregate $\mathbf{2_x}$ existing simultaneously. The system in equilibrium also provided good estimate for the size of the unknown aggregate. The DOSY of compound **2** in $CDCl_3/CS_2$ (1 : 1, v/v) indicated that hydrodynamic radius of the new species is 60% larger than the known tetramer $\mathbf{2_4}$ (Fig. 26b). Diffusion data suggested that the aggregate is most likely larger than the smallest possible species - a pentamer (of the composition $\mathbf{A_2B_2C}$) and gave an idea about the next possible self-assembled structure – a decamer $\mathbf{A_4B_4C_2}$.

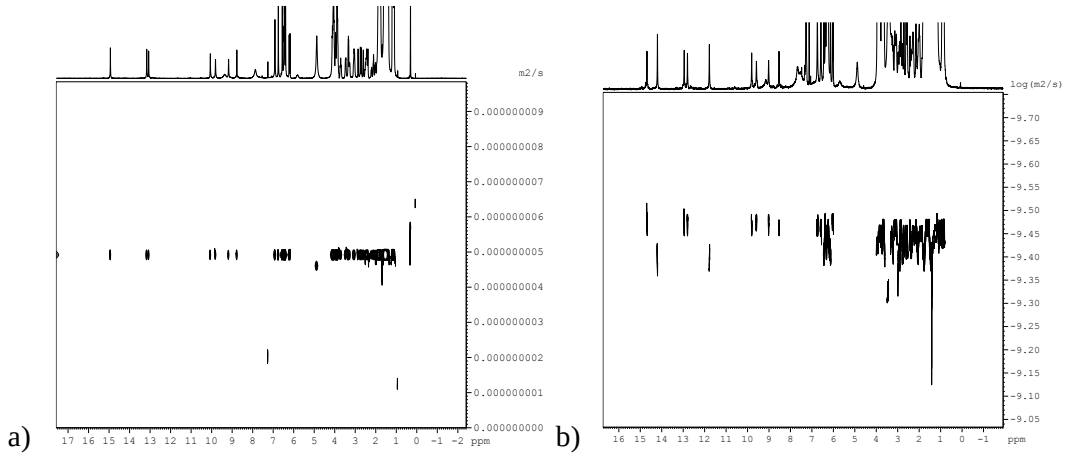

Figure 26. a) DOSY NMR spectrum of **2** in CS_2; b) DOSY NMR spectrum of **2** in $CDCl_3/CS_2$ (1:1, v/v) mixture.

4.2.3 TAUTOMERIC FORMS

Long range heteronuclear ^1H- ^{13}C couplings were used to map the resonances within the units and allowed to identify individual NH resonances. In the HMBC spectrum the protons from aliphatic region 6A, 12A, 6B, 12B and 6/12C gave correlations to carbon atoms 4' and 10' in the region 114 – 108 ppm (Fig. 27a). The same carbons then could be traced to the NH region (Fig. 27b).

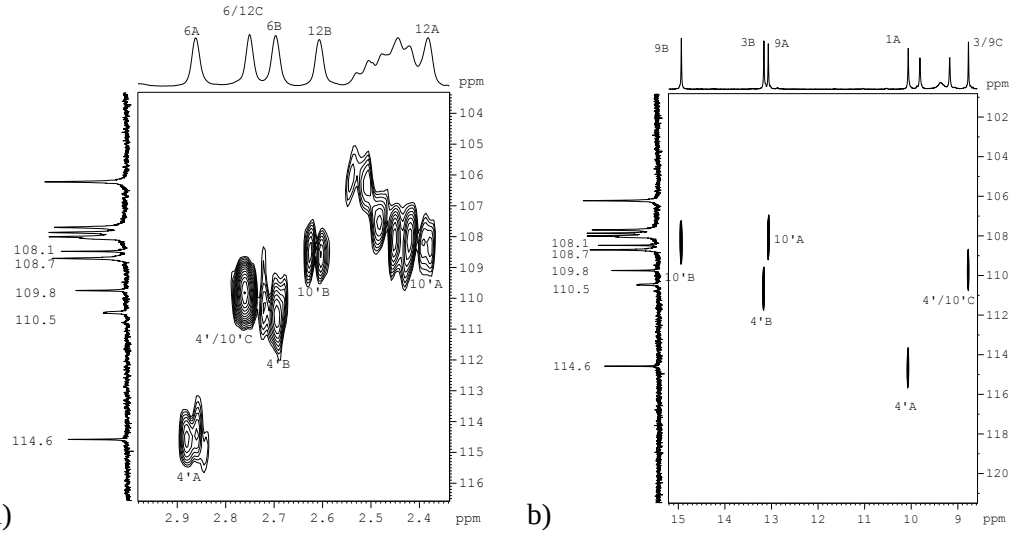

Figure 27. a) Part of HMBC spectrum showing long range scalar coupling from protons 6 to carbons 4' and protons 12 to carbons 10'; b) Part of HMBC spectrum showing long range scalar coupling from carbons 4' to protons 1 or 3 and from carbons 10' to protons 9.

Useful information about the tautomeric forms of the three units was gained from HMBC spectrum. As it is shown in Fig. 28a, all of the NH protons except the proton at 10.1 ppm (1A) give two bonds coupling to the carbonyl carbon atoms in the region of 163 -166 ppm labeled 4 or 10. Thus, the hydrogens must be located at the position *3H* in the Ic ring. The protons of this tautomer also correlated through three bonds to carbon atoms labelled 4' and 10' in the region 108 - 110 ppm. In contrast, NH proton at 10.1 ppm (1A) interacts differently: it correlates to the carbon at 146 ppm, i.e. proton 12', and thus is located at the 1 position, i.e. 1*H* tautomer. It also has three bonds scalar coupling to carbon atom 4'A at 114.6 ppm. These findings were also confirmed by ^{1}H-^{15}N HMBC experiment where cross-peaks from bridgehead protons 6 and 12 to nitrogen atoms 1 and 7 were observed. N1 nitrogen in unit **A** is the only protonated nitrogen at the position 1 (Fig. 28b) and thus, belongs to *1H* tautomer. Other protons 6A, 6/12C, 6B and 12B are coupled to aromatic nitrogen atoms in the region 205 – 199 ppm and therefore indicate that protonated nitrogen atoms are 3 and 7, i.e. *3H* tautomer.

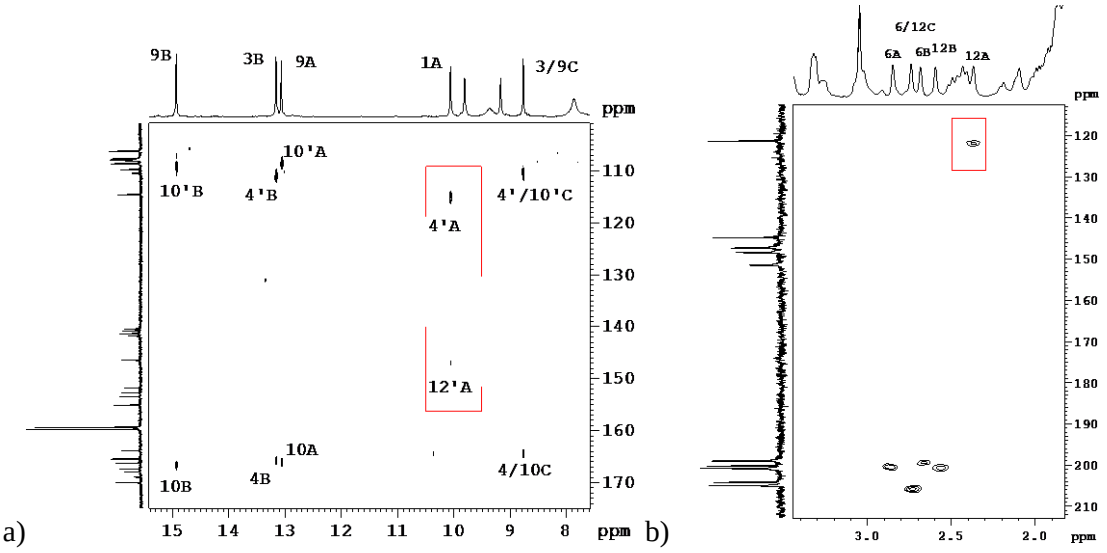

Figure 28. a) Downfield region of the HMBC spectrum of **2** in CS_2. Correlation pattern common for *3H* tautomer and *1H* tautomer (marked with a red square) emerges; b) Part of ^{1}H-^{15}N HMBC spectrum.

After having established the tautomeric forms, their distribution within the monomer units can be deduced: unit **A** is asymmetric and has two different tautomeric forms on the opposite ends of the molecule while the units **B** and **C** incorporate *3H* form on both ends of the units (Fig. 29).

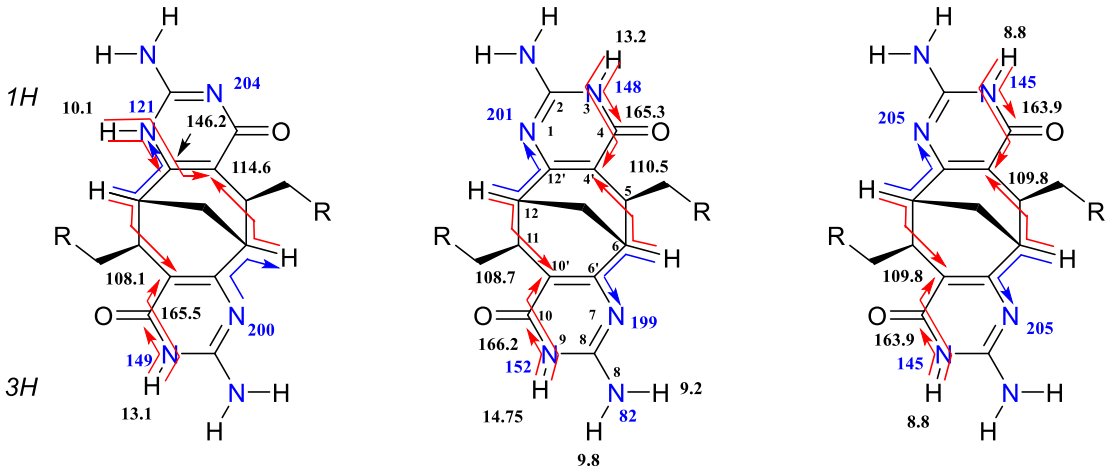

Figure 29. Proton, carbon and nitrogen (blue) atom assignment information and schematic representation of important long range heteronuclear couplings (^{1}H-^{13}C HMBC - red arrows, ^{1}H-^{15}N HMBC - blue arrows).

Unit **A** is intrinsically asymmetric due to different tautomers residing on the same molecule. Although unit **B** contains the same tautomeric forms on both sides of the molecule the two sites are chemically and magnetically nonequivalent. This may arise from different H-bonding interfaces at the two sites: 3H-bonding with the unit **A** on one side and 2H-bonding with either unit on the other side.

4.2.4 CONNECTIVITY OF THE UNITS

The connectivity of the units was established from ROESY spectra recorded at room temperature and at 258 K. After careful analysis several NOE interactions were identified in the spectrum among many TOCSY-like cross-peaks (Fig. 30). It was found that units **A** and **B** are indeed connected: proton 9A gives NOE's to 5B, 14aB and 3B while 3B correlates with 11A, 31aA and 9A. These are the NOE interactions across 3H-3H-bonding between *1H* and *3H* tautomeric forms in units **A** and **B**. The NH proton 9B on the other side of the unit **B** is connected with another side of the unit **A** and gives NOE interactions to protons 6A and 5A. Purely from symmetry considerations tetrameric ring composed of units **ABAB** could be deduced. No ROESY peaks could be found for unit **C** which strongly implies that the magnetically symmetrical unit **C** is not included into the ring system but is located outside the cyclic tetramer.

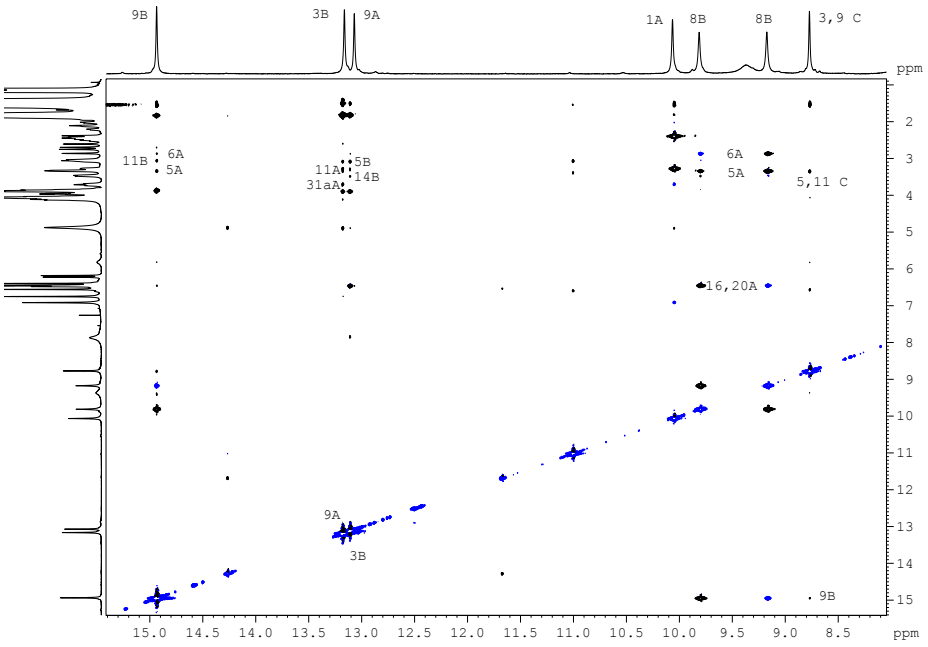

Figure 30. Part of the ROESY spectrum with the assignment information. Opposite phase crosspeaks (blue) correspond to TOCSY-type artifacts.

Low temperature ROESY (Fig. 31) revealed one important inter-unit correlation – unit **C** amino group 2/8C is coupled to the proton 11B. This interesting finding led to an idea that the tetramer ring **ABAB** is connected or capped with the unit **C**.

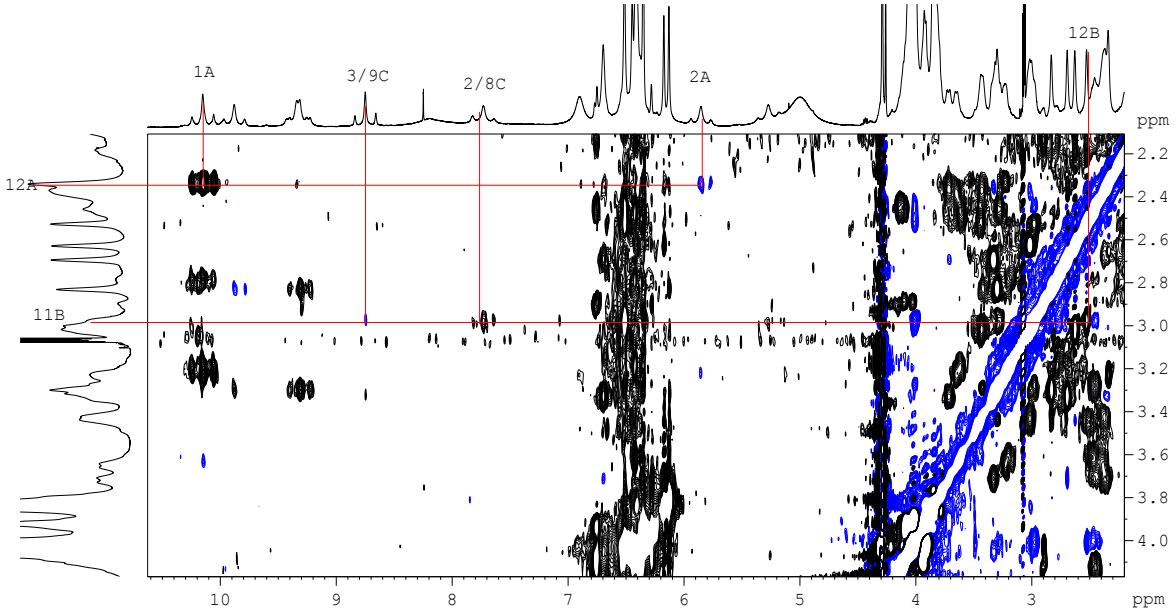

Figure 31. Part of ROESY spectrum at 258 K.

4.2.5 FINAL H-BONDING PATTERN ELUCIDATION

In the simplest scenario of a cyclic pentameric aggregate **A_2B_2C** according to the observed NOEs, the unit **A** must be connected to the unit **B** via 3H-bonding and on the other side with the unit **B** via 2H-bonding. In turn, the unit **C** then should bind to the unit **B** on one side and the unit **A** on the other side, via 2H-bonding i.e. **BACBA**. The suggested connectivity order stands against magnetic inequivalence of the monomers, because unit **C** should have the same binding mode on both sides. In addition some other contradictory findings such as DOSY and the absence of NOEs (comparing to very compelling NOE's between units **A** and **B**) including unit **C** strongly suggested that the cyclic pentamer is not the correct arrangement of the units, but instead the cyclic tetramer **ABAB** is the main structural component of the larger supramolecular entity. Trying to deduce other cyclic pentameric arrangements from units **A**, **B** and **C** failed to produce aggregate that would satisfy the findings discussed above. Therefore, the next larger entity – a decamer was considered.

The fact that four out of twenty Ic motifs exist as *1H* tautomer implies that four 3H-bonding modes and six 2H-bonding modes are established. The two distinct aggregation modes, *e.g.* 2H-bonding between two *3H* keto forms and 3H-bonding between *1H* and *3H* keto forms operating in one C_2-symmetric monomer may be responsible for the symmetry

breaking observed in unit **B** (*vide infra*). To confirm assembly through 3H-bonding HNN COSY experiment was pursued. HNN COSY experiment was developed by Grzesiek[67] to directly detect N-H···N hydrogen bonds in ^{15}N labelled nucleic acid pairs and other biomolecules. The experiment detects electron-mediated scalar couplings across the hydrogen bond (H-bond scalar couplings), which connect ^{15}N nuclei of the H-bond donor and acceptor. The outcome is a correlation which identifies donor nitrogen atom, acceptor nitrogen atom and hydrogen atom involved into H-bonded in a single spectrum. Since HNN COSY is usually applied to biomolecules, the exact duration of delays used in the pulse sequence suitable for small molecules was unknown. Moreover, absence of cross-peak not necessarily could mean absence of correlation, but rather unsuccessful NMR experiment. Therefore, experiment conditions were compared with a model compound **$^{15}N_1$-4** that was known to form N-H···N hydrogen bonds and was reported by Sijbesma et al. to give the expected HNN COSY cross-peak.[68] After several attempts and successful experiments on the model compound **$^{15}N_1$-4**, the same set of parameters were utilized for **$^{15}N_1$- 2** in CS_2. ^{15}N and ^{13}C isotope labeled monomer **2** was synthesized in the same way as in the original procedure[65] using $^{15}N_1$-guanidine hydrochloride or ^{13}C-guanidine hydrochloride (Fig. 32).

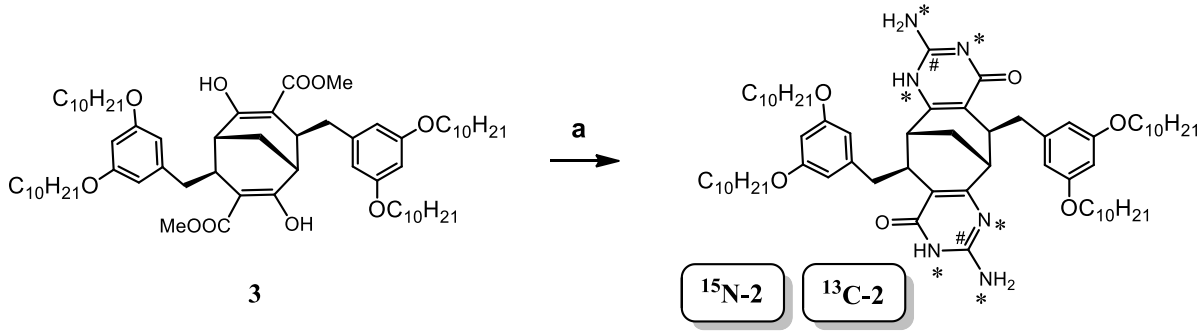

Figure 32. Synthesis of **^{15}N-2** and **^{13}C-2**. Nitrogen atoms marked with stars are enriched by 33 % by ^{15}N atoms. ^{13}C atoms marked with # are enriched by 99 %. Reagents and conditions: (a) $^{15}N_1$-guanidium chloride or ^{13}C-guanidinium chloride, KOBu^t, MeOH, yield 65 – 69 %.

Singly randomly $^{15}N_1$ labeled but not fully labeled $^{15}N_3$ analog was required for the HNN COSY experiment. If all nitrogen atoms are ^{15}N, all of them will be magnetically labeled in the initial step of the pulse sequence and subsequently magnetization will be transferred in all directions. In such scenario cross-peaks correlating all three nitrogen atoms within a residue will be observed. The HNN COSY of **$^{15}N_1$-2** is depicted in Fig. 33a. Indeed, the proton at 14.95 ppm correlates two nitrogen atoms at 152 ppm and 204 ppm (squared with

red line). The same experiment at low temperature allowed to identify amino group protons 2/8A and 2/8C, which were not resolved at room temperature.

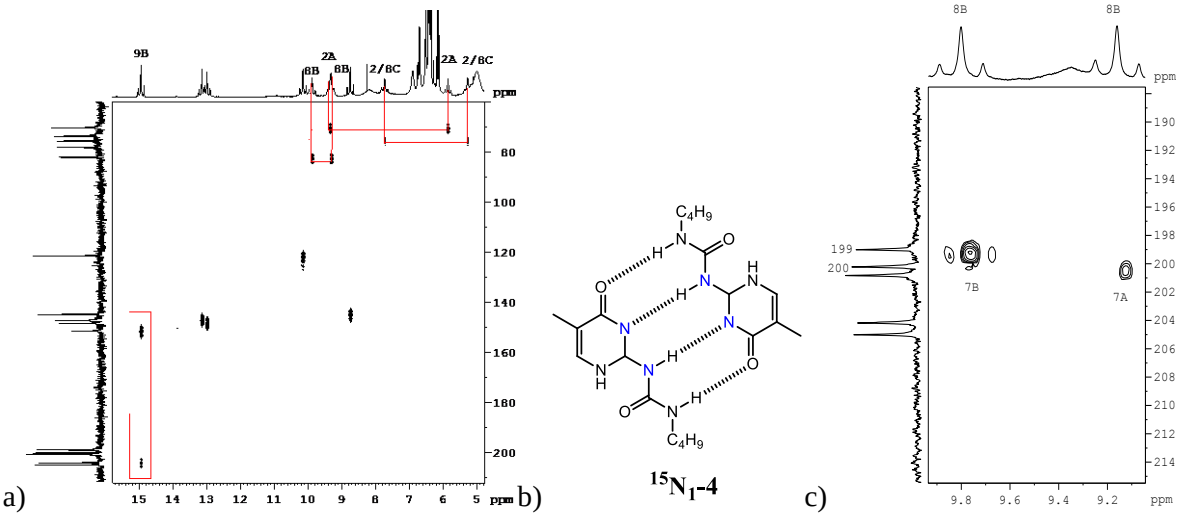

Figure 33. a) HNN COSY spectrum of **^{15}N$_1$-2** in CS_2 at 258 K; b) Molecular structure of the model compound **^{15}N$_1$-4**; c) Part of ^{1}H-^{15}N HMBC spectrum of **^{15}N$_1$-2**.

We therefore confirmed 3H-bonding arrays within tetramer **ABAB**. As it is known from low temperature ROESY, amino groups in the unit **C** are in proximity to bridgehead proton 11B. Fig. 34 schematically represents H-bonding patterns together with observed inter-unit NMR interactions. ^{1}H-^{15}N HMBC spectrum has one correlation from the unit **B** amino group at 9.2 ppm to aromatic nitrogen 7 in the unit **A**. This particular interaction is inter-tetramer and connects two tetramers through 8B amino group and aromatic nitrogen atom 7 of unit **A** *3H* tautomer.

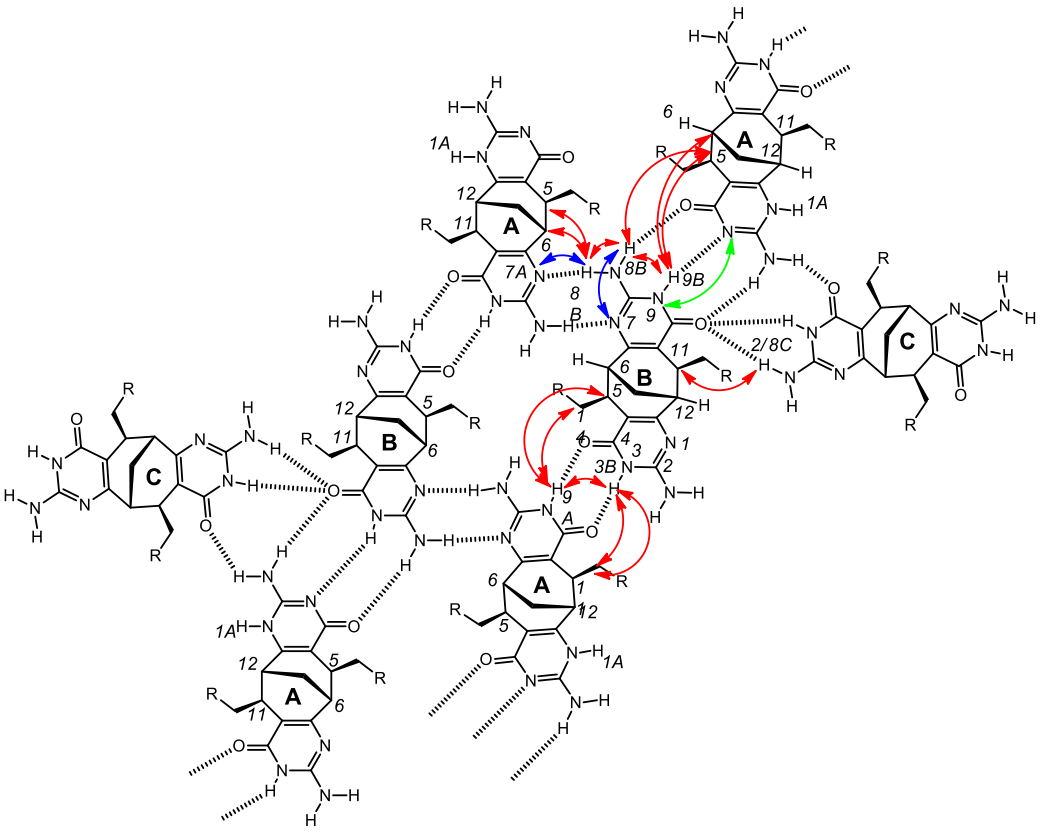

Figure 34. Schematic representation of monomeric unit's arrangement together with interunit interactions: ROESY correlations (red arrows), HNN COSY coupling (green arrow) and ^{1}H-^{15}N HMBC correlations (blue arrows). For clarity only one set of interactions is represented.

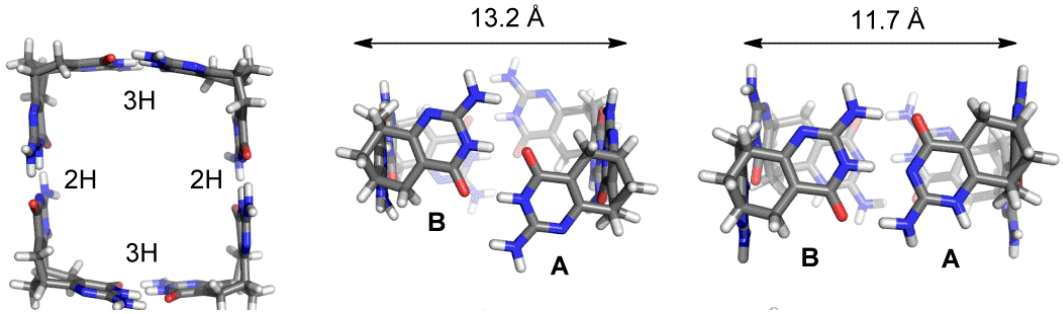

Figure 35. Molecular model of the tetramer **ABAB**.

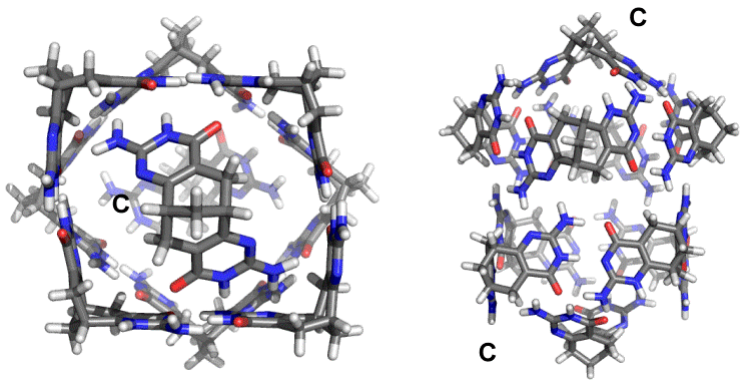

Figure 36. Molecular model of the final decameric capsule $\mathbf{2_{10}}$ top view and side view.

As it is seen from a molecular model, tetramer is held together by alternating 3H- and 2H-bonding arrays which makes the two pairs of opposite walls of the parent tetramer slightly different in length (Fig. 31). The wall that has 2H-bonding array is longer by 1.5 Å than the tighter packed wall with 3H-bonding interface. The two tetramers are connected though inter-rim hydrogen bonds between unit **B** amino group 8B and nitrogen 7 from unit **A**. For these inter-tetramer H-bonds to form, tetramers have to be rotated by 45 º with respect to each other. Such arrangement is further supported by ROESY correlations between proton 8B at 9.2 ppm and protons 5A and 6A in unit **A** (inter-tetramer). These protons are too far away from each other to give NOE if we would consider them to be located in **A** and **B** units within the same tetramer. Proton 8B resonating at 9.2 ppm also gives secondary NOE to protons 16/20A and 9B (within tetramer). Similarly, proton 8B at 9.8 ppm which is included into 3H-bonding, gives secondary NOE to 6A (inter-tetramer) but true NOE's to 5A, 16/20A and 9B (within tetramer), just as proton 9B gives inter-tetramer NOE's to 5A and 6A. The *1H* tautomer in unit **A** is positioned on the opposite side than inter-tetramer binding site and possibly its amino group interacts with the keto group of the unit **C**.

	Unit A			**Unit B**			**Unit C**		
Atom No.	^{1}H	^{13}C	^{15}N	^{1}H	^{13}C	^{15}N	^{1}H	^{13}C	^{15}N
1	10.08	-	121	-	-	201	-	-	205
2	5.80, 9.38	152-156	70	-	152-156	73.5	7.73, 5.27	152-156	75.5
3	-	-	204	14.95	-	147	8.8	-	145
4	-	170.0	-	-	165.5	-	-	163.9	-
4'	-	114.6	-	-	110.5	-	-	109.5	-
5	3.34	38.1	-	3.08	37.7	-	3.36	36.6	-
6	2.86	37.9	-	2.70	36.0		2.75	36.0	-
6'	-	167.4	-	-	168.0	-	-	169.0	-
7	-	-	200	-	-	199	-	-	205
8	N	152-156	78	9.8, 9.1	152-156	82	7.73, 5.27	152-156	75.5
9	13.08	-	149	13.17	-	152	8.8	-	145
10	-	165.3	-	-	166.2	-	-	163.9	-
10'	-	107.9	-	-	108.7	-	-	109.5	-
11	3.28	39.2	-	3.00	38.1	-	3.36	37.65	-
12	2.38	31.5	-	2.61	35.8	-	2.75	36.0	-
12'	-	146	-	-	167.4	-	-	169.0	-
13a	2.03	17.5	-	2.12	17.5	-	2.09	17.5	-
13b	1.85	17.5	-	2.21	17.5	-	2.09	17.5	-

Table 1. ^{1}H, ^{13}C and ^{15}N atoms assignment of $\mathbf{2_{10}}$ in CS_2.

Extensive chemical shift assignment for most of the proton, carbon and nitrogen atoms is given in the Table 1. Chemical shifts observed for Ic ring atoms in this study are in good agreement with chemical shifts for crystalline isocytosine reported by others.[11]

4.3 HOST-GUEST CHEMISTRY WITH C_{60}

The efficiency and the extent of the host and guest pairing is depends on the complementarity of the size, shape, and chemical surface of the guest with the cavity of the host. It is well recognized that along with the matching of these properties, solvation of host, guest and their complex play crucial role in molecular recognition process. In a host guest binding or encapsulation event, poor solvation of a guest molecule can enforce complex formation where entropic cost is compensated by large negative enthalpy changes. The large cavity size of the proposed decameric capsule $\mathbf{2_{10}}$ could be utilized as a suitable host for large size guests. Fullerene C_{60} has the hydrodymic radius of 10.1 Å and could fit inside the cavity. At least theoretically, two C_{60} molecules or its dimer C_{120} could be hosted as well.

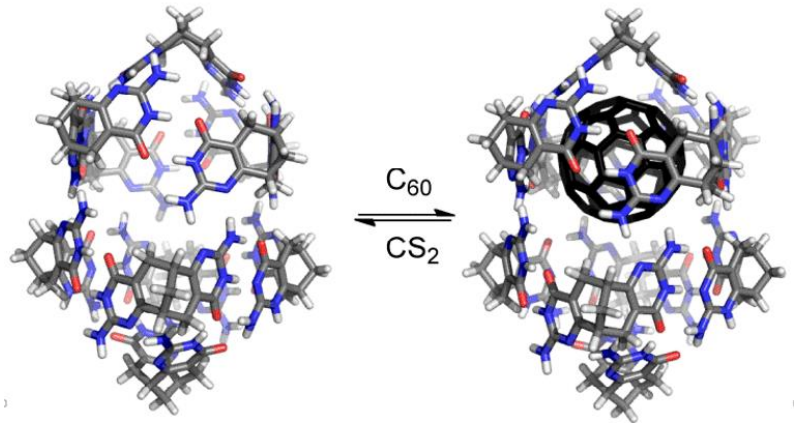

Figure 37. Encapsulation of C_{60} into decameric capsule $\mathbf{2_{10}}$.

Decamer $\mathbf{2_{10}}$ indeed produced inclusion complex (Fig. 37) with $\mathbf{C_{60}}$ although full complexation was never achieved even with an excess of $\mathbf{C_{60}}$. The complexation event is visible from the color change of the solution – purple color of the C_{60} gradually changes to brown color of the complex $\mathbf{2_{10}@C_{60}}$. The ^{1}H NMR spectrum contains resonances of the free decamer $\mathbf{2_{10}}$ and another more complicated set of peaks corresponding to the complexed species $\mathbf{2_{10}@C_{60}}$. DOSY NMR provided evidence that new species and the free host $\mathbf{2_{10}}$ has the same diffusion coefficient and therefore we assumed that complexation

induced no changes in the host structure and **C_{60}** molecule must be inserted into the host cavity. From the ^{1}H NMR spectrum it was evident that the new species are of reduced symmetry which probably arises from **C_{60}** residing at one end of the cavity. The slow exchange between the two identical binding sites of the cavity give rise to separate signals rather than average resonances (Fig. 38). Every NH signal is split into two signals for the inclusion complex. Complexation event also caused upfield shift of the C_{60} resonance in ^{13}C NMR spectrum – from 142.7 ppm to 141.7 ppm. As no structural rearrangement of the initial aggregate has taken place the integration of these resonances and their relative ratio were used to calculate stoichiometry of the parent aggregate.

4.3.1 STOICHIOMETRY DETERMINATION OF HOST GUEST COMPLEX

Stoichiometry of the inclusion complex **^{13}C-2@C_{60}** was established by integrating quantitative ^{13}C NMR spectrum and comparing relative integrals values of the complexed and the free **^{13}C-2** and the complexed and the free C_{60} individually.

The sample for stoichiometry determination was prepared from 18 mg (0.0164 mmol) of 98 % atom ^{13}C labeled compound **^{13}C-2** and 2.48 mg (0.0033 mmol, 0.2 eq.) of C_{60} ^{13}C enriched by 32 % dissolved in 0.5 ml of CS_2 and left to stand overnight to reach equilibrium. The sample was equipped with an inner insert tube which was filled with $(CD_3)_2CO$ to provide deuterium lock. T1 relaxation of carbon atoms was measured by inversion recovery experiment and was determined to be 14 s for the slowest relaxing C_{60} carbon atoms. Quantitative ^{13}C NMR was run using following parameters: d1 = 125 s, aq = 0.6 s, ns = 128. The integrated spectrum is given in Fig. 39. The peak at 143.3 ppm corresponds to the free C_{60} and peak at 142.3 ppm to the complexed C_{60}. This gives 33 % of all C_{60} complexed, which calculated from total amount of C_{60} added (0.0033 mmol), gives the amount of the complexed C_{60} 0.00111 mmol. Integrating peaks of **^{13}C-2** in the same manner gives 70 % of **2** being complexed which calculated to molar amount is equal to 0.00115 mmol. The molar ratio **^{13}C-2**/**^{13}C-C_{60}** then equals to 10.

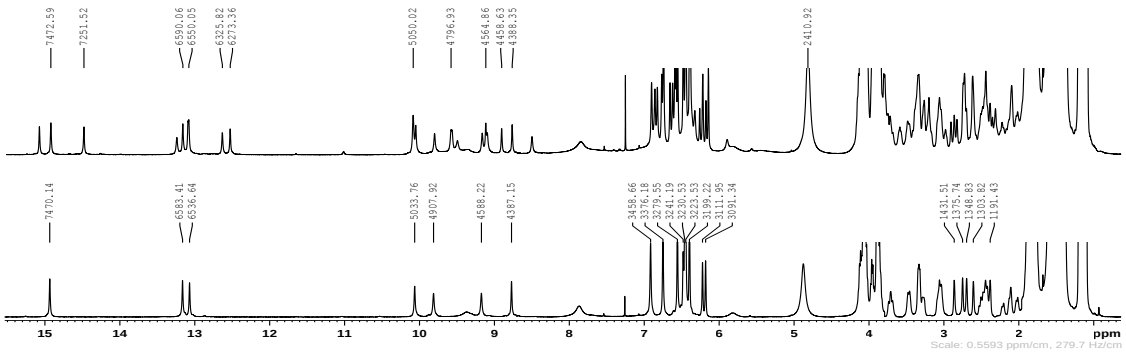

Figure 38. Stacked ^{1}H NMR of **2** (bottom) and inclusion complex $\mathbf{2_{10}@C_{60}}$ (top) in CS_2**.**

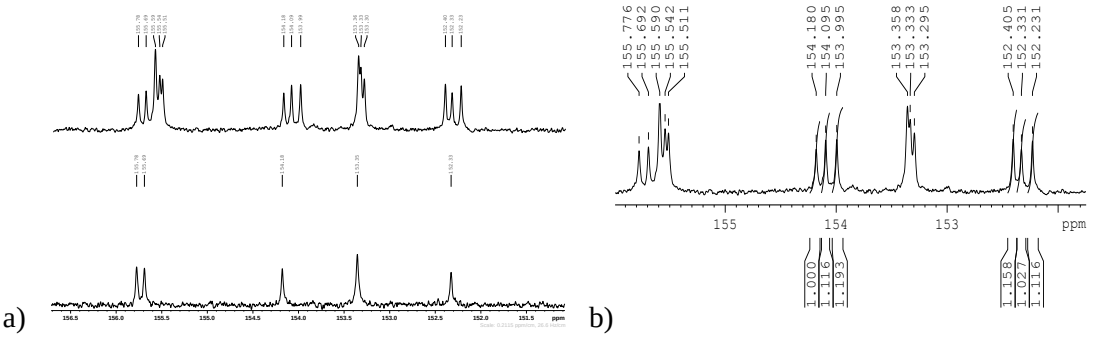

Figure 39. a) Stacked ^{13}C NMR spectra of free ^{13}**C-2** (bottom) and ^{13}**C-2@**^{13}**C-C$_{60}$** (top) in CS_2; b) Quantitative ^{13}C NMR spectrum of the inclusion complex ^{13}**C-2@**^{13}**C-C$_{60}$** in CS_2 showing the relative integrals of ^{13}**C-2**.

4.3.2 MOLECULAR DYNAMIC SIMULATIONS

Molecular dynamic (MD) simulations were employed in order to gain deeper insight into the mechanism of C_{60} encapsulation in CS_2 and the molecular structure of the complex obtained (Schrödinger Release 2014-1: Maestro, version 9.7, Schrödinger, LLC, New York, NY, 2014). In molecular mechanics (MM) calculations, the structure of the monomer **2** was simplified by exchanging the benzylic side chains with methyl groups. The observed $\mathbf{2_{10}}$ aggregate consists of three forms **A**, **B**, **C** of monomer **2** in the proportions 4 : 4 : 2 as indicated by the integration of ^{1}H NMR spectrum. Models of $\mathbf{2_{10}}$ aggregate in CS_2 were constructed in three steps: the cyclic tetramer **ABAB**, two stacked tetramers $\mathbf{(ABAB)_2}$ and stacked tetramers capped with the unit **C** at each end $\mathbf{C(ABAB)_2C}$. In every step weak distance constraints for the observed NMR interactions were applied as in Fig. 34 in a geometry optimization using the OPLS 2005 force field in the gas phase. MD simulations were performed on the gas phase decamer model, extended with a 2,4-ethoxy benzyl side chains as simplified version of the solubilizing groups using the Desmond molecular

dynamics simulations package with default settings (Schrödinger Release 2014-1: Desmond Molecular Dynamics System, version 3.7, D. E. Shaw Research, New York, NY, 2014. Maestro-Desmond Interoperability Tools, version 3.7, Schrödinger, New York, NY, 2014).

First, a 9.6 ns MD simulation of the decamer was performed in CS_2. Initially, the simulation had three solvent molecules in the cavity and it reached equilibrium after 4.5 ns with eight solvent molecules in the cavity. The inclusion complex with C_{60} was constructed from a snapshot of the equilibrated MD simulation in CS_2. All solvent molecules were removed except those in the van der Waals contact to the $\mathbf{2_{10}}$ aggregate. A $\mathbf{C_{60}}$ molecule was initially positioned at the center of the cavity and all overlapping solvent molecules were removed. A 48 ns MD simulation of this inclusion complex was then performed in CS_2. After equilibration, two CS_2 molecules were in the cavity close to one of the **C** units and C_{60} was asymmetrically placed in the cavity close to the other **C** unit molecule. The MD simulation thus confirmed that the partial solvation of the C_{60} molecule from one side with CS_2 is responsible for the symmetry breaking of the aggregate. During the equilibration of $\mathbf{2_{10}}$ with C_{60}, the C_{60} molecule moved toward the pole of the capsule whereas the corresponding interacting unit **C** moved slightly inward as compared to the equilibrium structure of $\mathbf{2_{10}}$ in CS_2. This fact indicates favorable van der Waals interactions between the C_{60} surface and the concave surface of the unit **C**. Since the movement of C_{60} molecule inside the cavity is accompanied by its partial desolvation, the above-mentioned interaction between C_{60} and unit **C** is obviously stronger than the interaction between C_{60} and CS_2.[26] The very slow exchange of C_{60} molecule between two poles can be understood taking into account the fact that the two encapsulated CS_2 molecules that are in close contact to C_{60} have to be simultaneously removed from the cavity in order for C_{60} to exchange the binding sites. Such a process must be kinetically very demanding.

5 ORGANIC NANOTUBES FROM BIS-IC MONOMERS BASED ON 9-AZABICYLO[3.3.1]NONANE AND BICYCLO[3.3.1]NONANE FRAMEWORKS

5.1 INTRODUCTION TO 9-AZABICYCLO[3.3.1]NONANE DERIVATIVES

9-azabicyclo[3.3.1]nonane (granatane) scaffold is found in numerous naturally occurring compounds e.g. pavine,[69] macroline, sarpagine, ajmaline[70] and related indole alkaloids, an important class of natural products with diverse biological activity (Fig. 40). It was incorporated into structures of drugs (granisetron[71]) and synthetic receptors[72a, 72b]. TEMPO analog 9-azabicyclo[3.3.1]nonane N-oxyl radical (ABNO) is less hindered and therefore notably more reactive oxidant.[73]

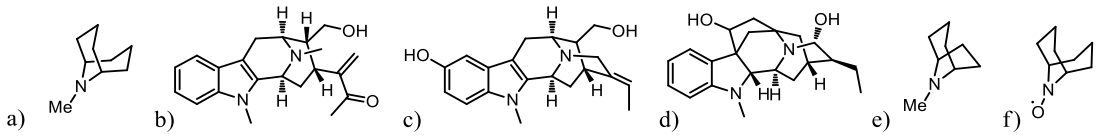

Figure 40. Molecular structures. a) Granatane; b) Macroline; c) Sarpagine; d) Ajmaline; f) Tropane; f) ABNO radical.

The strained nature of the bicylic skeleton is particularly interesting for conformational studies.[74a, 74b, 74c] The bicyclic ring in 9-azabicyclo[3.3.1]nonane derivatives is composed of two connected six membered rings with 3 possible conformations: *chair-chair* (*CC*), *chair-boat* (*CB*) and *boat-boat* (*BB*) (Fig. 41); the first one usually the most stable.[75] The stability of conformations in 9-azabicyclo[3.3.1]nonane derivatives follows the same trends as in bicyclo[3.3.1]nonane.

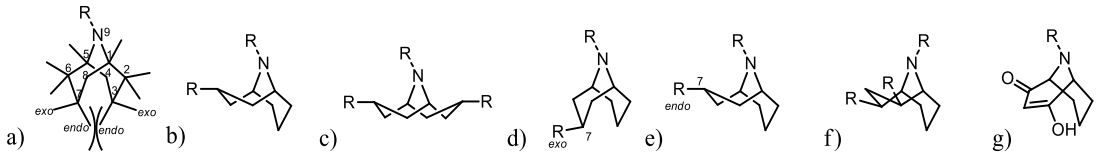

Figure 41. Possible conformations of 9-azabicyclo[3.3.1]nonane rings *CC*, *CB* and *BB* and preferred conformations of substituted derivatives.

Main destabilizing factor for the *CC* conformation is steric repulsion between substituents in 3-*endo* and 7-*endo* position (Fig. 41a). Any substituent bigger than hydrogen in one of those positions will cause to flip one of the rings and adopt the *CB* conformation (Fig. 41b).[76] In contrast, 3-*exo* or 7-*exo* substituted rings will not interfere to stay in *CC* position due to the absence of any steric interaction (Fig. 41d). In 2,4-disubstituted rings

CC conformation will be destabilized due to 1,3-diaxial repulsion, therefore *CB* conformation will be preferred (Fig. 41f). Substituents in 1 and 5 position usually have little effect and inherently most stable *CC* conformation is favored. The same is true for 2,6-disubstituted 9-azabicyclo[3.3.1]nonanes. sp^2 atoms in 2,3 and/or 4 positions in the bicyclic ring leads to the flattening of the six membered ring and flipping to the envelope conformation (Fig. 41g). This conformation is obtained for bicyclo[3.3.1]nonanes fused with aromatic rings, as it is in the case of macroline, sarpagine, ajmaline compounds and supramolecular synthons presented in this work.

5.1.1 SYNTHETIC ROUTES TO 9-AZABICYCLO[3.3.1]NONANE DERIVATIVES

Synthetic methods for 9-azabicyclo[3.3.1]nonane derivatives include classical Robinson condensation, Cooks synthesis for indole-fused 9-azabicyclo[3.3.1]nonanes and various transannular cyclization reactions. Radical cyclization was also reported for pavine derivatives.[77]

Condensation reactions. Historical Robinson-Schöpf reaction also called Robinson condensation is most widely used to obtain various 8-azabicyclo-[3.2.1]octane (tropane) derivatives. It is easily applicable for the construction of 9-azabicyclo[3.3.1]nonane (granatane) scaffold. [73, 78] Glutaric aldehyde **5** (in case of tropane, succinic aldehyde is used), acetonedicarboxylic acid **6** and methyl amine (aqueous ammonia in case of tropane) undergo multiple chemical reactions including double Mannich addition and subsequent decarboxylation (Fig. 42).

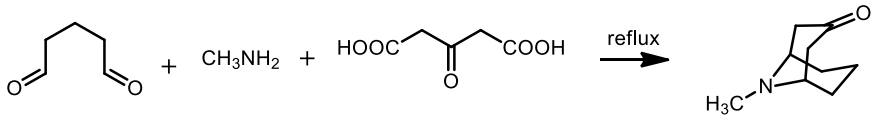

5 **6** **7**

Figure 42. Classical synthesis of 9-methyl-9-azabicyclo-[3.3.1]nonan-3-one **7** using Robinson condensation.

This method was used to prepare 9-azabicyclo[3.3.1]nonane analogs of cocaine as part of the research[79] aiming to evaluate different bicyclic analogs as cocaine-binding site ligands at the dopamine transporter.[80]The findings indicate that small structural difference (additional methylene group) between cocaine and 9-methyl-9-azabicyclo[3.3.1]nonane derivative studied caused 100-fold decrease in binding to the

dopamine transporter. These observations gave insight into fundamental molecular features of cocaine molecule and its binding fashion to the receptors.

Total syntheses of a large number of indole alkaloids of ajmaline, macroline and sarpagine families which embody the 9-azabicyclo[3.3.1]nonane scaffold fused with indole has been developed by Cook group.[81] The excellent review covers extensive work and achievements in total synthesis of the aforementioned alkaloids from the synthetic point of view.[70] In most if not all cases the indole alkaloid synthesis utilizes synthetic intermediate tetracyclic ketone **12** (Fig. 43). The key compound **12** was synthesized repeatedly in Cook's laboratories in 100 g scale. The seven step procedure gives **12** in 47 % overall yield starting from unnatural *D*-tryptophan. D-tryptophan **8** is easily transformed into N-methyltryptophanmethyl ester which is then converted into secondary amine **9** via reductive amination reaction with benzaldehyde. This transformation required careful control since the intermediate imine undergoes imine isomerization which in turn gives decreased ee% of **9**. The compound **9** then undergoes key synthetic transformation - the Pictet–Spengler condensation with 2-ketoglutaric acid **13** and forms six membered ring in compound **10** as the only diastereomer due to inherent selectivity of the Pictet-Spengler condensation. The subsequent intramolecular Dieckmann condensation leads to tetracyclic product **11** which after decarboxylation gives the so called tetracyclic ketone **12**.

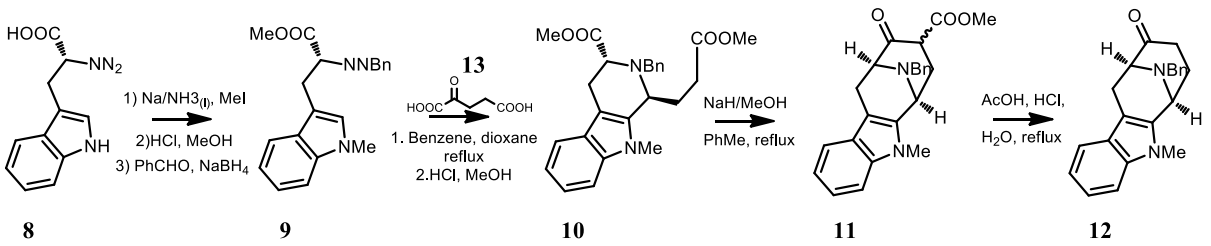

Figure 43. Cook synthesis of the key intermediate in the synthesis of indole alkaloids.

Transannular cyclization reactions. Another way to construct 9-azabicyclo[3.3.1] derivatives is transannular electrophilic cyclization of cyclooctane derivatives with primary amines. Several different procedures can be found in literature yet all of them share similar mechanism – formation of the mixture of [3.3.1] and [4.2.1] regioisomers and subsequent isomerization of the [4.2.1] isomer to the more thermodynamically stable [3.3.1] isomer.

Initially synthesis of 9-methyl-9-azabicyclo[3.3.1]nonan-2,6-diol **15** from 1,5-cyclooctadiepoxide was developed by Portman and Ganter during their research towards synthesis of 2-oxa-7-azatwistanes.[82] Diepoxide **14** and aqueous methyl amine were heated in MeOH to form two regioisomers **15** and **16** (Fig. 44). Mixture of the diols were acetylated to form corresponding diacetyl esters followed by thermal isomerization of the [4.2.1] diacetate **18** into [3.3.1] isomer **17**. 9-azabicyclo[4.2.1]nonane scaffold is found within the structure of cyanobacteria toxin Anatoxin-a.[83] The isomerization occurs in S_N2 fashion via quaternary ammonium ion intermediate forming after labile acetyl groups departs upon nitrogen attack.

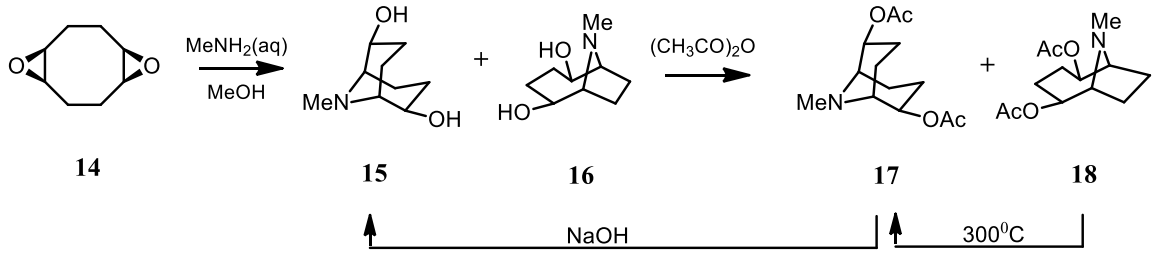

Figure 44. Synthesis of 9-methyl-9-azabicyclo[3.3.1]nonan-2,6-diol.

Later, the procedure of the double epoxide opening was greatly simplified[84] by exchanging methylamine for benzylamine and refluxing the mixture in water. Then the two isomers were converted into corresponding trifluoroacetyl esters followed by spontaneous isomerization to the more stable [3.3.1] regioisomer. In this way easily accessible 9-benzyl-9-azabicylo[3.3.1]nonane-2,6-diol was utilized in the synthesis of racemic tetracyclic ketone **12**.[85] This procedure was used to prepare gram quantities of the latter diol as starting material in this work.

Other transannular cyclization methods for *C_2* symmetric disubstituted 9-azabicyclo[3.3.1]nonane derivatives involve transannular electrophilic N-heterocyclization of 1,5-cyclooctadiene (1,5-COD) with NBS or NIS and then trapping the observed cation with nucleophile i.e. NH_2CN[86]; treating N-protected aminocyclooct-4-enes with iodine or bromine enables to tune reactivity towards the formation of a single regioisomer [3.3.1] or [4.2.1][87]; aminomercuration of 1,5-COD using different mercury (II) salts it is possible to get solely the kinetic [4.2.1] ($Hg(OAc)_2$/NaOAc) or the thermodynamic [3.3.1] isomer ($HgCl_2$) as well[88]; transannular double nucleophilic addition to a cyclic diketone leading to tetramethylated argemonine- or pavine-like

compounds.[89] 1,5-disubstituted 9-azabicyclo[3.3.1]nonanes can be synthesized from 2,6-diacetoxypiperidine via electrophilic transannular cyclization trapping the corresponding dienolate with 1,3-dibromoethane.[90]

5.1.2 PREPARATION OF ENANTIOMERICALLY PURE OF 9-AZABICYCLO[3.3.1]NONANE DERIVATIVES

Interest for obtaining 9-azabicyclo[3.3.1]nonane derivatives as single enantiomers mainly stems from the total synthesis of natural products such as ajmaline, macromaline, (-)-euphococcinine, (-)-adaline[91], (-)-argemonine[92] and others. In this chapter methods that enable access to enantiopure (*1R,5R*)- or (*1S, 5S*)-9-azabicyclo[3.3.1]nonanes will be discussed.

Asymmetric synthesis. One of the first attempts towards enantiopure 9-azabicyclo[3.31]nonane derivatives was pursuit by employing chiral amine in double Mannich reaction. Cyclization of the cyclooctadiene precursor with (*R*)-(α)-methylbenzylamine gave diastereomeric mixture (Fig. 45). Although the diastereoselectivity imposed by the chiral amine was low it allowed separating the two diasteromers by crystalization or chromatography. Hydrogenolysis gave alkaloid (-)-adenine in its enantiopure form.[93]

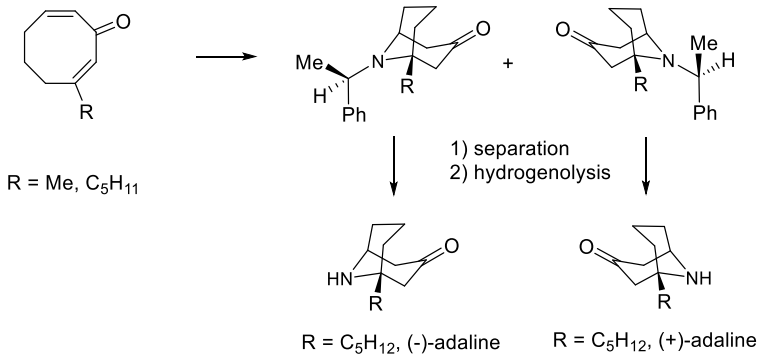

Figure 45. Transannular cyclization using chiral amine and subsequent diastereomer separation leading to enantiopure adaline alkaloid.

The same family alkaloids were synthesized in their enantiomeric from purposely designed chiral building block bearing p-methylphenylsulfamide substituent as a chiral auxiliary.[91]

Desymmetrization methods. 9-Azabicyclo[3.3.1]nonane is a C_2 symmetric molecule with distinctive *exo* and *endo* sites at 2/6 and 3/7 and 4/8 positions. The example of *endo,exo* desymmetrization is well illustrated in the synthesis of potential radiotracer **24** for positron emission imaging which expresses the necessary affinity to dopamine D_2, contains detectable ^{19}F atom and is antipsychotic.[76] For such application the target compound had to be purely in *endo* form which was achieved by protecting amine **21** with Boc protecting group and separating the products **22a** and **22b** chromatographically (Fig. 46).

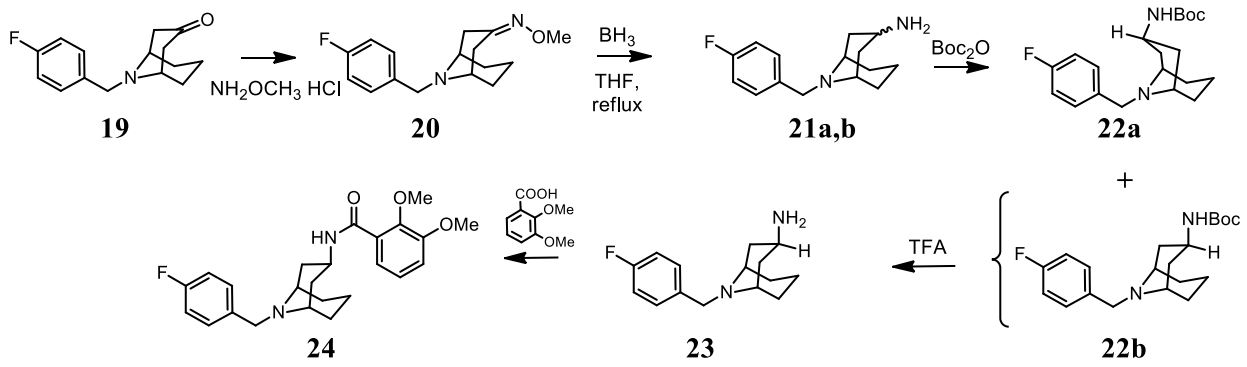

Figure 46. *Exo, endo* sites desymmetrization by introducing Boc protecting group.

Tandem Beckman an Huisgen-White rearrangement,[94a, 94b] Norrish Type I Photo-cleavage,[95] asymmetric aldol reaction,[96] and enantioselective deprotonation of alpha hydrogen[94b] were utilized for desymmetrisation of *meso*-ketones, for example 9-azabicyclo[3.3.1]nonan-3-one. Enantiopure derivatives are often utilized as substrates in double bond cleavage reactions for synthesis of chiral *cis*-2,6-disubstituted piperidine derivatives.

5.1.3 ENZYMATIC ENANTIOMER RESOLUTION METHODS

Main enzymatic reactions types used for chiral building block synthesis include enantioselective reduction, oxidation, hydrolysis, esterification and transesterification reactions.[97] Enzymes are often regarded to be active only in aqueous media, which is considered not suitable for majority of organic compounds due to their low solubility and promoted side reactions of sensitive reagents. However, enzyme powders prepared from aqueous solutions of pH range in which enzyme is active by freeze-dry method are active in organic solvents with little or no water added to the reaction mixture.[98] Another attractive feature is that stereoselectivity and the reaction rate can be controlled by the

choice of the solvent system and concentration. Among different chemical transformations that many enzyme classes known to date can catalyze, lipases hold a place. Depending on the conditions employed these versatile enzymes can catalyze both ester formation and ester hydrolysis.[99]

One of the first uses of hydrolytic enzymes in the kinetic enzyme catalyzed enantiomer resolution of bicyclo[3.3.1]nonane derivatives was utilized in hydrolysis reaction of the *meso*-diacetate ***rac*-25** (Fig. 47).[100] It was found that lipase from *Candida Rugosa* fungus (CRL) was fairly selective towards the bicyclic diacetate ***rac*-25** and after 24 h hydrolysis reaction in phosphate buffer (pH = 8) gave 95 %ee of the unreacted diacetate (-)-**25** and 81 %ee of the monoester **(+)-26**. The enantiomerically enriched products were separated chromatographically and reduced by $LiAlH_4$ to give the corresponding diols which after crystallization were obtained in enantiopure form as both enantiomers. Similar bicyclic derivative ***rac*-27** bearing dimethyl substituents on the position next to the ester functionality gave equally satisfactory results using pig liver esterase (PLE) instead of CRL.

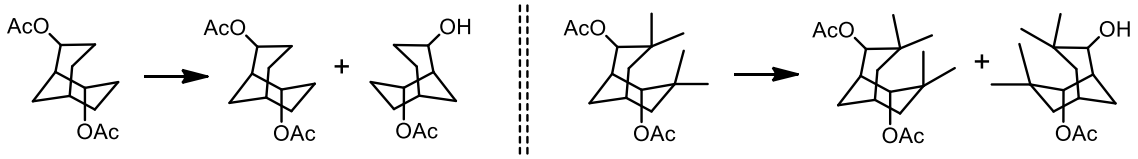

	rac-25	(-)-25	(+)-26	*rac*-27	(+)-27	(-)-28
CRL		95%ee	81%ee		53%ee	55%ee
PLE		31%ee	30%ee		86%ee	96%ee

Figure 47. Kinetic enzymatic resolution of bicyclic diacetates utilizing lipase catalyzed enantioselective hydrolysis reaction.

Few more successful attempts on kinetic enantiomer resolution of bicyclo[3.3.1]nonane-2,6-diol employing transesterification reactions catalyzed by different lipases such as lipase from *Alcaligenes sp.*[101] or lipase from *Pseudomonus sp.*[102] have been reported, yet all of them share similar reaction conditions and strategy. The established theoretical model based on the size of the substituents at the stereocenter reliably predicts which enantiomer of a secondary alcohol will undergo lipase (CRL and PCL (lipase from *Pseudomonas cepasia*) catalyzed esterification reaction faster.[103] The general rule, which is adapted from Prelog's model for ketones, implies that the faster reacting enantiomer

will have the larger substituent on the right hand side if the hydroxyl group is positioned in the paper plane:

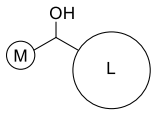

As for CRL only cyclic substrates can be predicted well, while acyclic secondary alcohols in most of the cases give low enantioselectivity. Although the rule has its limitations, as it does not predict why only particular lipase among other express increased enantioselectivity to some substrates, or does not explain the effect of other stereocenters present in a substrate, it could find use in confirming the absolute configuration in some cases.

Desymmetrization of *meso* compounds using biocatalysis is a very efficient way to obtain enantiopure compounds as the theoretical yields are not limited to 50 % as in the case of kinetic resolution. The *meso* bicyclic diol ***meso*-29** was employed in the lipase catalyzed transesterification reaction[104] (Fig. 48) which allowed to achieve 85 % yield and 90 %ee in the most successful case when the lipase from *Humicola lanuginosa* (HLL) and 2 eq. of vinyl acetate in diisopropyl ether was used. Oxidation of the monoacetate **(+)-30** to the ketone **(+)-31** and recrystallization from diisopropyl ether gave enantiopure **(+)-31** in 65 % overall yield.

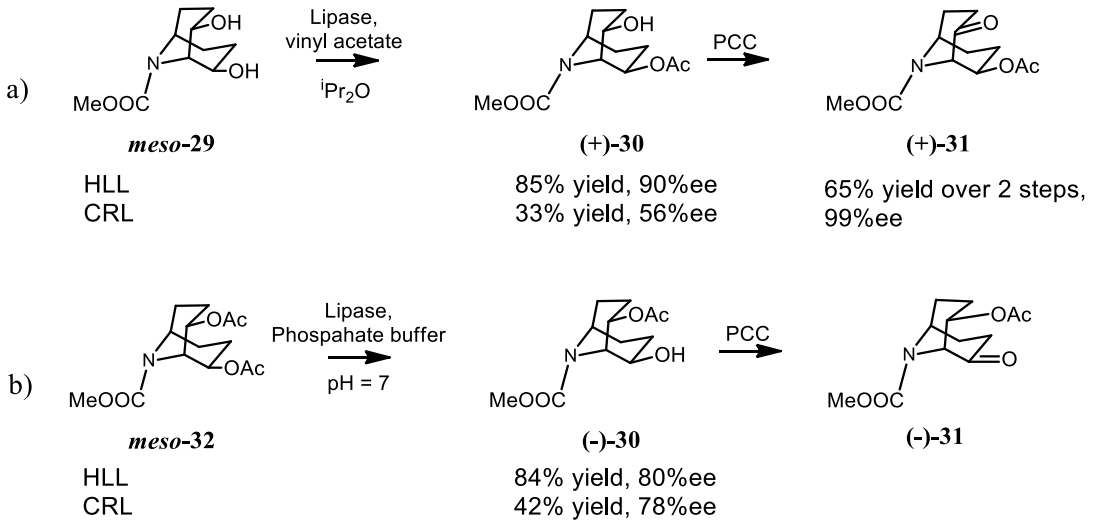

Figure 48. Enantiomer resolution of both enantiomers of 2,8-oxygenated-9-azabicyclo[3.3.1]nonane utilizing lipase catalyzed transesterification (a) and hydrolysis (b).

The second enantiomer is obtained by hydrolyzing the ***meso*-32** using lipase in phosphate buffer. The major drawback of this method is limited synthetic accessibility to the diol ***meso*-29** and its diacetate.[105]

Structurally very similar 9-oxabicyclo[3.3.1]nonane-2,6-diol was subjected to kinetic lipase catalyzed resolution of its enantiomers.[106] The transformation proved to be very useful in this case as it enabled easy separation of 9-oxabicyclo[3.3.1]nonane-2,6-diol **35** from otherwise inseparable 9-oxabicyclo[4.2.1]nonane isomer ***meso*-34** (Fig. 49). More active enantiomer was R-enantiomer as predicted by Kazlauskas rule. CRL was most successful among other lipases used.

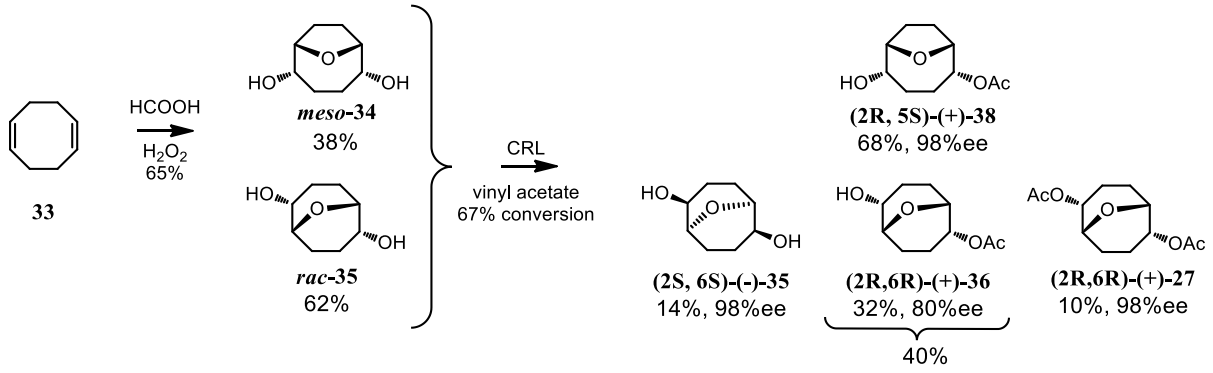

Figure 49. CRL mediated acetylation of the mixture of regioisomers of 9-oxabicyclononanes leading to easy separation of *(2S, 6S)*- and *(2R,6R)*-9-oxabicyclo[3.3.1]nonane-2,6-diols in enantiopure form.

As several different methods for enantiomer resolution of bicyclo[3.3.1]nonane-2,6-dione derivatives (yeast catalyzed reduction[66] of diketone and lipase catalyzed transformations[100, 107]) have been developed, its aza-congener stereochemistry is far less explored. Apart from the diol derived from *meso*-9-azabicyclo[3.3.1]nonane, enantiomer resolution of 9-azabicyclo[3.3.1]nonane derivatives remained scarce. The results are discussed in this part of the work.

5.2 INTRODUCTION TO H-BONDED SUPRAMOLECULAR POLYMERS

"Supramolecular polymers" is a broad term that represents great variety of polymeric arrays composed from a single or multiple monomeric units held together by noncovalent interactions and expressing polymeric properties in bulk and solution. The main feature of supramolecular polymers is their dynamic nature e.g. noncovalent bonds form and break on experimental time scale which leads to dynamic equilibrium between free monomers and long chains. This equilibrium is greatly dependent on monomer concentration and

sample temperature – adjustment of these parameters offers an easy way to tune degree of polymerization (DP) and so, the polymer bulk properties, such as rheology. Significant progress has been made in this area over the years that led to better understanding on the factors and driving forces that govern formation of long chains. These achievements are well illustrated by development of smart polymeric materials with unprecedented properties e.g. thermoresponsiveness and self-healing.[108a, 108b] Hydrogen bonds have been extensively employed in the construction of supramolecular polymers. Several excellent reviews cover recent achievements in the field of 3H-bonded polymers. [109] [110]

5.2.1 DESIGN PRINCIPLES AND DRIVING FORCES FOR THE FORMATION OF HIGH DP H-BONDED POLYMERS

Linear H-bonded supramolecular polymers are usually formed when bifunctional monomers bearing homo- or hetero-complementary H-bond arrays at both ends of the monomer are mixed together in a noncompeting solvent. For construction of high DP supramolecular polymers, strong and highly directional reversible interactions are required and the recognition units must only interact with their intended partners. There are two ways to build supramolecular polymers: main chain polymer and side chain polymers, also called grafted polymers. Main chain polymers can be obtained by assembly of small molecules or by assembly of telechelic monomers. Telechelic monomers have polymeric or copolymeric chain between two recognition sites. In contrast, when binding sites are attached at the side chains of the covalent polymer chain, side chain supramolecular polymers are obtained that can further aggregate and build complicated networks.

Strong association between H-bonded functionalities is a prerequisite for the formation of high DP polymers. As shown in the introductory section in chapter 4 (Fig. 4), 3H-bonding are usually not strong enough whereas quadruple arrays have met with success expressing association constants of 10^7 M^{-1} in $CHCl_3$. Many different H-bonded arrays has been developed with varying strength, homo- or heterocomplementarity, different orthogonality and synthetic accessibility.[9] Introduction of quadrupole H-bonded motif, 2-ureido-4[1H]-pyrimidinone (UPy) (Fig. 50) and its incorporation into structures of various homo- and hetero monomers by Meijer and Sijbesma[111] was a breakthrough in the field of H-bonded supramolecular polymers.

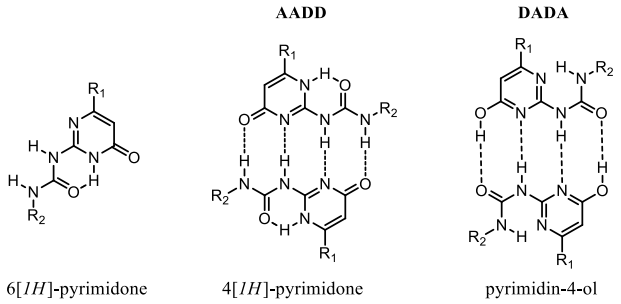

Figure 50. Tautomeric forms of the UPy motif and their dimerization.

UPy can exist in three tautomeric forms preorganized by intramolecular H-bonding: 6[*1H*]-pyrimidinone, 4[*1H*]pyrimidinone and pyrimidin-4-ol, the latter two being self-complementary and capable of strong dimerization (Fig. 50). The lactim form pyrimidin-4-ol has ADAD H-bonding arrays and as expected dimerizes with lower affinity than 4[*1H*]-pyrimidinone which has DDAA motif. Library of substituted 2-ureidopyrimidinone compounds was synthesized and investigated by ^{1}H NMR. The results have shown that the dimer of 4[*1H*]-pyrimidinone tautomer is indeed the existing structure in $CDCl_3$ and toluene-d_8 when the R_1 substituent in pyrimidinone ring is alkyl group. Very high dimerization constants $6 * 10^7$ M^1 in $CHCl_3$, $1 * 10^7$ M^{-1} in wet $CHCl_3$ and $6 * 10^8$ M^{-1} for 4[*1H*]-pyrimidinone in toluene as were determined by excimer fluorescence, using model compound bearing fluorescent perylene ring system at the urea end.[112]

Effect of complementarity and stoichiometry on binding can be well understood using main chain linier supramolecular copolymers as examples. Linear polymers can be composed of AA + BB or AB type ditopic monomers (where A is complementary to B, but not self-complementary) (Fig. 51). The first strategy uses two different complementary monomers and it was found that DP strongly depends on *stoichiometry balance*.

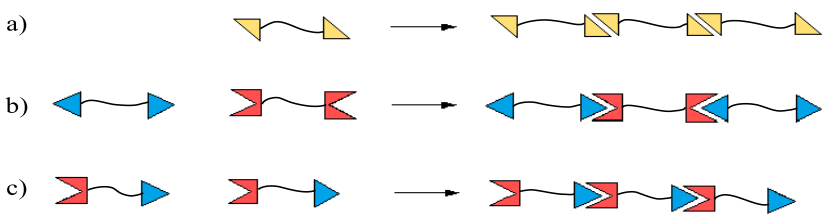

Figure 51. Schematic representation of main chain supramolecular polymers formation. a) Homoditopic self-complementary monomers (AA type); b) Homoditopic heterocomplementary monomers (AA BB type); c) Heterotopic heterocomplementary monomer (AB type).

Very small excess of one of the monomers acts as a chain stopper and effectively prevents formation of long chain hetero polymers. The effect of chain stopper molecule was demonstrated[113] in the case of 3H-bonded polymer formed from bifunctional self-complementary bis-UPy monomer by adding monofunctional UPy chain stopper Fig. 52. An instant drop of viscosity was observed after adding very small amounts of monofunctional derivative (Fig. 52c) which confirms high reversibility of H-bonded polymers and in turn the scope for tunable properties. It also stresses that high purity of bifunctional monomers, free from monofunctional impurities is necessary.

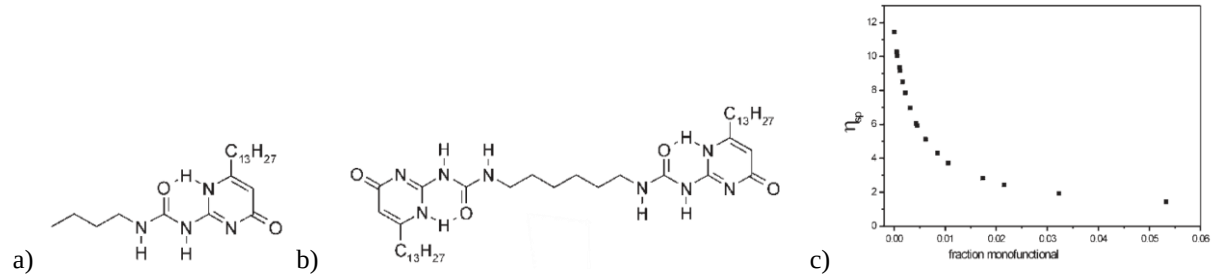

Figure 52. a) Structure of chain stopper; b) Structure of bifunctional monomer; c) Plot of specific viscosity against mol fraction of chain stopper on 40 mM solution of bis-UPy in $CDCl_3$.

Ring chain equilibrium. One of the UPy tautomers, 6[*1H*]-pyrimidinone, strongly binds to 2,7-diamino-1,8-naphtyridine (Napy) functionality (a non-self-comlementary DAAD array) with K_a of $6 * 10^6\ M^{-1}$ through ADDA array in concentrations above 100 mM and heterocomplexation is favored over UPy dimerization. This situation could be beneficial for copolymer synthesis, where slight access of UPy-UPy monomer would solve the stoichiometry problem. However, as it will be discussed shortly, strong self-association over hetero-association also leads to stoichiometry imbalance. UPy-UPy and Napy-Napy homoditopic monomers were utilized for the formation of linear AA-BB type polymer by adding Napy-Napy monomers into preexisting UPy-UPy polymer.[114] Heterocomplexation and subsequent formation of copolymer was dependent on the linker length in the UPy-UPy monomer. Short linkers form cyclic heterodimers over the whole concentration range. When the long chain UPy-UPy monomer is diluted with Napy-Napy comonomer, only slight decrease in viscosity was observed, which was attributed to the formation of heterocyclic dimers to small extent. Most of the added Napy-Napy is incorporated into polymeric chain until strict alternating copolymer is observed. If more than 1 eq. of Napy-Napy is added, the excess of it acts as a chain stopper and viscosity

drops dramatically. In this way 3H-bonded copolymers of various composition could be constructed depending on the fraction of Napy-Napy monomer added.

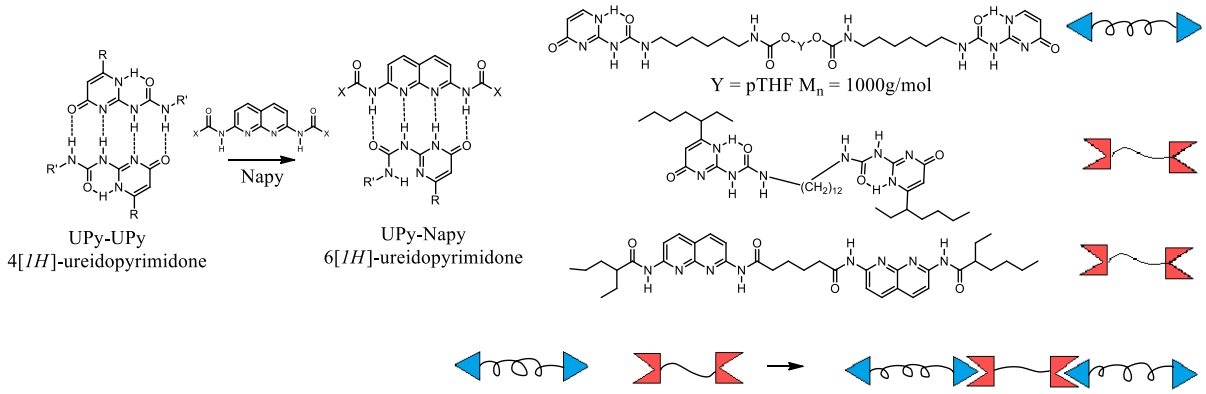

Figure 53. a) UPy-Napy equilibrium; b) Molecular structures monomers used for construction of of AA-BB type H-bonded polymer.

On the other hand, in the case of heteroditopic AB monomers, the stoichiometry imbalance was expected to be eliminated and high DP polymers were anticipated. When UPy-Napy heteroditopic monomer was utilized, long chain polymer was not obtained, due to the small, yet observable UPy-UPy homocomplexation (Fig. 53).[115] The uncomplexed Napy ends are not complementary and stop the chain growth. Strong tendency of UPy motif to self-associate limits heterocomplexation fidelity and results in the lack of control over selective assembly process. In the ideal scenario where homocomplexation is completely suppressed, H-bonded polymers should reach high DP values.

5.2.2 Bulk properties of H-bonded polymers

When low molecular weight monomers spontaneously assemble into long chains via reversible noncovalent interactions, viscous solutions, gels or elastic materials can be obtained within high concentrations ranges (>20 mM). These assemblies have reasonably well defined microscopic and macroscopic organization and display properties of macromolecules such as, entanglement of chains rheology, glass and melting transitions,. General tendency is that by increasing DP, viscosity of solutions increase accordingly. For conventional polymers viscosity measurements can provide good estimate of DP when viscosity of several samples at different concentrations are measured and calibration curve is derived from known samples. In the case of reversible supramolecular polymers viscosity measurements provide qualitative insight into DP and usually are not used as a method for determining number of monomeric units bound within a chain.

Phase separation of block supramolecular polymer. Covalent block copolymers are able to form different morphologies through a process called phase separation when chemically unlike chain blocks of polymeric chain segregate and form distinct nano or micro domains. If not the covalent bonds, two immiscible phases would separate macroscopically. Although block copolymers offers variety of morphologies and thus new properties, their processing is elaborate due to high viscosities and long annealing times. The use of noncovalent interactions in stabilizing nanostructures could help to improve block copolymers processability and also bring new morphologies (Fig. 54).[116] [117]

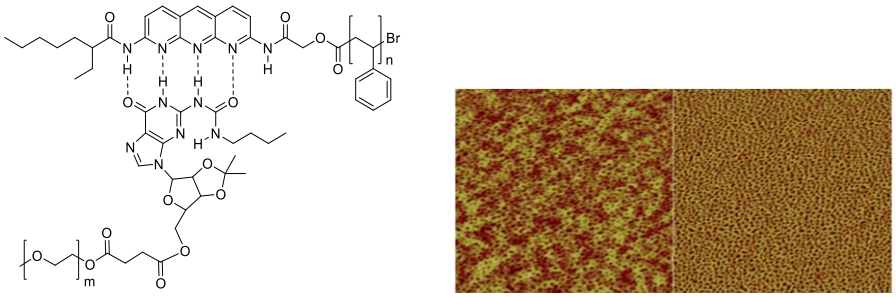

Figure 54. a) Molecular structure of H-bonded block PEG/PS copolymer; b) AFM height and phase images from a thin film of the latter (PS: MW =13 kDa, PEG: MW = 5 kDa).

Introducing H-bonded recognition sites enables the preparation of homogeneous mixtures of otherwise phase separating copolymers. Two normally immiscible polymers poly-(butyl)-methacrylate (PBMA) and polystyrene (PS) were blended together after they were randomly decorated with few percents of 4H-bonded functionalities.[118]

Healable materials. Stimuli responsive reversible polymers which can assemble and disassemble through selective noncovalent interactions are perfect candidates for *healable* and *self-healing* materials. Due to reversibility on intermolecular bonds it is possible to temporarily reduce molecular weight and break down polymers to oligomers or monomers by applying external stimulus such as temperature or UV light. The resulting decrease in MW and, hence viscosity enable the polymer to flow and fill cracks and gaps before the original polymeric material is restored by shifting equilibria back to the formation of macromolecules. UPy recognition units were incorporated in the chains of covalent polymers by Meijer et al. The material is now commercially available under the name Suprapolix and SupraB.[108b] *Thermoreversible* telechelic polymers can be prepared by decorating various polymeric chains (polysiloxanes, poly(ethylene/butylenes), polyethers, polyesters, and poly(meth)acrylates) with UPy functionalities at both terminus. As a

result, materials that combine mechanical properties of conventional polymers and the characteristics of solution, such as low melt viscosity, were obtained. Heating the rubber-like polymer to 140 °C results in decreasing of H-bonded interaction between polymer chains and consequently melting of the material. Cooling down brings back association between H-bonded functionalities and so the properties of the initial rubber. The concept of healable elastomeric materials was extended to create *light-healable supramolecular nanocomposites*. In the composite synthesized by Foster and Weder [119] cellulose nanocrystals modified on their surface with UPy motifs (UPy-CNC) were used as nanofiller and telechelic polymer with UPy groups at both ends as a polymeric matrix. The samples containing 15 – 20 % of CNC-UPy and few percents of UPy-UPy showed sufficient optical absorption and complete restoration of original state of material after healing with UV radiation.

In summary, supramolecular polymers express number of tunable bulk properties such as thermoreversibility, nano- or microphase separation that enables the preparation of polymers of different morphologies, or the opposite e.g. enabling to prepare homogeneous blends of otherwise immiscible phases; thermoresponsive morphology, adjustable chain length, cross-linking degree, viscosity, viscoelasticity etc. and specific functions arising from hierarchical order assemblies.

5.2.3 HIERARCHICAL SUPRAMOLECULAR POLYMERS

Cooperative supramolecular polymers are multimolecular systems that follow hierarchical aggregation order established by monomers capable of several orthogonal noncovalent interactions. Cooperativity can be seen as the outcome of minimized entropic effects of the system. In the absence of strong enough repulsive interactions, monomers or small supramolecular species aggregate further in order to reduce entropic cost. This effect is highly influenced by the solvation efficiency. Many advanced hierarchical systems developed to date combine multiple hydrogen bonds with other noncovalent interactions, usually π - π interactions or hydrophobic forces. While the main chain supramolecular polymers usually follow an isodesmic polymerization mechanism, hierarchical polymers almost exclusively forms by cooperative mechanism.[120] Supramolecular polymers that

are built from ditopic monomers can undergo a ring-chain polymerization mechanism if equilibrium between small rings and monomers/oligomers exist. Which mechanism is in action can be deduced from a shape of isotherm, relating the concentration of monomer with a fraction of aggregated monomer, the latter being derived from a certain physical property sensitive to concentration (Fig. 55). According to isodesmic model, the fraction of the polymer is increasing gradually and will give sigmoidal curve. In contrary, cooperative mechanism firstly predict nucleation step (formation of small supramolecular units) and then elongation step (further assembly of these units) the two appearing as distinctive regimes in the plot.

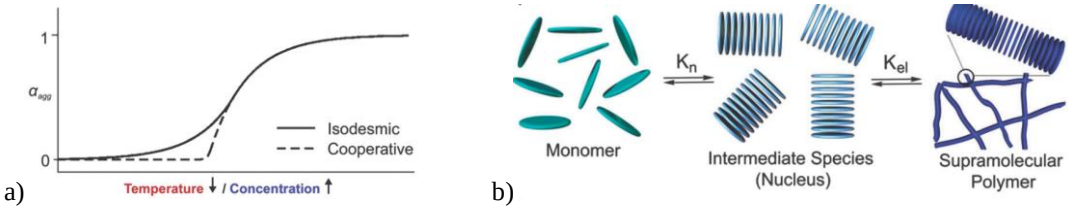

Figure 55. a) Schematic representation of plot of aggregated fraction against decreasing temperature or increasing concentration; b) Schematic representation of nucleation-elongation polymerization mechanism.

The cooperative polymers formed this way, unlike the main chain supramolecular polymers, express high degree of order and form well defined fibers, layers, stacks, ribons or other aggregates. One of most celebrated examples is the assembly of oligo(p-phenylenevinylene)s (OPVs) derivatives, monofunctionalized with ureido triazine functionality (Fig. 56).[121] In dodecane, these building blocks first form dimers via quadruple self-complementary ureido triazine functionality which subsequently aggregate into chiral stacks.

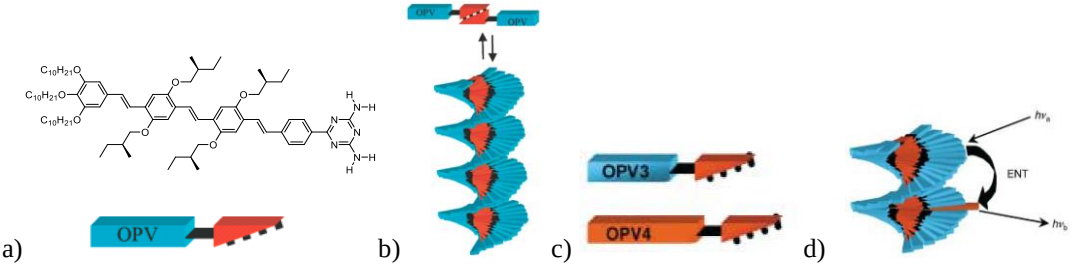

Figure 56. a) Molecular structure of the monomer; b) Schematic representation of its hierarchical assembly into columnar stacks in dodecane; c) Incorporation longer OPV chain monomer (by one p-phenylenevinylene fragment) into the stack.

Well defined structure of columnar stacks, provides ordered arrangement of conjungated OPV groups which sets the scene for possible energy transfer. Indeed, when longer OPV

monomers are incorporated into the helical stacks very efficient energy transfer from shorter OPV molecules to longer OPV molecules occurs (because the absorption maximum of longer OPV unit is red shifted as compared to shorter OPV unit). Adding as little as 2.6 % of monomer having longer OPV functionality causes the effective energy transfer because then longer conjungated molecules are isolated and act as energy trap.[122] By controlling the structure of a single monomer, construction of hierarchical supramolecular polymers of high complexity and degree of order from relatively simple molecules enables to create new smart materials with the functions and features implemented at the molecular level.[123a, 123b]

5.3 ENANTIOMER SEPARATION OF 9-BENZYL-9-AZABICYCLO[3.3.1]NONANE-2,6-DIOL

During ongoing studies towards construction of various cavity aggregates from C_2 symmetric supramolecular synthons which have Ic rings fused with bicyclo[3.3.1]nonane skeleton we were interested to explore association of analogous monomers that would have the solubilizing side chains positioned further away from the H-bonding sites. 9-azabicyclo[3.3.1]nonane framework is a suitable precursor as the nitrogen atom at 9 position in the bicyclic ring system could accommodate the solubilizing chains which would not interfere in binding with other monomers. For the synthesis of 9-azabicyclo[3.3.1]nonane derivatives the protocol by Michel and Rassat[84] was used as a scalable synthetic procedure to obtain C_2 symmetric diol **39** (Fig. 57). Starting material for this reaction, *syn*-diepoxide **13** is accessible in one step synthesis from 1,5-COD following procedure developed by E. Orentas, which required the careful control of addition rate of aqueous Oxone® solution to the buffered solution of 1,5-COD. Transannular double epoxide ring opening of **13** with benzylamine gave two regioisomers: **39** and **40**. Isomerization of the corresponding trifluoroesters of the two isomers and subsequent saponification with NaOH gave the thermodynamic product diol **39** as the sole product in high yield >95 %.

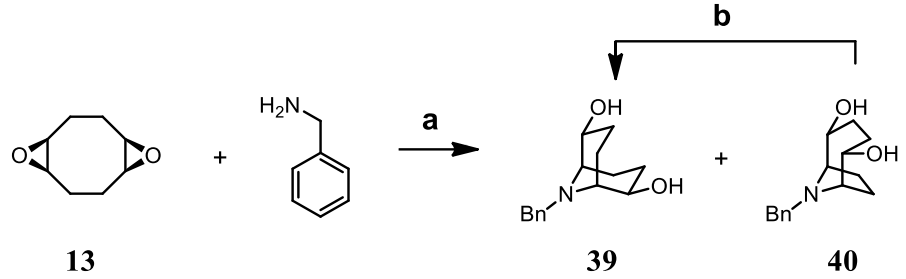

Figure 57. One pot synthesis of the bicyclic diol **39**. Reagents and conditions: a) H_2O, reflux; b) (i) TFAA, DCM, -60 ºC; (ii) TEA, DCM, reflux; (iii) 2.5 M NaOH, THF, rt, yield of **39** > 95 %.

Although several methods for obtaining enantiopure 9-azabicyclo[3.3.1]nonane derivatives employing asymmetric synthesis exist, there is a lack of convenient methodology for enantiopure 2,6-disubstituted derivatives. The compound of interest **39** is a diol and could be conveniently subjected to enzymatic esterification reactions hoping that one of the enantiomers will be more reactive than the other. It was shown by Naemura et al.[100] that lipase from *Candida Rugosa* microorganisms (CRL) is active towards bicyclo[3.3.1]nonane-2,6-diol with sufficient enantioselectivity. Likewise, CRL gave satisfactory results in enantioselective esterification of mixture of 9-oxa derivatives **34** and **35**.[106] The stereochemical outcome and the reaction rate of enzymatic reactions are often hard to predict *a priori*. Slight differences in molecular structure of substrate can result in complete loss of reactivity of particular enzyme due to misfit of the substrate and catalytic site in the active center of the enzyme. Therefore the choice of the right enzyme from many commercially available is not a trivial task. Several papers on enzymatic reactions of the bicyclic compounds of similar structure[106] encouraged us to try lipase CRL for kinetic enantiomer resolution of 9-benzyl-9-azabicyclo[3.3.1]nonan-2,6-diol **39**.

Resolution of diol *rac*-**39** and *rac*-**41** enantiomers at our laboratory was first attempted by converting diols into diastereomeric diesters of chiral acids. The most successful case was the ester obtained from diol *rac*-**39** and (-)-(*S*)-camphanic choride which after crystallization from methanol gave enantiomerically pure (+)-**43** in 31 % yield (Fig. 58). Analogously, another enantiomer was fractionally crystalized from concentrated mother liquor in slightly reduced yield of 20 %. Although the enantiomerically pure **39** and **41** could be obtained via fractional crystallization of the camphanate esters in reasonable yield, the procedure suffers from low reproducibility as it relies on several subsequent

crystallization steps and stoichiometric use of camphanic acid. Therefore, we directed our efforts toward more economical kinetic resolution using lipases.

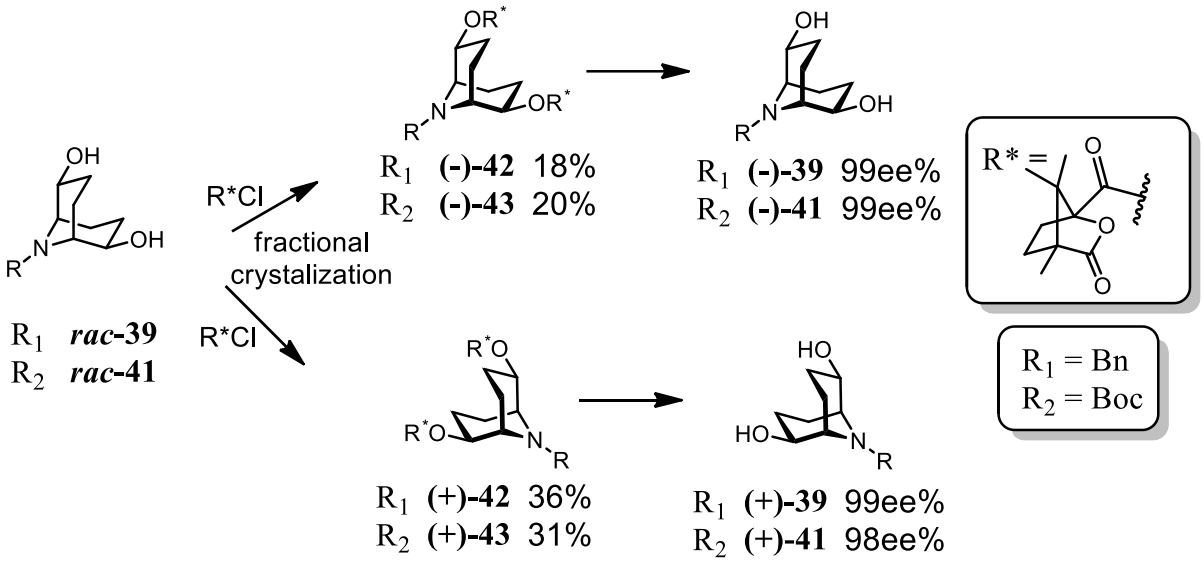

Figure 58. Diastereomeric camphanate ester formation, fractional crystallization and hydrolysis leading to enantiopure diols **39** and **41**.

Enzymatic esterification using CLR in vinyl acetate which served as a solvent and irreversible acetate donor was tested on Boc-diol **41** and Bn-diol **39**. Enzymatic reaction of *rac*-**41** was very slow and resulted in low conversion at room temperature even after one week reaction time. Bn analog *rac*-**39** reached approximately 50 % conversion as judged by TLC in a few hours giving mixture of enriched unreacted diol **39**, monoacetate **44** and diacetate **45** (Fig. 59).

To monitor the enzymatic reaction efficiency and to determine the exact point of 50 % conversion, kinetic study was pursuit by taking aliquots every 30 min and filtering the lipase through the pad of Celite® to stop the reaction. The reaction conversion at every time point was determined by GC-MS, integrating the corresponding peak areas in GC chromatogram. The enantiomeric excesses of the diol **39** and monoacetate **44** were measured first converting them into diacetate (using standard conditions Ac_2O, DMAP, DCM) and then analyzing by chiral HPLC and comparing the chromatograms of the samples with racemic **39**. The results obtained are plotted in Fig. 60.

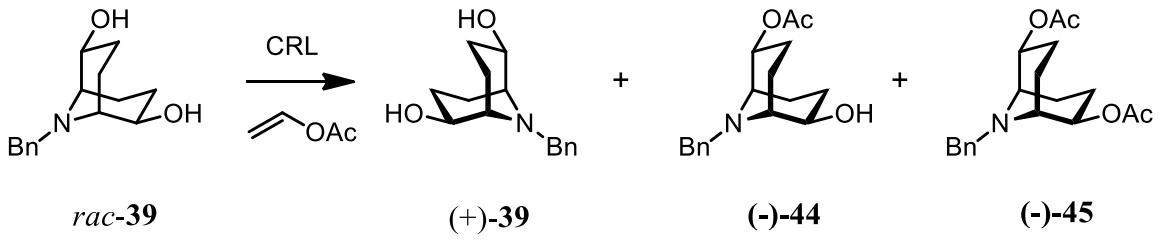

rac-**39** (+)-**39** **(-)-44** **(-)-45**

Figure 59. Enzymatic esterification of *rac*-**39** catalyzed by CRL.

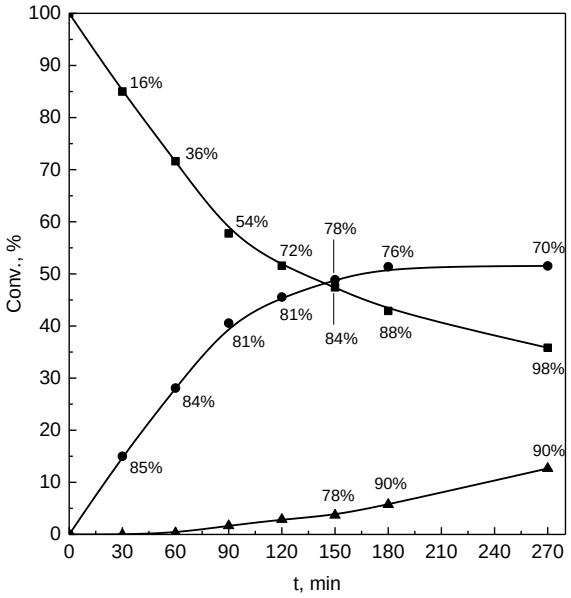

Figure 60. Conversion (diol **39** - ■; monoacetate **44** - •; diacetate **45** -▲) and enantiomeric excesses of the CRL catalyzed acetylation reaction of 2.0 g of *rac*-**39**, 100 ml vinyl acetate and 400 mg of CRL at 20 ^{o}C.

The reaction slows down considerably after 90 min. i.e. when reaching 40 % conversion. Approximately 50 % conversion was reached after 150 min showing moderate enantioselectivity towards the substrate: 78 ee% of the formed monoacetate **44** and 84 ee% of the unreacted diol **39**. As reaction proceeds further, the ee of the monoacetate **44** decreases because it is consumed in the subsequent acetylation. After 270 min, the ee% of the monoacetate **(-)-44** is decreased to 70 ee%, whereas the ee of diacetate **(-)-45** is is increased to 90 ee%. The remaining 35 % of unreacted diol has 98 ee% at this point. Considering the fact, that in most cases 80 ee% is needed for further enantioenrichment using crystallization, we reasoned that the optimal point to stop the reaction is at 50 % conversion, i.e. after 150 min, because equal amounts of comparably enriched mixtures of **39** and **44 + 45** are accessible. The optical purity can then be improved to virtually 100 ee% by simple recrystallization.

On 3 g scale, the reaction was stopped after 150 min by filtering off the enzyme. After separation of the unreacted diol and the combined acetates on column chromatography, the acetate fraction was hydrolyzed to diol. The enriched diols were then recrystallized from $CHCl_3$/petroleum ether (1 : 1, v/v) mixture to give enantiopure materials: **(+)-39** in 27 % yield from unreacted diol, and **(-)-39** in 23 % yield from corresponding monoacetate. 47 % of the remaining material recovered from mother liquors could be combined and subjected to the second enzymatic reaction. Although the enzymatic esterification proceeds only with moderate enantioselectivity, the easy and quick procedure allows obtaining both enantiomers in combined 50 % yield.

5.4 SYNTHESIS OF BIS-IC DERIVATIVES BASED ON 9-AZABICYCLO[3.3.1]NONANE AS NEW SUPRAMOLECULAR SYNTHONS

Synthetic methods for all target bis-Ic compounds were first optimized with racemic substrates and the successful protocols were applied for enantiopure compounds. Only enantiomerically pure samples were used in the aggregation studies unless otherwise noted. The synthetic route for novel 9-azabicyclo[3.3.1]nonane based monomers is outlined in the Fig. 61. Bicyclic diol **39** was required to be oxidized to the corresponding diketone. For this reason the N-benzyl protecting group had to be replaced with Boc protecting group. N-benzyl group is easily removed by standard catalytic hydrogenation procedure H_2/Pd/C in MeOH. Reaction mixture is then filtered through a pad of Celite©, concentrated under reduced pressure and reacted with Boc_2O in DCM. In the next step, β-keto ester **47** was synthesized by forming dienolate and trapping it with ethyl cyanoformate at low temperature. Dimethyl carbonate was also tested as enolate trapping reagent in this reaction, but fail to react. To provide necessary solubility in organic solvents long chains had to be incorporated into the structure of the monomers. TFA deprotection of the Boc group in **47** and subsequent reductive amination under classical conditions[124] with a corresponding aldehyde afforded β-keto esters **48** and **49**. The target compounds **52** and **53** are then obtained via condensation reaction with guanidinium carbonate.

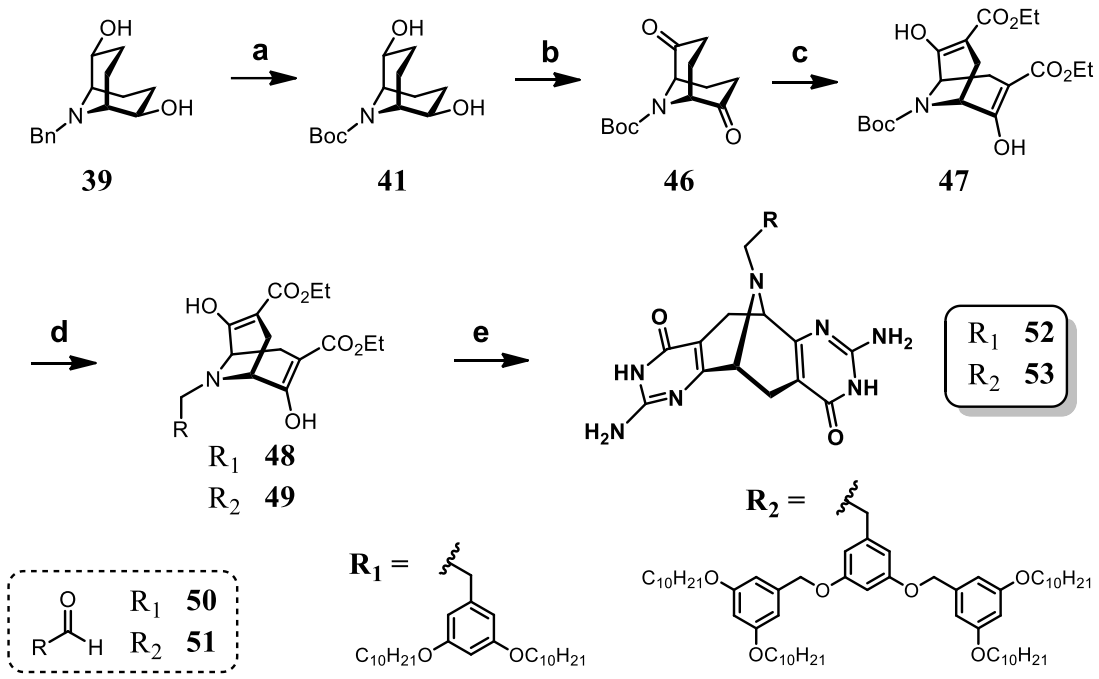

Figure 61. Reagents and conditions: a) (i) H_2/Pd/C, MeOH; (ii) Boc_2O, DCM, TEA, 75 %; b) PCC, DCM, rt, 70 - 90 %; c) (i) LiHMDS, THF, -78 ºC; (ii) HMPA, Et(CO)CN, -78 ºC; (iii) H_2O, 71 %; d) TFA, DCM, Aldehyde **50** or **51**, TEA, DCM, $Na(OAc)_3BH$, rt, 81%; e) guanidinium carbonate, K_2CO_3, EtOH, reflux, 75 %.

Monomer **56** was synthesized as presented in the Fig. 62. Precursor **55** was obtained via copper mediated decyl magnesium bromide addition to dienone **54**. Condensation of **55** with guanidinium chloride gives monomer **56** in high yield.

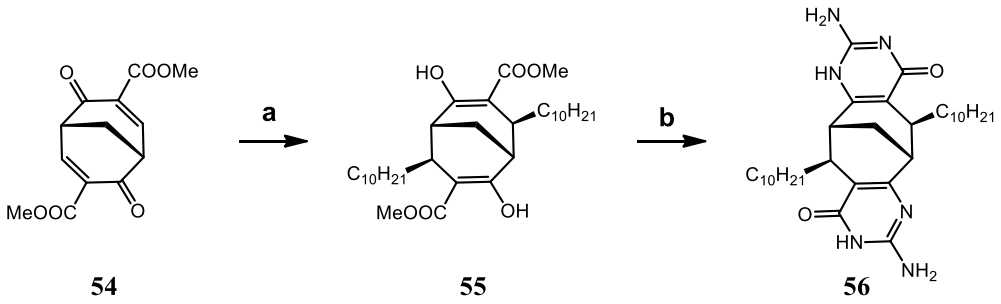

Figure 62. Synthesis of the monomer **56**. Reagents and conditions: a) (i) CuCN, THF, $C_{10}H_{21}MgBr$, -30 ºC; (ii) **54**, -78 ºC; (iii) $NH_4Cl_{(aq.)}$; b) guanidinium chloride, $KOBu^t$, MeOH, 100 ºC, 82.6 %.

5.5 SUPRAMOLECULAR TUBULAR POLYMERS OBTAINED FROM NEW BIS-IC MONOMERS

The new bis-Ic compounds **52** and **53** synthesized from enantiopure 9-benzyl-9-azabicyclo[3.3.1]nonane-2,6-diol **39** together with bis-Ic compounds **2** and **56** based on bicyclo[3.3.1]nonane scaffold were found to display exceptionally strong aggregation in

nonpolar solvents. It was demonstrated, that despite of the similar molecular structure and shape in the series of bis-Ic synthons (Fig. 63), different aggregation modes were observed as a result of steric crowding imposed by different side chains.

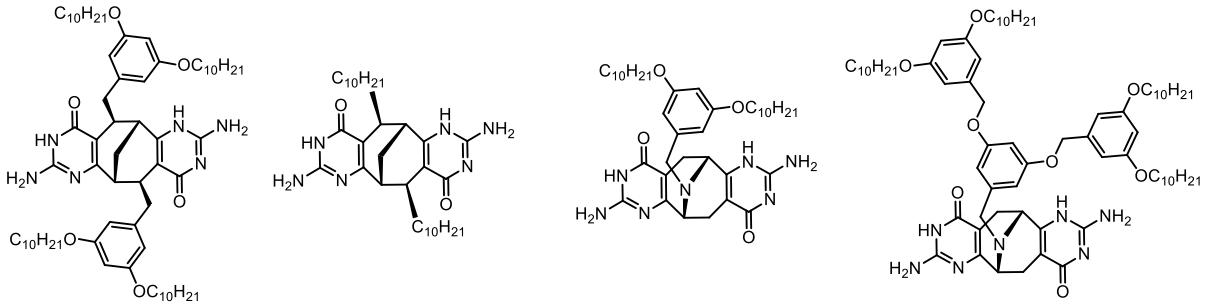

Figure 63. Series of bis-Ic monomers.

Monomer **2** has the bulky 3,5-bis(decyloxy)benzyl side chains incorporated right onto bicyclic skeleton therefore further stacking of tetrameric rings is efficiently precluded and the sole supramolecular entity the tetramer exists in $CDCl_3$ and toluene solutions.[65] In highly nonpolar solvent CS_2, the H-bonding is significantly stronger and the tetramers now can approach each other, albeit in a bit distorted manner and the decamer is formed (see Chapter 4). Monomer **56** which has decyl chains in the same positions, behaves like a polymer, but has a very limited solubility. Small amounts of **56** can be dissolved in $CDCl_3$ by heating which leads to the formation of a gel after cooling to ambient temperature.

When the side chains are located further away from the H-bonding sites, it enables the tetramers to approach each other and bind through orthogonal >C=O...H-NH- H-bonds between the two tetramers. Stacking of tetramers then propagates into a polymeric tube. Solubility of **52** in $CHCl_3$ was found to be very low. The ^1H NMR spectrum in $CDCl_3$ confirmed the presence of supramolecular polymer and as a result of extensive association, extremely broad signals were obtained (Fig. 64).

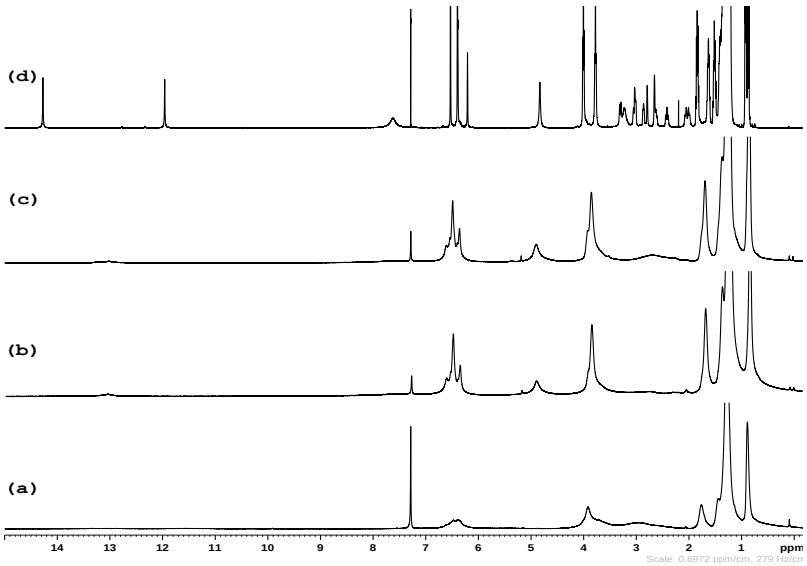

Figure 64. ^{1}H NMR spectra of bis-Ic series of compounds in $CDCl_3$: a) **52**; b) **53**; c) *rac*-**53**; d) **2**. Spectrum of **56** in $CDCl_3$ could not be acquired due to low solubility.

The obtained polymer was remarkably stable because more than 20 % of DMSO was necessary to break it, upon which the compound **52** precipitated. To break the polymers into monomeric units by adding DMSO was therefore not possible and addition of TFA was necessary (Fig. 65d). ^{1}H NMR spectrum of monomeric **52** in $CDCl_3$ with TFA allowed to confirm molecular structure as well as the purity of **52**. The degree of aggregation of H-bonded supramolecular polymer is mainly dependent on monomer concentration. To improve solubility and hence to obtain soluble polymers of high DP, more bulky side chains were introduced into structure of new monomer **53**. As a result, **53** had excellent solubility in nonpolar solvents and formed H-bonded polymers as its analog **52**. Diluting the **53** sample in toluene-d_8 to 0.01 mM concentration, the extremely broad resonances, typical for polymers, are obtained. Further dilution was beyond NMR spectrometer sensitivity limits. Nevertheless, it was clear that compound **53** undergoes very strong association and solely exists in associated state throughout all concentrations.

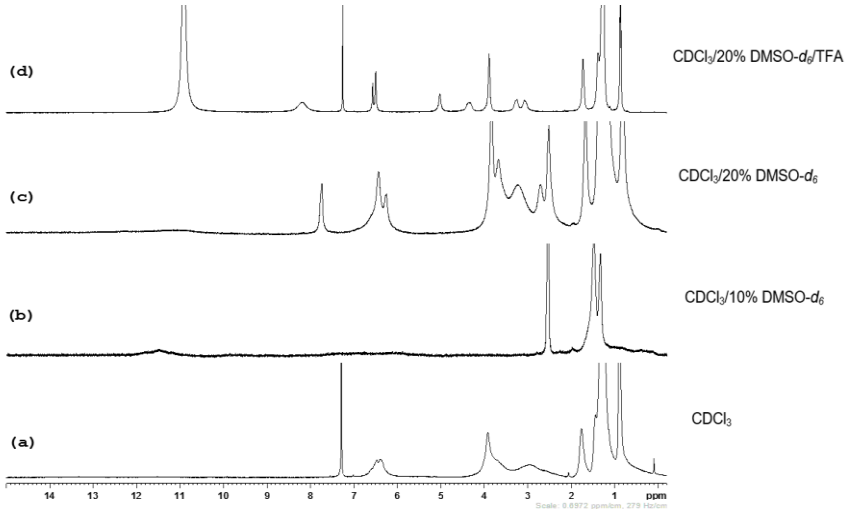

Figure 65. ^{1}H NMR spectra of **52** in $CDCl_3$ with increasing amounts of DMSO-d_6 and TFA.

Noncovalent polymers have a distinctive high viscosity as compared to assembled cyclic structures whose viscosity is only slightly dependent on concentration.[125] Transition from H-bonded extended chain polymers to cyclic species upon dilution have been described using viscosity profile.[126] From viscosity measurements of the solution of **53** at different concentrations in toluene (0.01 to 5 mM), concentration dependent degree of association of **53** was observed. Higher than 5 mM concentrations were too viscous for measurements using falling ball viscometer because it caused the ball to stop in the middle of the run. In dilute conditions (less than 0.1 mM), compound **53** behaved like a polymer – nonlinear specific viscosity against concentration profile was observed (Fig. 66). As concentration increases, extensive polymerization of **53** resulted in further nonlinear increase of the viscosity. Indeed, solutions of **53** became very viscous as concentration reaches 0.5 mM. Increasing temperature from 20 ºC to 40 ºC has little effect on viscosity. Warming up the sample to 60 ºC more H-bonding gets disrupted and viscosity drops significantly, however, still displaying the same non-linear dependence.

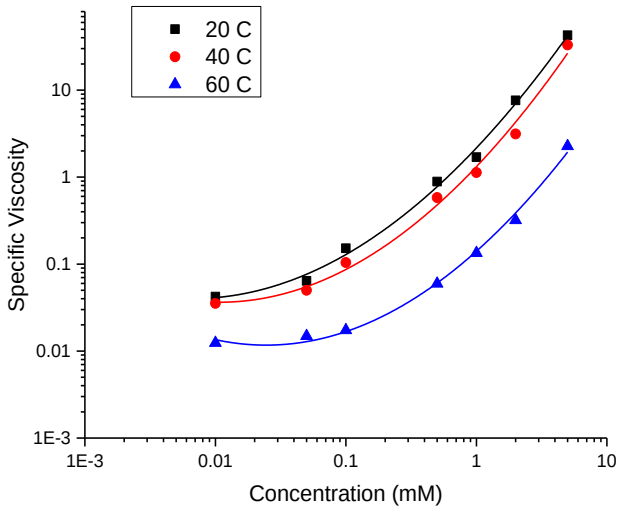

Figure 66. Double logarithmic plot of specific viscosity against concentration at different temperatures of **53** in toluene.

Interestingly, racemic sample ***rac*-53** (Fig. 64c) associates into oligomers as well as indicated by ^{1}H NMR, although its viscosity remains low at 20 mM concentration. This difference might be attributed to formation of shorter linear zig-zag shaped oligomers compared to more stable and dense tubular stacks formed from enantiomerically pure **53.** Another factor possibly contributing to nonlinear viscosity profile of the enantiopure sample compared to the racemic sample, is that the tubes act as a weak gelator. Part of the solvent molecules gets trapped inside and around the tubes resulting in their restricted motion. Long side chains entanglement does not contribute to the increased solution viscosity in this case, but rather results in decreased molecular motion due to long stacks.

To determine the stability of the novel supramolecular polymer, TGA analysis of **56**, **52** and **53** in powder form was performed. From TGA curve (Fig. 67a) it is evident that monomers are stable under nitrogen atmosphere up to 345 ºC. For monomer **53** weight loss of more than 70 % is observed in the temperature range 345 – 450 ºC (not shown) could be associated with degradation and loss of solubilizing chains. Exactly the same behavior is observed for racemic **53** sample (not shown). Polymers differs essentially from low molecular weights compounds in their thermal behavior as they have glass transition point but lacks crystallization and often melting phase transitions. Therefore thermograms are often diagnostic for amorphous polymeric state in solid form. DSC thermogram of **52** and **53** (Fig. 67b) shows pronounced glass transitions T_g (transition from chain frozen state

to chain movement state, i.e. rubbery state) at around 80ºC in the case of **52** and 120 ºC in the case of **53** which is followed by transition to melt state at around 160 ºC and 260 ºC, respectively.

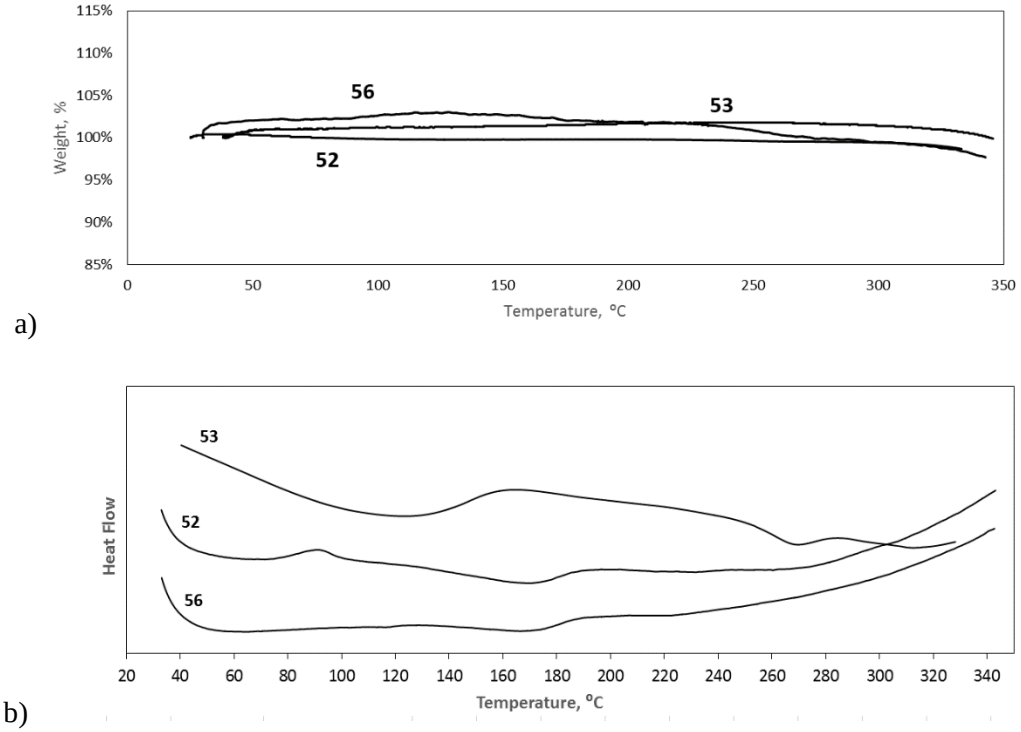

Figure 67. a) TGA curves of solid **56, 52** and **53**; b) DSC scans of solid **56, 52** and **53**.

Melting of polymers does not give sharp peak as do crystalline compounds, but rather result in gradual transition from rubbery state to melt state. Measuring melting point of **53** in air resulted in decomposition starting from 230 ºC, but in nitrogen atmosphere melting temperature is 282 ºC without observable decomposition, as evident from TGA. Thermogram of **56** has weak T_g transition at 115 ºC which is followed by the transition to melt state at 160 ºC.

5.5.1 MOLECULAR MODELING

Further support for tubular structures comes from molecular modeling. Structures of monomers were minimized using B3LYP method with the basis set 6-31G* in *Spartan'14* molecular modeling application. Then these building blocks having two different tautomers on the opposite side of the molecule were used to build tetramer and larger tubes which in turn were minimized using molecular mechanics (MM). Molecular models of aggregates of **52** and **53** (Fig. 68) and **56** (Fig. 69) revealed that the tetramers have the propensity to stack into tubes. Eight inter-tetramer H-bonding holds two adjacent

tetramers. The total energy is lower by adding more tetramers to the stack, as evident from MM minimization of two and three tetramer stacks.

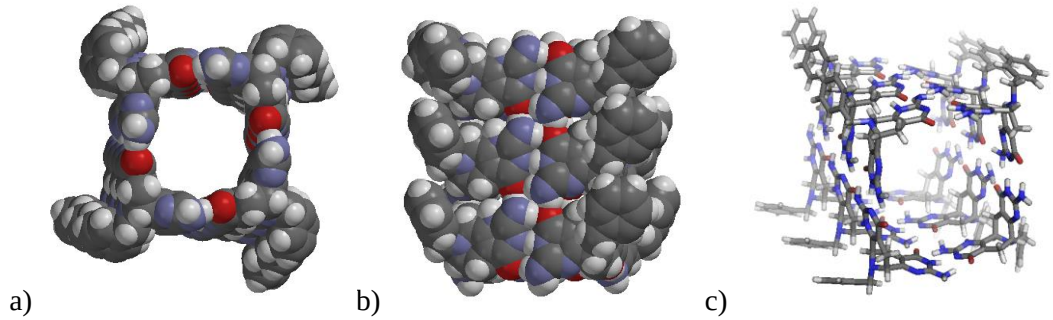

Figure 68. Organic self-assembled tube composed of **52** or **53** monomer. a) Top view; b) Side view; c) Perpectivce view. $OC_{10}H_{21}$ chains in **52** and $(OCH_2C_6H_3(OC_{10}H_{21})_2)_2$ chains in **53** were omited for simplifiction. Distance between opposite walls 12.6 Å, hinge angle 110.8 deg.

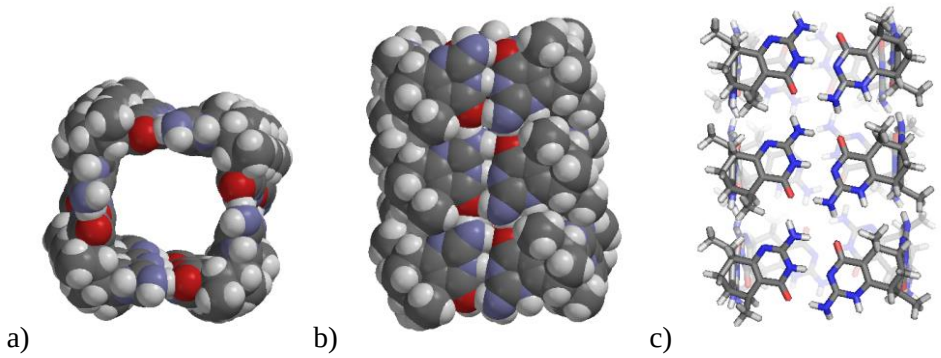

Figure 69. Molecular model of organic nanotube composed of **56** monomers. a) Top view; b) Side view; c) Side view showing H-bonding. $C_{10}H_{21}$ chains were replaced with CH_3 groups. Distance between the opposite walls 11.1 Å, hinge angle 109.6 º.

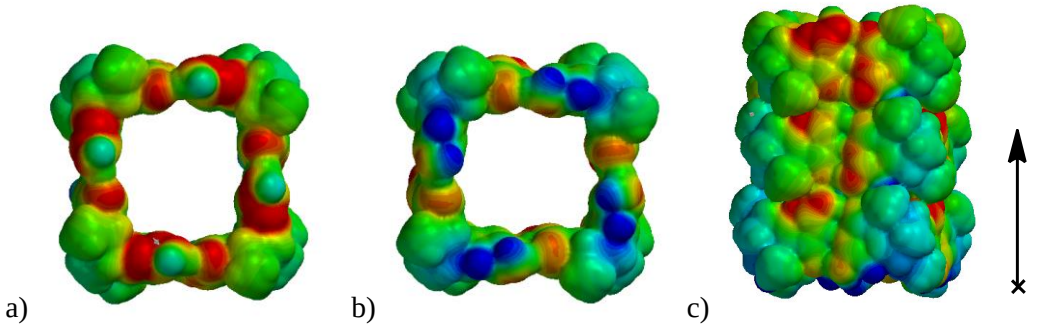

Figure 70. Electrostatic potential map of the tetramer composed of **56** monomers. a) Top view; b) Botom view; c) Stacked tube, side view along with dipole moment vector. Red color represents regions of high electron density (oxygen), blue color - low electron density regions.

Stacking efficiency could be compared in terms of inter-tetramer H-bond N-H···O lengths which in the case of **52** and **53** is 2.74 Å and in the case of **56** is 2.84 Å. The slightly longer hydrogen bond in tube **56** is probably due to side chains creating additional steric

crowding. The tetramers from **52** and **53** are able to approach each other closer. Apart from side chains position, another difference in monomer structures of **56** and **53** is the hinge angle between Ic ring planes. According to molecular models, monomers based on 9-azabicyclo[3.3.1]framework have hinge angle wider by more than 1 degree, that is more than 4 degrees per four monomers, which cause round offs of the tetramer corners and in turn increased distance between the opposite walls to 12.6 Å as compared to 11.1 Å in tube of **56**.

Electrostatic potential maps can be useful to qualitatively map molecule's charge distributions i.e. electron rich and poor regions displayed on van der Waals surface. In such way the interactions between molecules and their attraction centers can be foreseen by matching red regions (electron rich, acceptor) of one interacting partner with blue regions (electron poor, donor) of another partner. In this case, tetramer made of **56**, a building block for organic nanotube, was used to illustrate electron density distribution in this type of associate (Fig. 70). The two sites accessible for stacking of the parent tetramer have the opposite electron density distribution (Fig. 70a and 70b), or in other words express dipole moment, which helps to drive 1D assembly.

5.5.2 SOLID STATE NMR

As this type of compounds forms viscous gels in solution, structural information about their binding in solution was no longer accessible by solution NMR techniques. Solid state NMR could provide the important information on local magnetic environments of the NH protons in the powder state and therefore confirm the proposed molecular arrangement of monomers within tubular structures. $^{1}H - {}^{1}H$ DQ/SQ MAS experiment was run on the **56** sample as it was available at hand in gram quantities. We expected tubular structures to exist in powder state as well as in solution. The $^{1}H - {}^{1}H$ DQ/SQ MAS data, collected at 850 MHz and at 60 kHz spinning rate, supports the 3H-bonding between two monomers. In such an experiment cross peaks are observed when protons are within dipolar coupling distance (approximately 3.5 Å). In Fig. 71 important contacts are highlighted which relate to the proposed H-bonding structure.

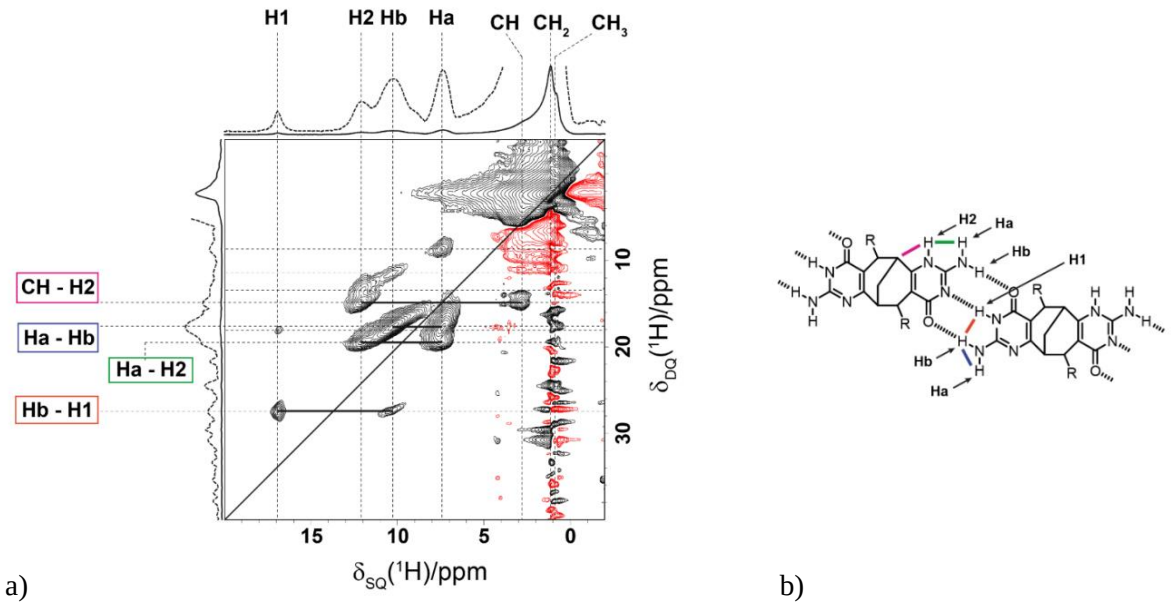

Figure 71. a) $^{1}H - {}^{1}H$ DQ/SQ MAS spectrum with the assignment information; b) Molecular structure of **56** showing the triple hydrogen bond between two monomers.

The NH protons in Ic ring are arbitrary labeled H1 and H2 for convenience. The first evidence for the proposed structure involving two tautomers is the presence of four distinct NH environments. The two NH protons at approximately 7.5 ppm and 10 ppm are assigned to the NH_2 pair of protons since the distance between them is small and consequently the dipolar coupling is large due to the intrinsic relationship between the dipolar coupling strength and the interatomic distance. They also form what could be described as a characteristic pair of cross-peaks for this type of environment. The NH proton at 12 ppm is assigned to the H2 environment and is based upon the observation of contacts between itself and Ha at 7.5 ppm and CH protons at approximately 3 ppm; H1 being too far away to couple to such environments. However, from the schematic H-bonding structure it is unclear why this proton resonates at 12 ppm, a characteristic chemical shift for a moderate strength H-bonded proton. Comparable chemical shift of 12.7 ppm has been observed in SS NMR of unsubstituted isocytosine for the *1H* tautomer[11] where the isocytosine was found to self-dimerize through its two tautomers without indication of stacking (Fig. 72a). Diffraction data confirms isocytosine co-crystal of two H-bonded tautomer,[127]. The *1H* proton is not H-bonded as X-ray data

suggests. Therefore, the large chemical shift observed for this hydrogen must be inherent for this particular Ic ring position and not the result of H-bonding.

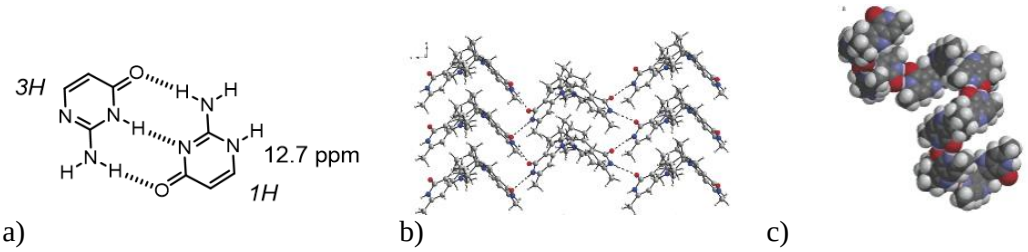

Figure 72. a) Isocysine dimer in crystal; b) Bis-2-pyrimidinone monomer packing in crystal; c) Helical structure from bis-2-pyrimidone monomers determined in solution.[128]

The H1 proton involved in the 3H-bonding interface is easily assigned due to the contact with Hb. Interestingly, this proton seems to interact, albeit weakly, with some unknown proton within the alkyl chain. Although stacking of the tetramers could not be observed in the $^{1}H - {}^{1}H$ DQ/SQ MAS measurement, 3H-bonding between the monomers were unambiguously assigned which, in principle, supports the formation of tubular structures. It should be always acknowledged, that absolute correlation between structures in condensed state and solution should be made with care. A good example of such situation is helical oligomer composed of C_2-symmetric monomer with complementary 2-pyrimidone binding sites fused with bicyclo[3.3.1]nonane framework reported by our research group earlier.[128] X-ray analysis (Fig. 72b) revealed different packing in crystal than the aggregation into helical oligomer (Fig. 72c) as it was determined by spectroscopic methods in solution. As in the favorable case of **52**, **53** and **56**, hydrogen bond directed packing into condensed matter as tubular stacks is very likely to take place. Especially, considering the factors that favor self-assembly – chelate cooperativity of the bidendate monomers, strong 3H-bonding, rigidity of the monomers, orthogonal H-bonding, good shape match and the absence of steric hindrance from the side chains.

5.6 BIS-UPY TYPE QUADRUPOLE H-BONDING SYNTHONS

New cyclic aggregates with well-defined inner space and functional substituents could be easily synthesized from bis-Ic compounds by modifying the NH_2 group of the Ic ring to give novel rigid structure bis-UPy derivatives. The UPy H-bonding array is self-complementary and associates strongly by the virtue of DDAA – AADD 4H-bonding. These monomers are expected to form very stable discreet cyclic structures in nonpolar solvents as further stacking propagation into polymeric tubes should be prevented by the urea substituent. The new bis-UPy type synthons are especially attractive for the possibility of functionalization the urea moiety (Fig. 73). The very strong aggregation which is the result of 4H-bonding between monomers could be used to spatially position substituents at the urea functionality. This strategy could provide means to control the arrangement of functional motifs in respect to each other. Therefore, our objective was to develop well-defined cyclic structures that could be easily modified at the urea end.

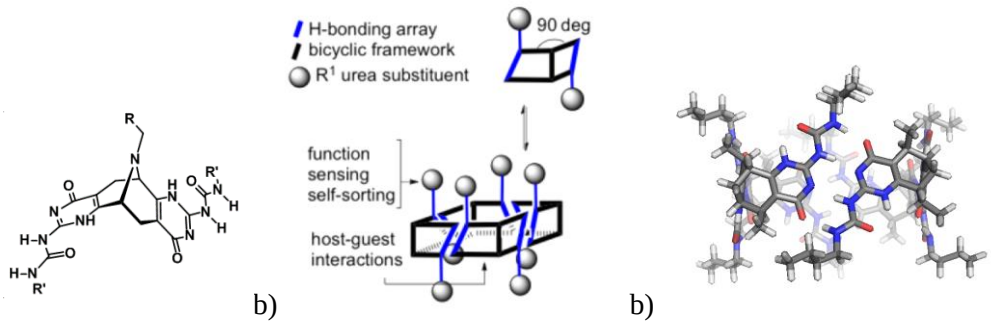

Figure 73. a) General molecular structure of the synthesized bis-UPy monomers; b) Schematic representation of bis-UPy aggregation fashion; c) molecular model of a tetramer from bis-UPy type compounds.

The widely used synthetic method for UPy synthesis is the corresponding isocyanate addition to the Ic.[111] The bis-Ic compounds of this type are sterically hindered and this significantly reduces their reactivity. Due to limited availability of highly functionalized isocyanates, we aimed to introduce urea substituents that would have either protected NH_2 or protected COOH functionalities for later derivatization (substituents **R'3** and **R'4**). Reacting Ic

compounds with 8 eq. of the corresponding isocyanate in dry pyridine gave the desired products in 1 h at 80 °C (route 1 in Fig. 74). Compound **16** was synthesized using carbonylimidazole precursor (route 2 in Fig. 74). Molecular structures of the novel bis-UPy type derivatives is shown in Fig. 74.

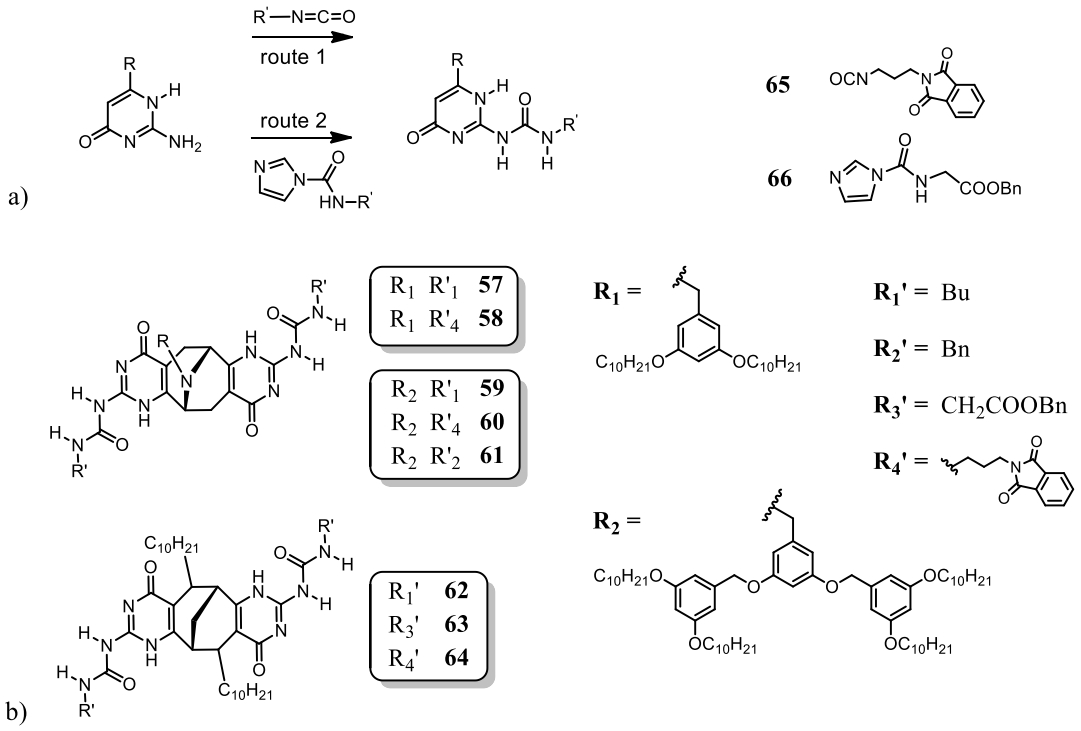

Figure 74. a) Synthetic methods used for bis-UPy monomers synthesis; b) Molecular structure of synthesized bis-UPy monomers based on Ic compounds **56**, **52** and **53**.

From previous studies it was known that Bu and Bn bis-UPy compounds **67** and **68** derived from **2** assemble into cyclic tetrameric structures in chloroform and mixture of tetrameric and pentameric aggregates in toluene after aging.[129]

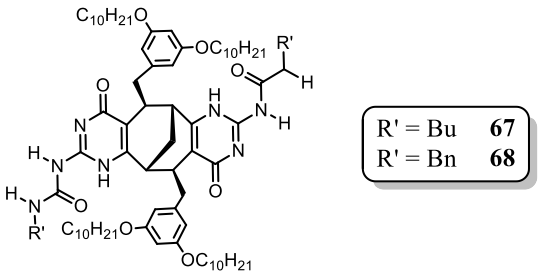

Figure 75. Bis-UPy monomers known to self-assemble into cyclic structures. [129]

Both entities give distinctive three NH resonance pattern. We were interested to test bis-UPy monomers derived from **52**, **53** and **56**. First, to screen bis-UPy type

monomer aggregation, bis-UPy derivatives were synthesized from Ic monomers based on 9-azabicyclo[3.3.1]nonane framework**.** The obtained derivatives **57**, **58**, **59**, **60** and **61** did not expressed the expected aggregation profile as seen from ^{1}H NMR spectrum (Fig. 76).

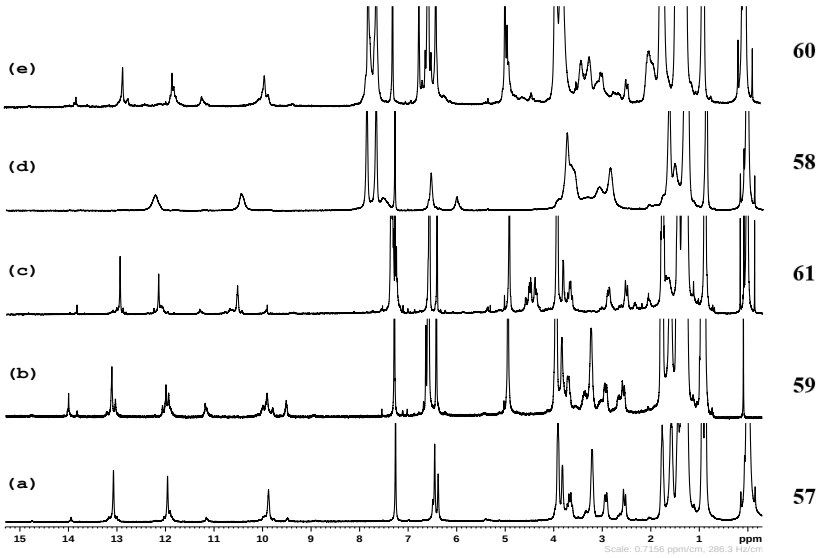

Figure 76. Stacked ^{1}H NMR spectra of butyl and benzyl bis-UPy's derived from **52** and **53** in $CDCl_3$.

As it became clear, subtle balance in molecular structure i.e. side chains and urea substituents was prerequisite for high fidelity aggregation into a single discreet species. Interestingly, bis-UPy monomers **57**, **58**, **59**, **60** and **61** gave tetramers as main species together with small amounts of unknown aggregates in $CDCl_3$ (Fig. 76). In toluene-d_8 the same monomers were aggregating into a polymer (Fig. 80). What type of noncovalent forces induce such excessive aggregation remains unclear. For bis-UPy type compounds, at least according to a model, further binding in orthogonal direction should be prevented by urea substituents.

The low intensity resonances belong to lactim form and its associates. UPy can undergo lactam-lactim tautomerism (Fig. 77a) with the lactim form being self-complementary by the virtue of DADA 4H-bonding. Meijer at al. investigated lactam-lactim tautomerism of various 6-substituted UPy derivatives and found that amount of lactim form depends on substituents at 6-position and to the lesser extend to urea substitution.[111] Lactim form was found to dominate for the UPy's

with electron withdrawing substituents. There is a small conformational change as urea substituent in the lactim form is brought closer to the bicyclic region and hence might interfere with the side chains (Fig. 77b). We noticed that in the series of butyl bis-UPy monomers, higher content of lactim form aggregates is observed for monomers containing less bulky chains i.e. **57**, **59** and **62**, whereas bis-UPy **68** with the large 3,5-bis(decyloxy)benzyl chains attached to the bicyclic region solely gives the aggregate of lactam tautomer. Steric crowding from the 3,5-bis(decyloxy)benzyl chains prevents the butyl substituent to park in this position. In the case of **57**, **59** and **62** side chains do not impose steric hindrance and butyl substituent can fit into space near the bicyclic framework and equilibrium is shifted slightly more towards the lactim form.

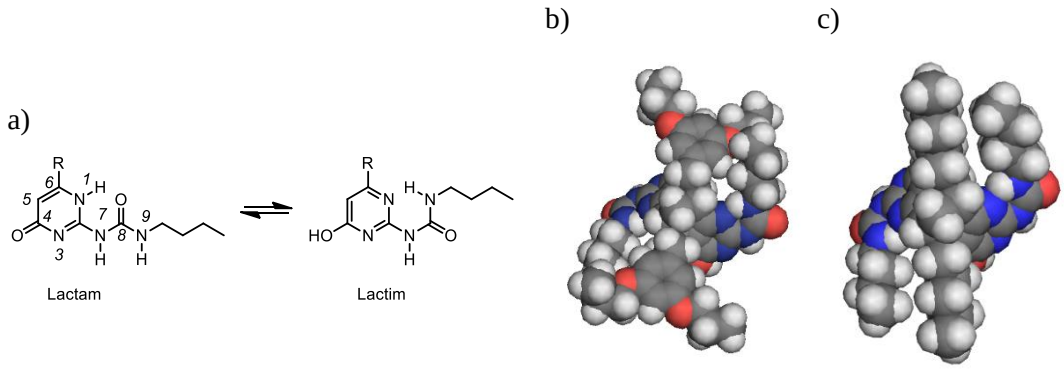

Figure 77. a) Lactam-lactim tautomerism of UPy derivatives; b) Steric crowding imposed by side chains in lactim form of **65**; c) lactim form of **62** and less steric crowding from decyl chains.

^{1}H-^{15}N HSQC experiment confirmed existence of lactim form aggregates. The most downfield resonance at 14.4 ppm did not produce correlation to nitrogen atoms, whereas other low intensity resonances had couplings with nitrogen atoms (Fig. 78a). The same proton resonating at 14.4 ppm showed long range correlations in ^{1}H – ^{13}C HMBC spectrum with carbon atoms 4 and 5, at 169 ppm and 111 ppm, respectively. Such chemical shifts are remarkably different from lactam form, which signals are present simultaneously as the main species in the same ^{1}H – ^{13}C HMBC spectrum in Fig. 78b. The change in chemical shifts observed for lactim tautomer associates in **62** agree with the reported trend for such change.[130]

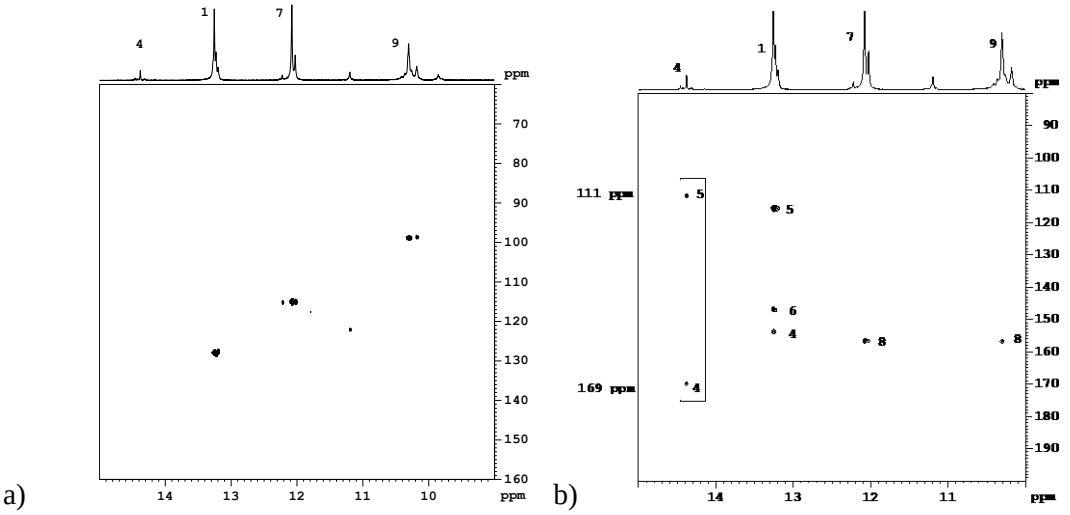

Figure 78. a) ^{1}H-^{15}N HSQC of **62** in toluene-d_8; b) ^{1}H-^{13}C HMBC spectrum of **62** in toluene-d_8.

Another compelling evidence that proton resonating at 14.4 ppm is OH and not NH came from T1 measurement by NMR. Inversion recovery experiment showed that this proton has longer T1 (approximately 1 s) as compared to the rest of NH protons (approximately 0.7 s). In general, NH protons relax faster due to coupling to ^{14}N quadrupole nuclei, whereas OH does not experience this relaxation pathway.

Our efforts on 9-azabicyclo[3.3.1]nonane framework based bis-UPy monomers assembly into well-defined cyclic aggregates met little success, whereupon synthesis of bis-UPy's from **56** were pursued. Deprotection of **63** and **64** could provide precursors for structurally complex next generation synthons. One type aggregate could be obtained for **62**, **63** and **64** in $CDCl_3$ (Fig. 79). In toluene, however, main tetrameric entities were accompanied by lactim form aggregates, the situation earlier seen for monomers **57**, **58**, **59**, **60** and **61** in $CDCl_3$.

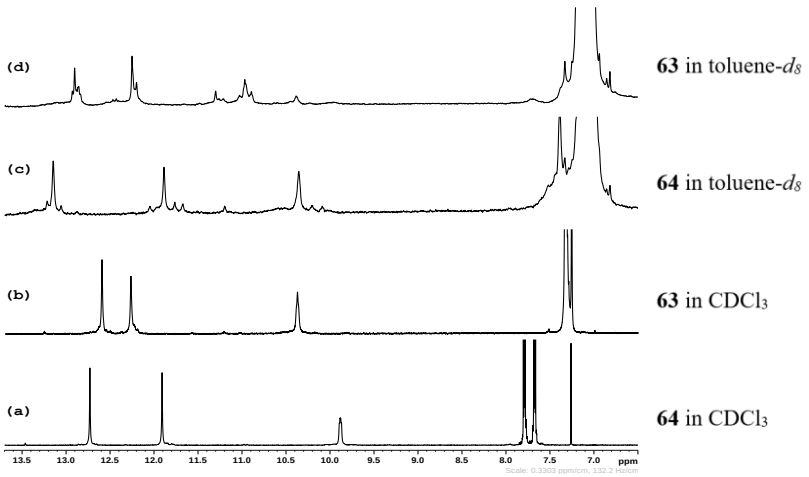

Figure 79. Stacked ^{1}H NMR spectra of bis-UPy's derived from **56** $CDCl_3$ and toluene-d_8. For clarity only NH region is displayed.

As it was mentioned above, bis-Upy's derived from 9-azabicyclo[3.3.1]nonane in toluene aggregate into polymers (Fig. 80) and form gels, even though bis-UPy monomers lack possibility for directional inter-tetramer hydrogen bonds.

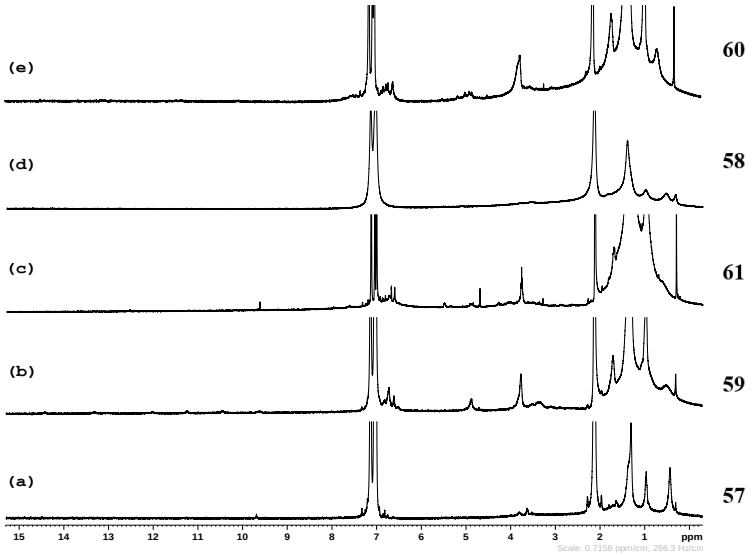

Figure 80. Stacked ^{1}H NMR spectra of bis-UPy monomers **57**, **58**, **59**, **60** and **61** in toluene-d_8.

Molecular modeling suggests, that close packing of tetrameric rings is possible if the tetramers are turned approximately by 45 º in respect with each other (Fig. 81a and 81b). Urea substituents are not interfering sterically, as they are pointing outwards from the tetrameric ring. In the case of azabicyclic bis-UPy monomers

57, **58**, **59**, **60** and **61**, side chains are also conveniently located further away from the tetrameric core and do not impose any steric barriers.

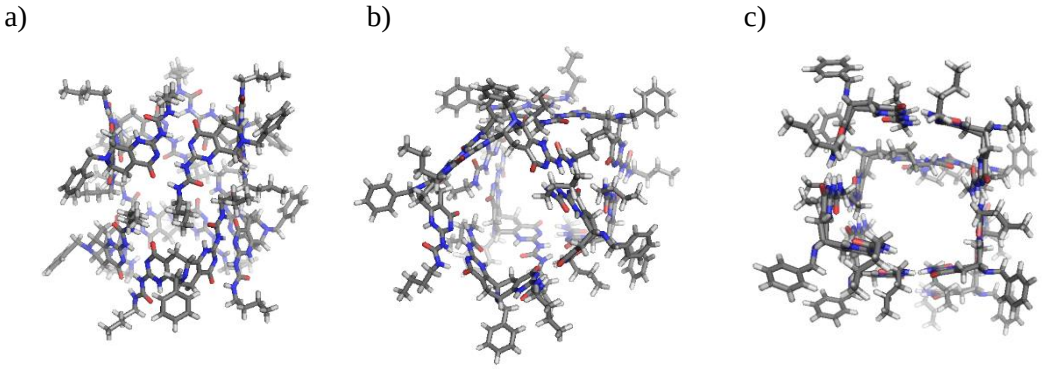

Figure 81. Molecular models minimized using MM for plausible aggregation of bis-UPy monomers based on 9-azabicyclo[3.3.1]nonane framework in toluene. a) Stacking of the two tetramers side view; b) Stacking of the two tetramers, perspective view; c) Helical supramolecular polymer.

Another possibility for this type of bis-UPy monomers to build supramolecular polymers is the formation of helix via 4H-bonding (Fig. 81c). Which exact aggregation mode is operating in toluene is not clear at this point and requires further investigation. Nevertheless, it could be concluded that excessive aggregation of azabicyclic bis-UPy derivatives **57**, **58**, **59**, **60** and **61** in toluene is the outcome of solvophobic effects and the absence of steric crowding near the H-bonding sites. The importance of the position of the side chains and their bulkiness on the aggregation mode can be rationalized by comparing series of bis-UPy monomers. Bis-UPy monomers **67**, **68, 62, 63** and **64** associate into cyclic tetrameric rings in $CDCl_3$ and toluene-d_8 since their stacking is efficiently prevented by 3,5-bis(decyloxy)benzyl or decyl side chains, which are attached near H-bonding sites. In the case of bis-UPy monomers **57**, **58**, **59**, **60** and **61**, derived from **52** and **53**, the side chains are too far away to interfere with the tubular aggregation.

6 OCTAMERIC TUBE FROM C_1 SYMMETRIC MONOMER: GUEST INDUCED REARRANGEMENT AND SELF-SORTING BEHAVIOR

6.1 INTRODUCTION TO MOLECULAR SELF-SORTING

Molecular self-organization, self-sorting or self-recognition are the collection of recognition events when mixture of molecules spontaneously organize themselves into specific assemblies rather than random aggregates.[131] High fidelity orthogonal molecular recognition processes give rise to the exclusive formation of selective assemblies over many possible combinations. Self-sorting of organic or biomolecules in highly complex multicomponent systems that leads to perfect selectivity of biological processes is a fascinating phenomenon. High integrity recognition processes are governed by the same noncovalent intermolecular forces as any complexation, association or assembly event – hydrogen bonds, coordination bonds, π-π stacking, donor-acceptor pairing, electrostatic interactions and hydrophobic or more general, solvophobic effects. New emerging area of supramolecular chemistry - systems chemistry - is dealing with the whole system rather its components individually.[28] Among the factors that control the outcome of interaction of several components most prominent are the intrinsic structural features, which include size, shape, complementarity and steric crowding.[131] The degree of self-sorting thus highly depends on the structural differences between molecules of interest and decrease when these differences become less and less pronounced. Therefore, clever design of every component of the system is prerequisite for self-sorting to occur and for molecular organization to weight out the entropic cost of the assembly. Most of the artificial H-bonded self-sorting systems functions under thermodynamic control. Increase of temperature causes temporary disruption of the assemblies due to higher exchange rate, but when the temperature is brought back to room temperature, the assemblies are restored with little or no crossover species formed.

Classification of self-sorting events. Self-sorting originally had the meaning of describing events associating with molecules recognizing self from nonself in

the presence of other competitive molecules. To describe these situations, the terms *social* and *narcissistic self-sorting* were introduced by Isaacs.[132] Exclusive formation of either homomeric or heteromeric species from a mixture of components (more desirable situation) leads to *absolute* self-sorting, whereas formation of mixture containing both homomeric and heteromeric species (situation more similar to statistical scrambling) is referred as *non-absolute* self-sorting. In between these two extreme situations there is also *partial* self-sorting, or in other words amplified self-sorting, where some aggregates form in higher amounts than the others (Fig. 82).[133]

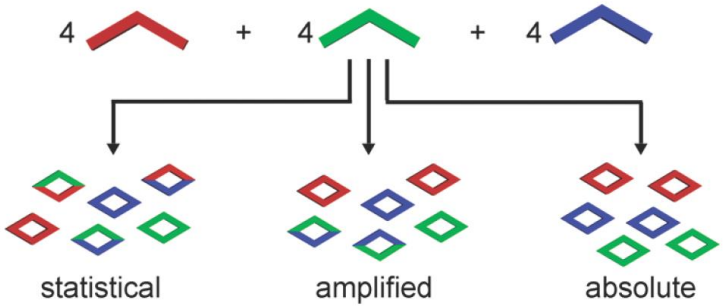

Figure 82. Schematic representation of different degrees of self-sorting: no self-sorting (statistical), partial self-sorting (amplified) and exclusive self-sorting (absolute). Taken from ref.[133]

External factors that influence self-sorting such as solvent, temperature, pH and concentration have huge impact on dynamic self-sorting mixtures, which could be taken as an advantage for various switching mechanisms from one state to another induced by kinetically driven changes.

Isaacs explored the question if self-sorting is expected in mixtures of compounds whose complementary components are appropriately designed. He conducted an experiment by mixing well defined H-bonding systems reported in literature (Fig. 83) in $CDCl_3$ and followed their behavior in the mixture by ^1H NMR.[132] The original assemblies were formed exclusively without scrambling of the components over random mixed entities. High fidelity self-association driven by spatial orientation and H-bonding patterns was governing the system of 9 components even though these components had more than one complementary partner to interact e.g. **69** and **70**, **69** and **75**, **72** and **70**, **72** and **74** or **76**.

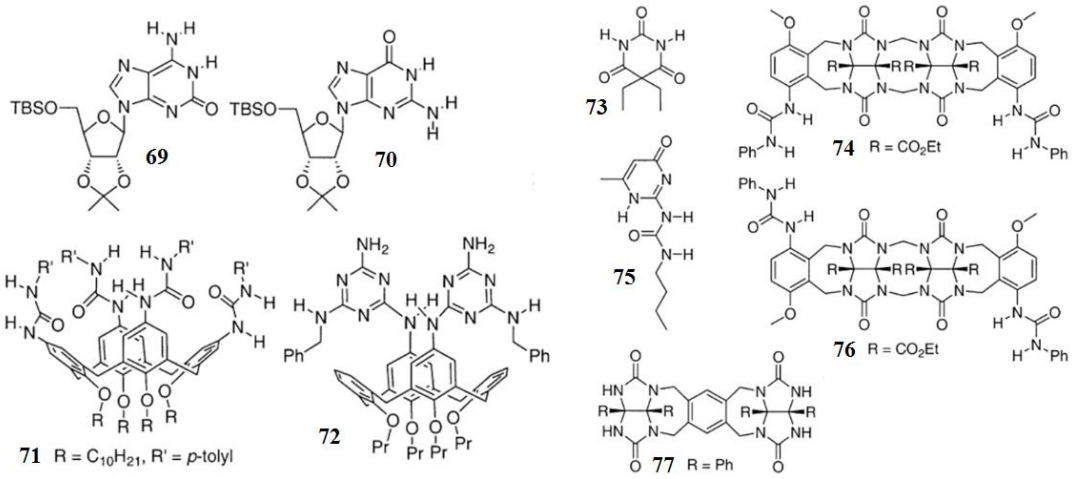

Figure 83. Well known H-bonded assemblies $\mathbf{69}_{10}\cdot Ba^{2+}$ + 2Pic$^-$, $\mathbf{70}_{16}\cdot 2Ba^{2+}$ + 4Pic$^-$, $\mathbf{71}_2$, $\mathbf{72}_3\cdot\mathbf{73}_6$, $\mathbf{75}_2$, $\mathbf{74}_2$, $\mathbf{76}_2$, $\mathbf{77}_2$ used to test self-sorting fidelity in Isaac's experiment.[132]

The effect of temperature, binding strength and mole fraction of the components for self-sorting were also examined. It was found, that K_a differences as small as 10-fold between two possible association pathways, i.e. homomeric or heteromeric, is enough to shift equilibrium one way or another. Narcissistic self-sorting for all investigated pairs was by far predominant in $CDCl_3$ solution due to directional and specific H-bonding between the partners. In aqueous media, however, these interactions are weakened considerably and nondirectional hydrophobic and electrostatic forces become dominant. To answer the question if narcissistic self-sorting would persist in such situation, Isaacs designed a similar experiment by selecting known examples of host-guests pairs in water (Fig. 84).[134] Again, the compounds had more than one complementary partner to associate with. Mixing equimolar amounts of 6 hosts and 6 guests in D_2O yielded clean narcissistic self-sorting under thermodynamic control. ^{1}H NMR spectrum of 6 pairs (12 components) mixture was the same as superimposed spectrum of the individual components.

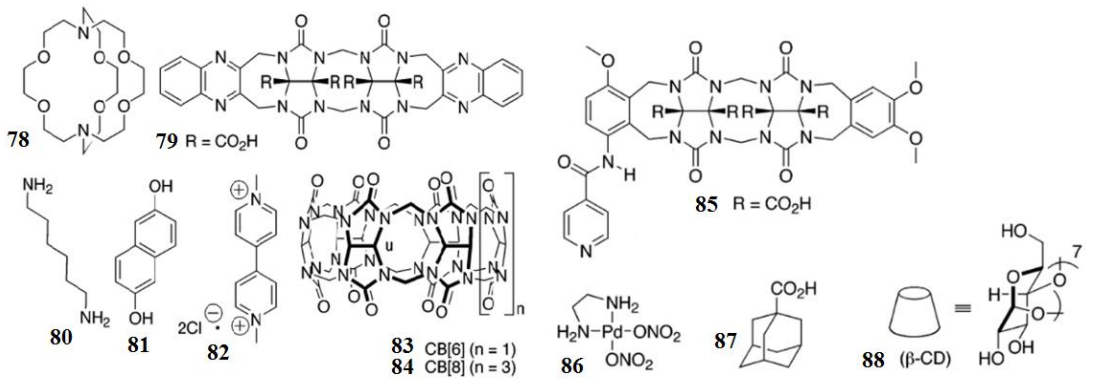

Figure 84. Components of host-guest systems **78**·K^+, **79**$_2$, **83**·**80**, **84**·**81**·**82**, **85**$_2$·**86**$_2$, **87**·**88** investigated in self-sorting experiment in water.[134]

Upon raising the temperature to 338 K some resonances becomes more complex and broad indicating change in certain component's binding, which is not restored after lowering the temperature back to 291 K. According to the authors, this emerging property is the outcome of kinetic social self-sorting, because raising the temperature imposed no changes in separate host-guest pairs. The two experiments provided excellent demonstration of the extent of self-recognition to which high integrity of artificial systems in organic media and water is achieved by rational molecular design of the components.

Intrinsic structural properties that influence self-sorting. Geometrical fit determines how strong the noncovalent interactions used for the binding will become. Steric effects in the form of intentionally introduced bulky substituents are the general strategy to promote binding with one partner while inhibit the binding with another, or the opposite, to form a well-defined mixed entities. Steric effects were successfully applied to guide the self-sorting events between structurally similar building blocks. In the case of hexameric rosette[135] (Fig. 85), monomeric units **89** and **90** with the side chains of different bulkiness undergo slow process of social self-sorting as monitored by SEC in toluene. Shortly after mixing the two components broad SEC curve was obtained, which sharpened considerably after extended period of mixing. The discreet species was assumed to be symmetric alternating aggregate.

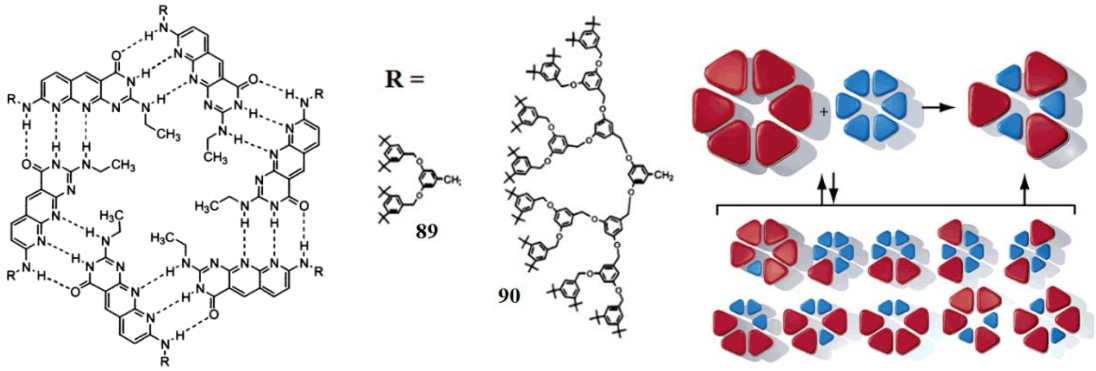

Figure 85. Sterically induced social-self sorting into alternating H-bonded aggregate via possible mixed entities.[135]

Orthogonal hydrogen bond motifs

Orthogonal hydrogen bond sites usually bear the meaning of being noncomplementary and thus not able to associate with each other but rather bind with their complementary partners. An example of orthogonal H-bond motifs could be a wedge type hydrogen bond array and a linear array. Such motifs are useful in hierarchical assembly, but they are limited to participate in only one recognition pathway each. Wilson et al. showed that affinity of certain linear H-bond motifs can be strongly influenced by other H-bond motifs present in the mixture.[136]

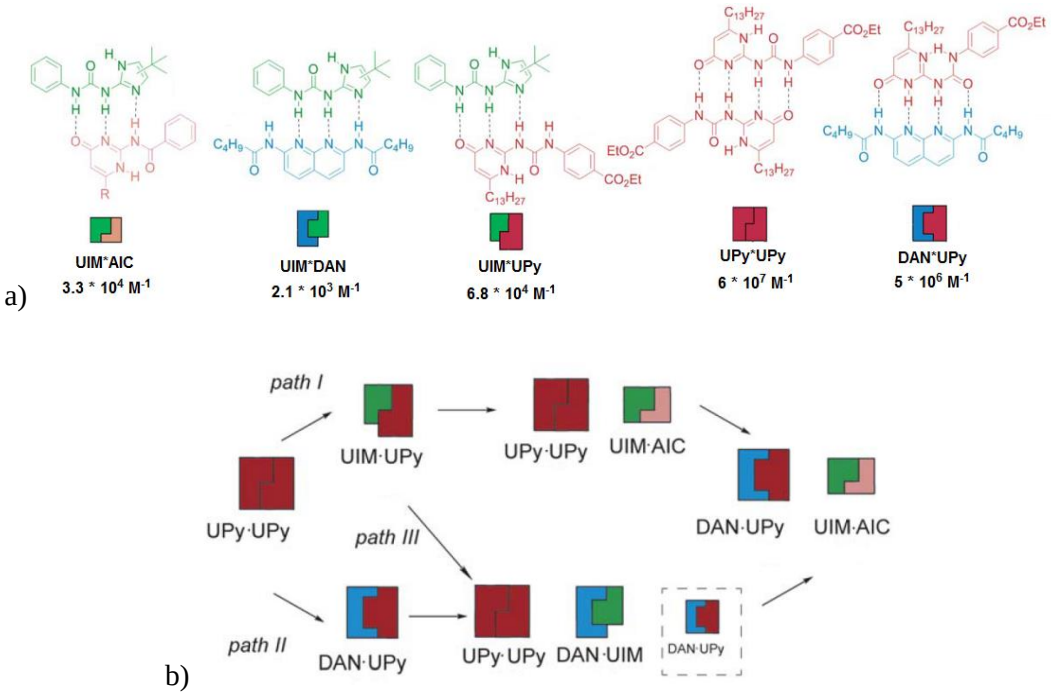

Figure 86. a) Complementary H-bond motifs utilized in sequential self-sorting events; b) Self-sorting pathways with different order of components addition.[136]

Fidelity of these self-sorting events is determined by K_a of the separate association processes and the establishment of the maximum number of H-bonding in a given situation. This behavior allowed to construct cascade self-sorting pathways with several high fidelity successive states (Fig. 86b). For such sequence of self-sorting events to be successful, it is prerequisite to use one motif, that has high affinity to one of the other components (e.g. AIC) and one motif that can bind to various components (e.g. UPy). It was also found, that maximum number of H-bonding established in the final distribution is the driving force for social self-sorting and the individual affinities do no weight out: UPy·UPy has the highest binding constant, but it is easily included into UPy·UIM or UPy·DAN heterodimers so that total number of H-bonding would be maximized. Simultaneous and sequential recognition pathways (Fig. 86b) were demonstrated to work with high integrity without formation of random hetero assemblies. These and plenty of other systems reviewed earlier by Würtner at al.[131] are capable of establishing order to particular extent in a mixture of other competitors. It highlights that with enough knowledge about affinities between the components and appropriate design, self-recognition events with multiple recognition modes can be devised.

6.2 SYNTHESIS OF THE UPY-IC MONOMER AND CHARACTERIZATION OF THE OCTAMERIC TUBE

Monomer **91** is obtained from bis-Ic compound **56** appended with linear decyl chains by using 1 eq. of butyl isocyanate. The desired product **91** is obtained in the statistical mixture with the unreacted isocytosine **56** and bis-UPy aduct **62**. **91** is separated by column chromatography on silica gel as the product of intermediate polarity in approximately 25 % yield (Fig. 87). Together is obtained bis-UPy monomer **62**. Monomers **92** and **68** are obtained in the same manner.

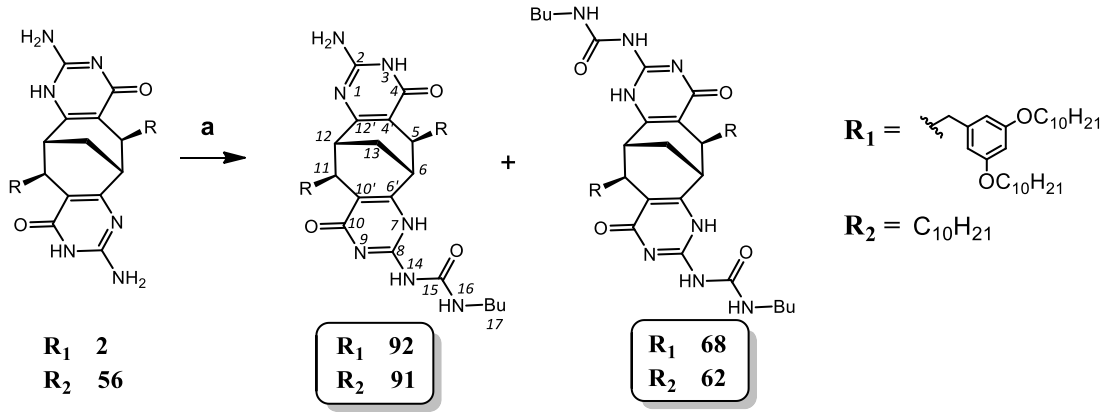

Scheme 87. Synthesis of the Ic-UPy monomers **91** and **92**. Reagents and conditions: (a) 1 eq. BuNCO, py, 80 ºC, chromatographic separation.

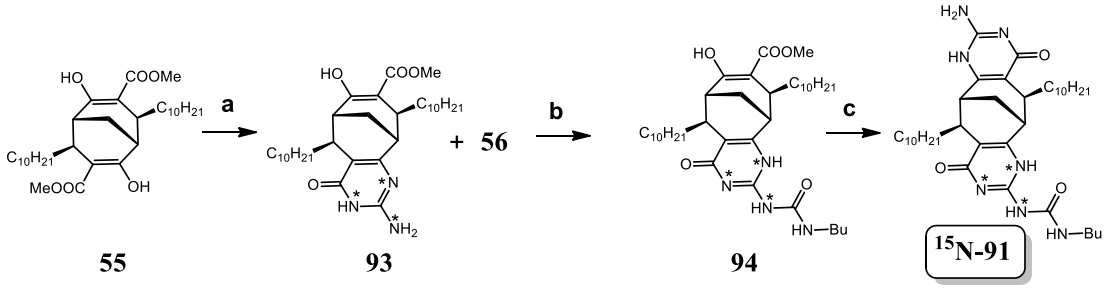

Figure 88. An alternative synthetic pathway to ^{15}N labeled monomer **^{15}N-91**. Guanidine of 99 % atom labelling of one nitrogen atom was used. Reagents and conditions: (a) 2 eq. ^{15}N-Guanidinium carbonate, MeOH, 100 ºC; (b) 1 eq. BuNCO, py; (c) Guanidinium hydrochloride, KOBu^t, MeOH, 100ºC.

To aid distinguishing between the Ic and UPy protons and to facilitate unambiguous structure assignment, singly randomly ^{15}N labeled **^{15}N-91** was synthesized (Fig. 88). Protons located on ^{15}N nitrogen atoms appear as triplets in proton NMR spectrum due to 33% of protons being split by ^{15}N nucleus into a doublet which overlaps with the singlet from nonlabeled portion of **91**. In the

alternative synthetic pathway (Fig. 88) utilized for the synthesis of **^{15}N-91,** desymmetrization of the two equal sites was achieved in the earlier synthesis step by preparing the corresponding mono-β-ketoester-mono-isocytosine **93**. In this transformation the use of guanidinium carbonate instead of guanidinium chloride was crucial to obtain the desired product. The use of strongly basic conditions at elevated temperatures in the latter case resulted in decomposition of the product and starting material. The modified synthetic route is thus more efficient as the symmetric products **56** and **55** can be recovered and subsequently utilized in the synthesis of **91**. All target compounds can be obtained in excellent purity in the powder form after precipitation from concentrated chloroform solution with methanol.

^{1}H NMR spectrum of the enantiopure monomer **91** in several solvents tested displayed very distinct set of signals. In toluene the aggregation profile was very well defined while in $CDCl_3$ and 1,2-dichlorobenzene-d_4 residual peaks of other tautomeric forms and/or possible aggregates could be detected. (Fig. 89) ^{1}H NMR spectrum indicates highly symmetrical aggregate formed from magnetically equivalent C_1 symmetry monomers. Interestingly, racemic sample displays the same resonance pattern, which suggests that homochiral sorting occurs during the formation of supramolecular aggregate.

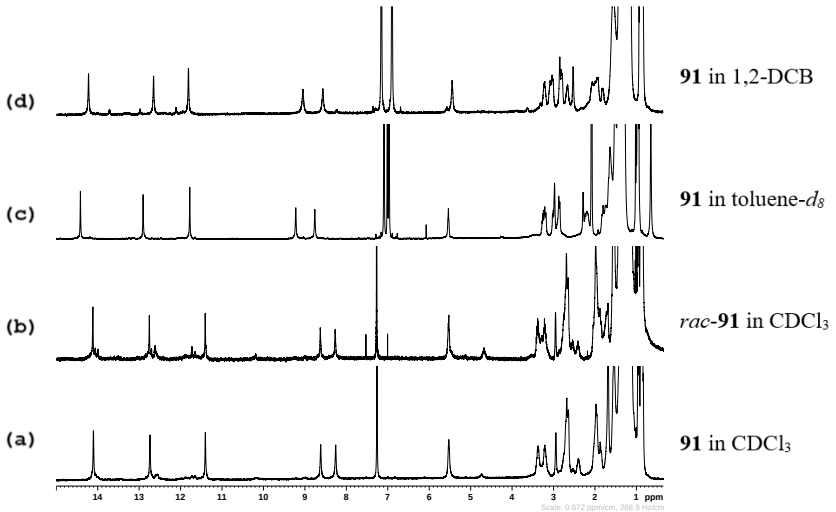

Figure 89. ^{1}H NMR spectra of **91_8** in different solvents.

In the ^{1}H NMR spectrum of **91** (Fig. 90), the most upfield NH signal at 5.56 ppm belongs to urea functional group as it is coupled to methylene protons 17 in butyl group as it is evident from the COSY spectrum and triplet multiplicity. According to its chemical shift, this NH proton is left outside the hydrogen bond array which implies that UPy – UPy quadrupole hydrogen bond is not formed. The two signals at 8.7 ppm and 8.3 ppm correspond to NH_2 group protons 2 of the Ic ring. The fact that both of them are in the downfield region indicates that they do participate in H-bonding. Proton resonating at 8.7 ppm is involved in strong 3H-bonding between UPy and Ic and proton resonating at 8.3 ppm is involved into inter-tetramer hydrogen bond (Fig. 91b).

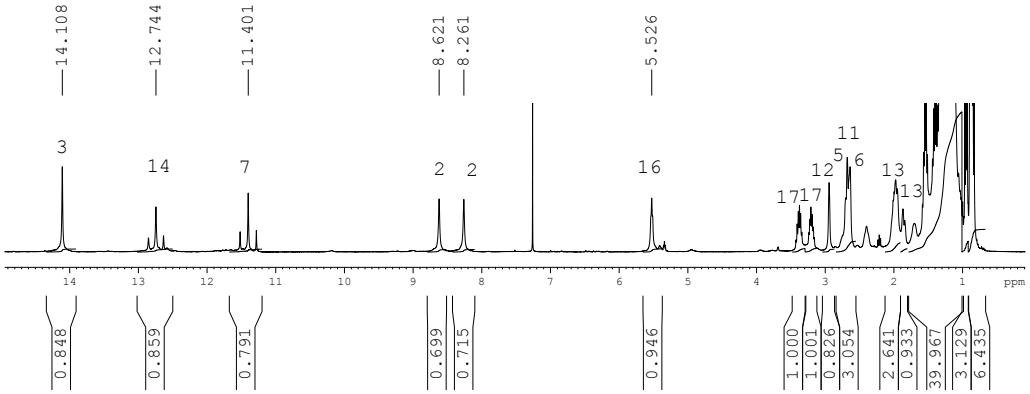

Figure 90. ^{1}H NMR spectrum of **91$_8$** in toluene-d_8 with integrals and the assignment information.

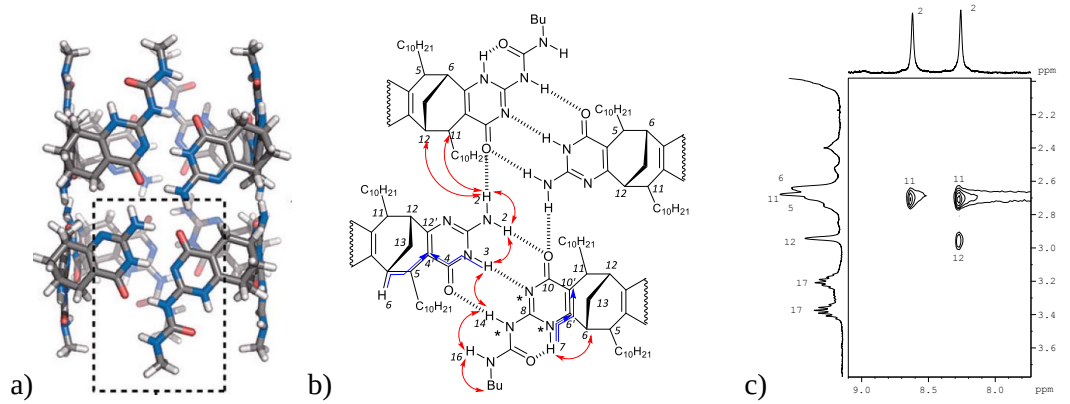

Figure 91. a) Molecular model of **91$_8$**; b) Schematic representation of two tetramers junction and important NMR correlations: red arrows – ROESY, blue arrows - HMBC ; c) ROESY correlations of Ic amino group protons 2.

Proton 3 resonating at 14.5 ppm from Ic ring interacts to carbon atom at 108.8 ppm which according to its chemical shift is assigned as the carbon atom 4'. This particular carbon atom in turn is coupled to proton 6 in the bicyclic region, which

gives rise to the signal at 2.64 ppm. Although, such HMBC correlation map does not prove neither of tautomeric forms of the isocytosine, proton 3 is assigned as *3H* tautomer in Ic ring based on the strong indication for the latter to be involved in H-bonding. It gives ROESY correlation to nearby proton 2 and proton 14 across 3H-bonding interface. Protons 14 and 7, that have the signals at 12.9 and 11.8 ppm appear as triplets and thus belong to UPy functional group. Proton 14 has NOE to the proton 16, whereas proton 7 displays NOE to the proton 6. Schematic representation summarizes the important correlations in Fig. 91b.

a)

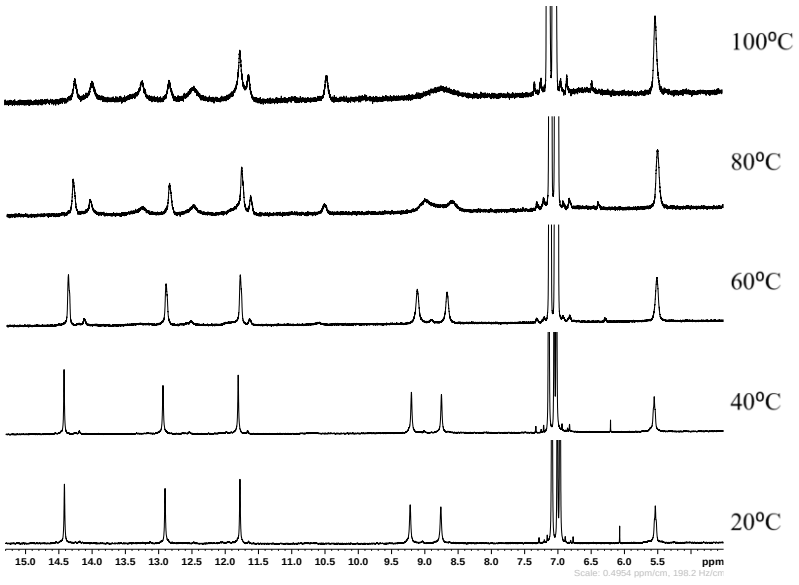

Figure 92. VT NMR of $\mathbf{91_8}$ in toluene-d_8. Only NH region is displayed for clarity.

The octamer $\mathbf{91_8}$ is a relatively stable aggregate as it is evidenced by VT NMR (Fig. 92). At 80 °C coalescence of the amino group resonances is observed which is accompanied by the emergence of the new set of peaks which indicates partial dissociation of aggregates. After cooling down the sample original resonance patter of the octamer is restored.

6.3 GUEST INDUCED REARRANGEMENT

It was known from our previous works that structurally similar compounds are good hosts for fullerenes. Therefore, the octameric tube was utilized as a host for several guests including C_{60}, C_{70} and C_{120}. Indeed, addition of excess of solid C_{60} to the toluene solution of **91** yielded very clean and entirely different

aggregation profile. The complexation happened to be quite slow and transient species could be captured at low fraction of the guest added, as shown in the third spectrum from the series in Fig. 93. The NH resonance pattern of the intermediate species matched the pattern observed for the initial octamer, hence, it is ascribed as C_{60} complexed octamer **91_8@C_{60}**. Conversion of the intermediate species **91_8@C_{60}** into the final species is too fast for more time demanding NMR experiments to be performed, nevertheless, proton spectrum was informative enough to draw conclusions about the topology of the intermediate species. DOSY experiment of the sample at low C_{60} concentration containing initial octamer **91_8** and the final inclusion complex **91_4@C_{60}**, showed that complexed aggregate is smaller than the octamer (Fig. 94a). It is obvious that the next possible smaller entity is a tetramer.

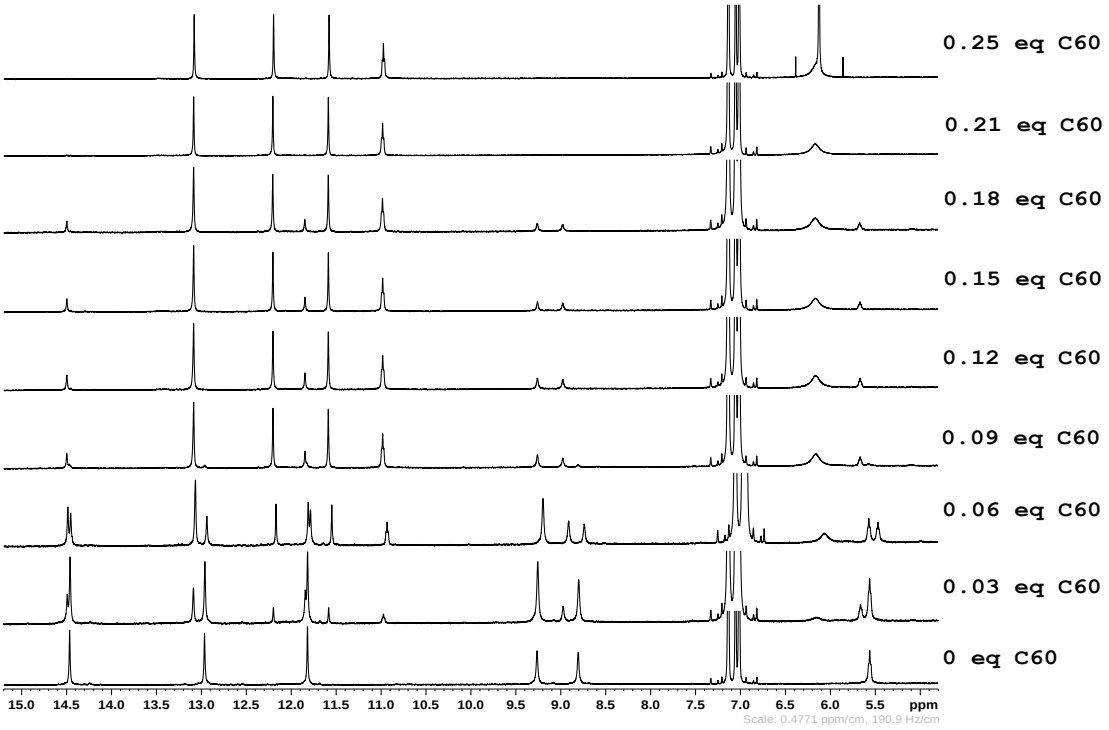

Figure 93. a) ^{1}H NMR titration of **91_8** in toluene-d_8 with increasing amounts of C_{60}. Only NH region is displayed for clarity.

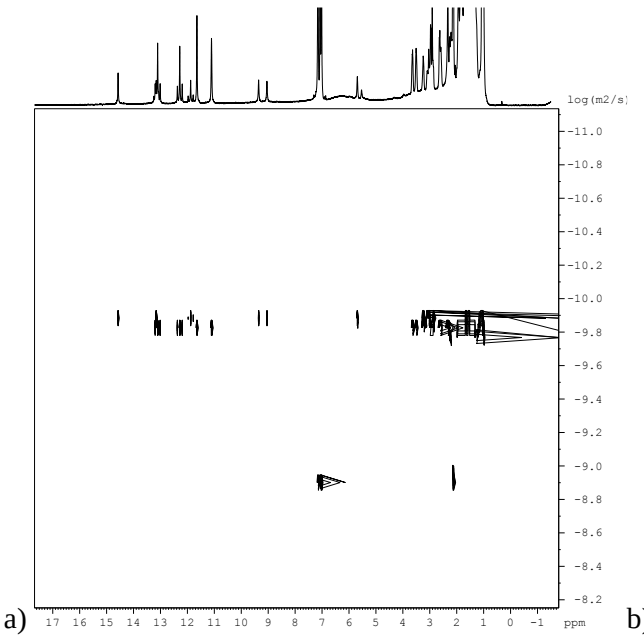

a) b)

Peak	Diff. Constant
14.572 ppm	1.262e-10 m2/s
11.878 ppm	1.252e-10 m2/s
9.352 ppm	1.257e-10 m2/s
9.044 ppm	1.264e-10 m2/s
Average	**1.258e-10 m2/s**
12.282 ppm	1.339e-10 m2/s
11.645 ppm	1.343e-10 m2/s
11.101 ppm	1.347e-10 m2/s
Average	**1.343e-10 m2/s**

Figure 94. a) DOSY spectrum of **91_8@C_{60}** and **91_4@C_{60}** in toluene-d_8; b) Diffusion coefficients for the individual peaks and averaged for the two species.

The new species, supposedly a tetrameric inclusion complex, contains 4 sharp NH signals in the downfield region and one broad NH_2 signal at 6.2 ppm. The free NH_2 group in Ic moiety together with remarkable simplification of the NH resonances (Fig. 95a) implies that the parent aggregate is built from one kind of monomers which amino group is not included in H-bonding.

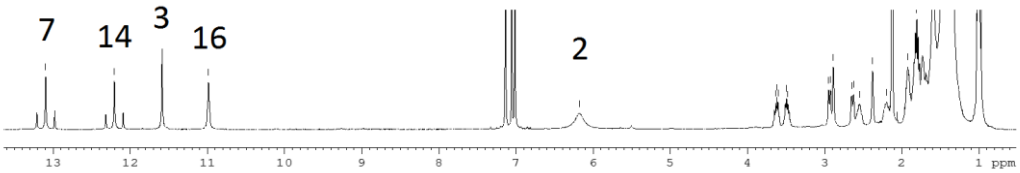

a)

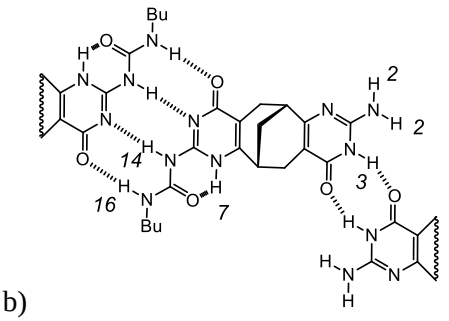

b)

Figure 95. a) ^{1}H NMR spectrum of **91_4@C_{60}** in toluene-d_8 with proton assignment; b) Molecular structure and hydrogen bond pattern in the **91_4@C_{60}**.

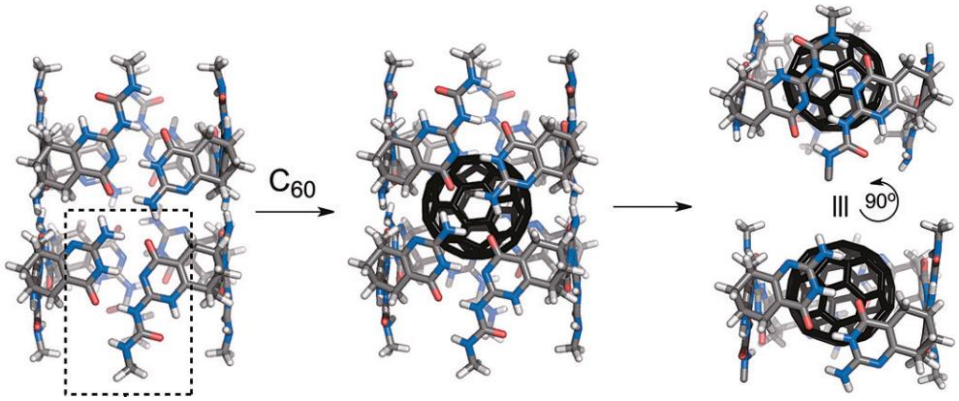

Figure 96. Molecular modeling showing C_{60} induced rearrangement of **91**$_8$;

For C_{70}, the same series of complexation stages involving the formation of the intermediate inclusion complex **91**$_8$**@C**$_{70}$ was observed (Fig. 97). Single set of resonances observed for **91**$_8$**@C**$_{70}$ and for **91**$_4$**@C**$_{70}$ suggests that C_{70} is accommodated in the octameric tube and tetrameric cavity symmetrically, i.e. at the middle. The complexation events occurred at comparable rate as with C_{60}. When excess of C_{70} is added, along with the main **91**$_4$**@C**$_{70}$ inclusion complex minor species are observed which increases in concentration after larger amount of complexed tetramer **91**$_4$**@C**$_{70}$ is produced in the sample. The unknown species could be accounted for asymmetric complex **91**$_8$**@C**$_{70}$ where C_{70} is located in one side of the cyclic tetramer rather than in the middle.

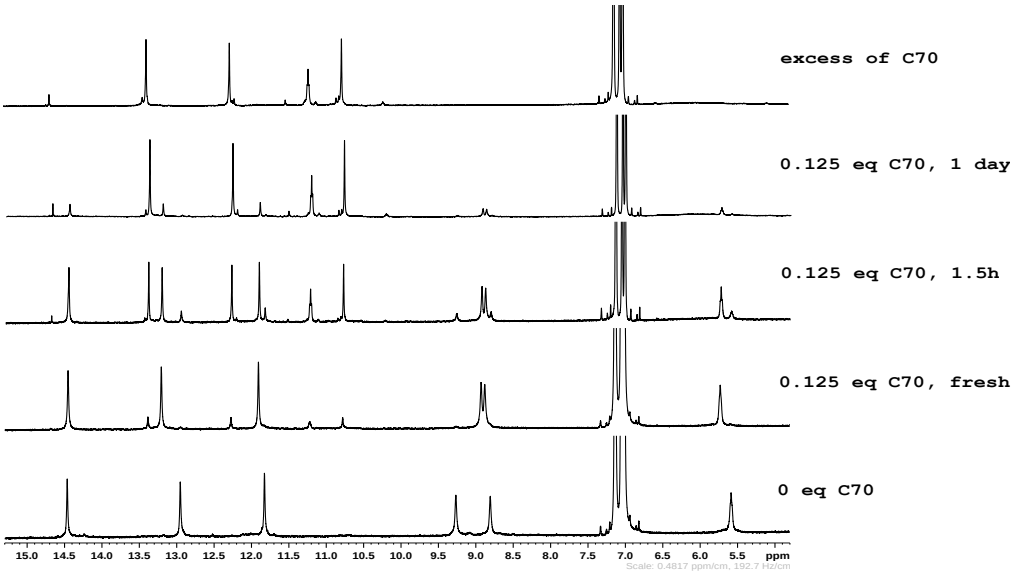

Figure 97. Series of ^{1}H NMR spectra of **91** in toluene-d_8 in the presence of C_{70}. Only NH region is displayed for clarity.

The cavity of the octameric tube is large enough to include fullerene dimer **95**, however even using excess of **95** failed to produce inclusion complex to any substantial degree (Fig. 98). High degree of preorganization is required for such complexation, i.e. C_{120} has to align itself at the open end of the tube at particular angle to enter the cavity. Such alignment out of many possible rotational movements that tumbling C_{120} molecule can adopt is rare and thus, entropically highly demanding. The same is true for guest **96.**

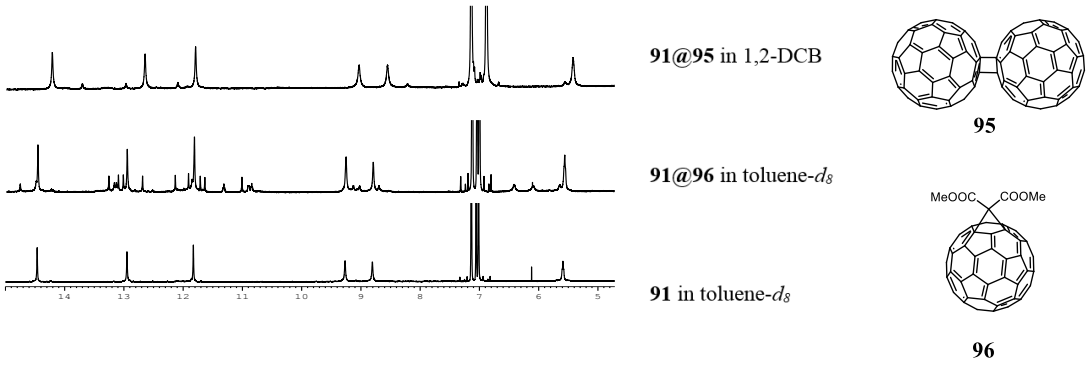

95

96

a) b)

Figure 98. a) Complexation of **91** with other guests; b) Molecular structure of the intended guests **95** and **96**.

6.4 COMPLEXATION INDUCED SELF-SORTING OF STRUCTURALLY SIMILAR COMPOUNDS

Modulation of the molecular recognition by reversible interactions such as complexation of guest molecules can lead to specific functional and responsive (adaptive) systems. Even more attractive situation is when the responsive system can function in a mixture of other similar compounds. The integrity of **91** complexation with C_{60} was tested in the presence of another structurally similar hosts. Two bis-UPy derivatives **68** and **62** were chosen for their perfectly matching geometry (Fig. 99). The Ic motif of **91** could form 3H-bonding interface with **68** and **62**, where the rest of the H-bonds would make use 4H-bonding UPy-UPy interface. NMR experiments were performed on the samples where two hosts $\mathbf{91_8}$ and $\mathbf{68_4}$ or $\mathbf{91_8}$ and $\mathbf{62_4}$ are mixed in equimolar amounts.

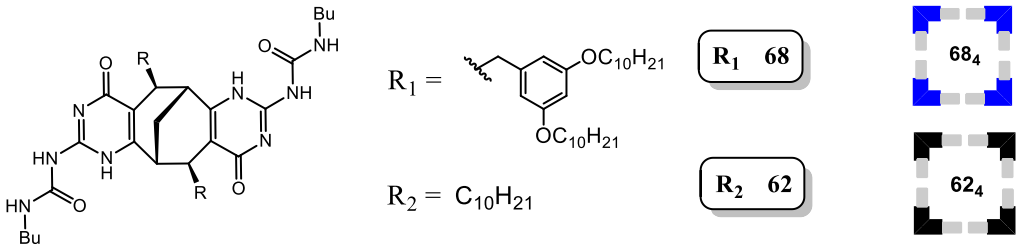

Figure 99. Molecular structure of the monomers tested in self-sorting experiments with $\mathbf{91_8}$.

In principle, two contrary scenarios could be expected. In the first scenario, the initial aggregates $\mathbf{91_8}$ and $\mathbf{68_4}$ or $\mathbf{91_8}$ and $\mathbf{62_4}$ do not scramble and stay within "their own kind" associates, i.e. remains narcissistically self-sorted. In the second scenario, full scrambling of the monomers could be foreseen without clear dominating entity, i.e. social self-sorting owning to the good match in shape and complementarity of the binding sites of the two monomers. In reality, situation somewhere in the middle is also likely to happen due to the small structural differences between **91** and **68** or **62**. To test these assumptions and also to probe C_{60} induced sorting, self-sorting experiments involving two different monomers were engaged.

Dissolving monomers **91** and **68** in $CDCl_3$ resulted in slow scrambling of the monomers and formation of hetero aggregates (Fig. 100c) which is indicated by the disappearance of the resonance patterns of the initial homo aggregate $\mathbf{91_8}$ (Fig. 100a) and appearance of large number of new resonances. The absence of $\mathbf{91_8}$ in the mixture indicated that monomer **91** was included the hetero-assemblies. The resonances corresponding to $\mathbf{68_4}$, are more intense than other resonances, but that could be accounted for twice as many protons contributing to these resonances compared to the heteroaggregates (Fig. 100c). Addition of 0.25 eq. of C_{60} to this mixture results in partial self-sorting of $\mathbf{91_4}$ which is driven by the formation of the stable species $\mathbf{91_4@C_{60}}$. From previous studies it was known, that $\mathbf{68_4}$ do not complex C_{60} in $CDCl_3$ solution. This quality is transferred to the mixed aggregates which clearly do not complex C_{60} (marked with the blue stars in Fig. 100d).

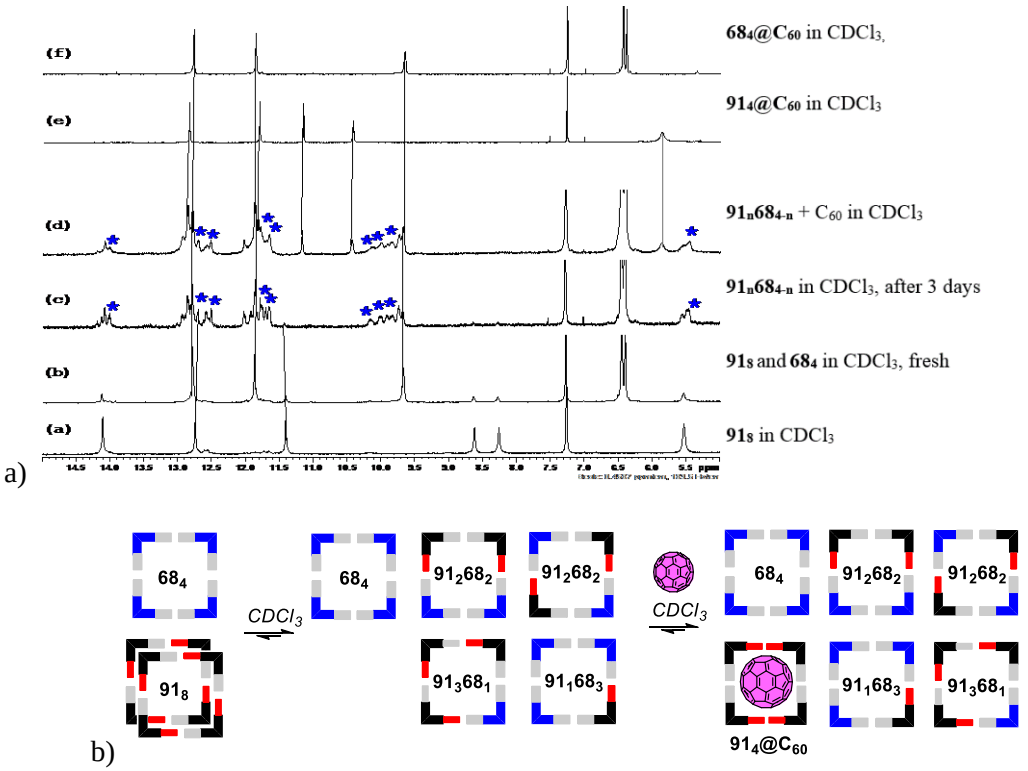

Figure 100. a) Self-sorting of **91** and **68** in $CDCl_3$. Scrambled non complexed aggregates are marked with the blue stars. b) Schematic representation of all assemblies.

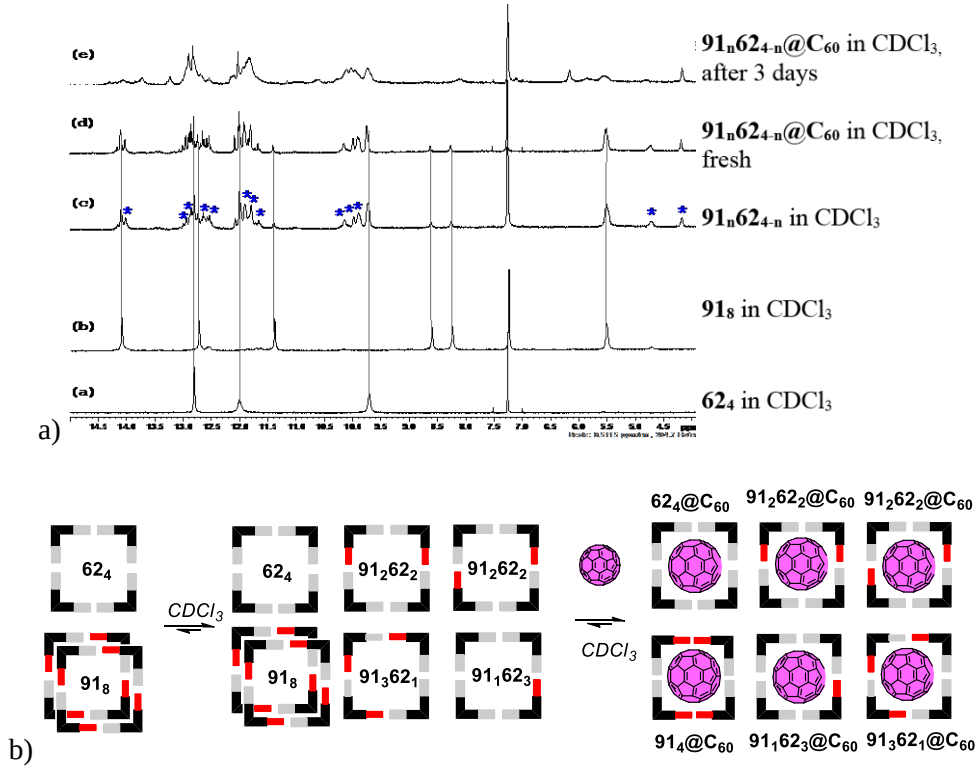

Figure 101. a) Self-sorting of **91** and **62** in $CDCl_3$. Scrambled noncomplexed aggregates marked with blue stars. b) Schematic representation of all assemblies.

The statistical mixture of monomers **91** and **68** within tetrameric aggregates $\mathbf{91_1 68_3}$, $\mathbf{91_2 68_2}$, $\mathbf{91_3 68_1}$ was obtained in $CDCl_3$, from which homo aggregates of $\mathbf{91_4@C_{60}}$ could be restored to significant extend upon C_{60} complexation. The efficient mixing of the host molecules can be explained by energetically favored "dilution" of the bulky side chains in **68**. Partial self-sorting of $\mathbf{91_4@C_{60}}$ from the mixed aggregates is driven by high-affinity recognition of C_{60}, since $\mathbf{91_4}$ is the only host for fullerene present in the mixture of aggregates.

In principle, using **62** instead of **68** could result in less pronounced mixing. In the tetramer $\mathbf{62_4}$ the smaller linear decyl chains would not be imparting large steric strain and thus, would reduce the tendency for mixed aggregate formation. Only the innate binding properties of H-bonding sites will govern self-sorting events. However, this effect was weak and mixing of **91** and **62** in $CDCl_3$ resulted in almost complete scrambling of the host monomers (Fig. 101c) as in the previous case. Addition of C_{60} resulted in complexation of mixed cyclic tetramers with no tangible self-sorting.

In contrast, in toluene both combinations **91 + 68** and **91 + 62** resulted in monomer exchange to rather small extend. Upon complexation with C_{60} no changes in monomer distributions between homo- and heteroaggregates were observed. The nonscrambled fraction of $\mathbf{91_8}$ underwent switch to $\mathbf{91_4@C_{60}}$. If the complexation is performed before mixing event, the homoaggregates $\mathbf{91_4@C_{60}}$ and $\mathbf{68_4@C_{60}}$ are "kinetically frozen" and scrambling is prevented due to exeptionally high stability of these inclusion complexes (Fig. 102d). The same effect is observed when competing monomer **68** is added to the preformed host-guest complex $\mathbf{91_4@C_{60}}$ - homo complexes persist in the solution for prolonged periods of time.

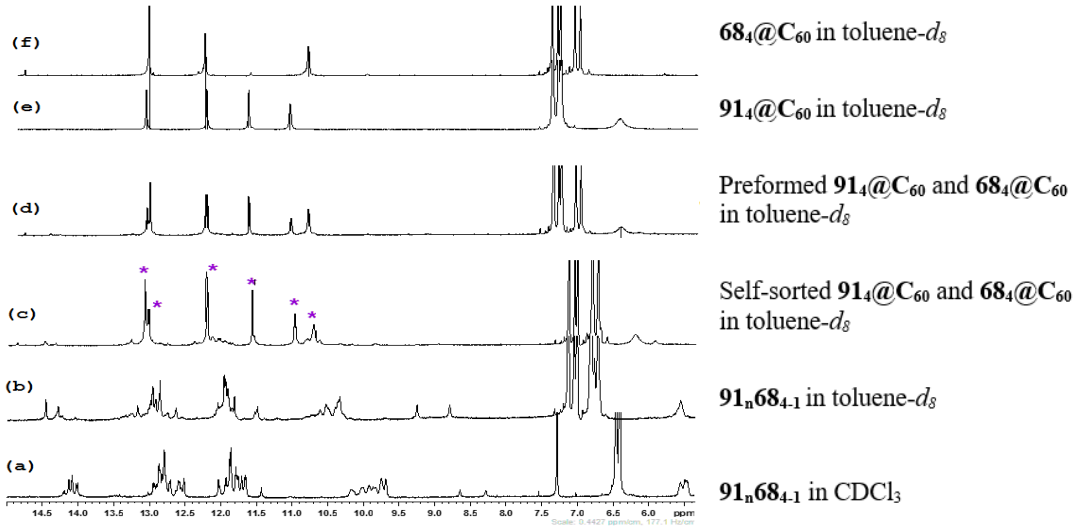

Figure 102. Self-sorting of **91** and **68** in toluene-d_8.

The two opposite situations obtained for the equimolar mixture of **91** and **68** i.e. formation of heteroaggregates in $CDCl_3$ and homoaggregates in toluene, can be utilized in successive myriad of self-sorting events. First, monomer **91** and **68** are allowed to form heteroaggregates in $CDCl_3$ (Fig. 102a). After exchanging solvent to toluene**,** heteroaggregates persist, although they would not normally form in this solvent (Fig. 102b). Addition of C_{60} guest to the established kinetically trapped state induce self-sorting into homoaggregates (Fig. 102c).

In order to probe the effect of urea substituent and solubilizing group, several other Ic-UPy monomers were synthesized. In compound **98**, the butyl substituent at the urea moiety was replaced with the CH_2COOBn functionality. The restricted motion of this large group resulted in less clean ^1H NMR spectrum, most likely due to the presence of several conformers. Unexpectedly, replacement of decyl solubilizing chains with shorter butyl groups in monomer **97** also afforded a complicated aggregation profile as evident by ^1H NMR (Fig. 103c). Likewise, when the side chains are more bulky, as in the case of **92**, mixture of unknown supramolecular entities is obtained (Fig. 103b). As it can be seen comparing NMR spectra (Fig. 103) delicate balance of all functionalities in the structure of this type of monomers has to be attained in order to obtain the desired octameric nanotube.

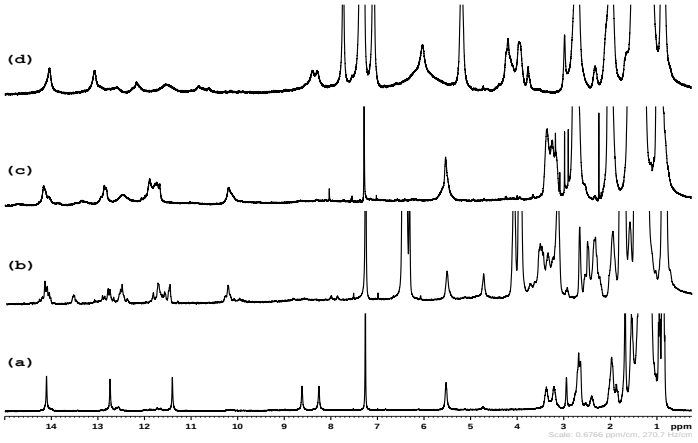

a)

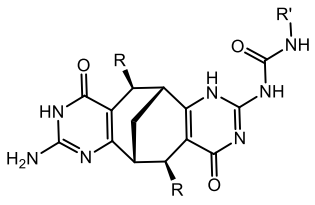

91 R = $C_{10}H_{21}$ R' = Bu
92 R = 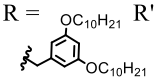 R' = Bu

97 R = C_4H_9 R' = Bu
98 R = $C_{10}H_{21}$ R' = CH_2COOBn

b)

Figure 103. Stacked ^1H NMR spectra of Ic-UPy type derivatives: a) **91** in $CDCl_3$; b) **92** in $CDCl_3$; c) **97** in $CDCl_3$; d) **98** in toluene-d_8.

In theory, controllable size organic nanotubes could be synthesized by mixing bis-Ic monomer **56** with the appropriate amount of **91** as the end capping agent. In practice, however, very low solubility of **56** hampers such experiment. Instead, soluble bis-Ic monomer such as **53** could be used to test this idea.

7 CONCLUSIONS OF THE THESIS

1. Formation of a complex H-bonded decameric capsule assembled from a rigid bis-Ic monomer in carbon disulfide is presented. The assembly is driven by solvent induced tautomerization of Ic motif, i.e. heteroleptic aggregation, and simultaneous establishment of 3H- and 2H-bonding modes between the monomers. The supramolecular structure was unambiguously elucidated using modern NMR techniques. In addition, ^{15}N and ^{13}C isotope labelling of the bis-Ic monomer was utilized for more specific NMR experiments to aid full characterization of the self-assembled capsule $\mathbf{2_{10}}$.
2. The large cavity of the decameric capsule $\mathbf{2_{10}}$ was utilized for guest C_{60} inclusion. Molecular dynamic simulations corroborated the proposed host-guest structure and provided valuable insight into inclusion event.
3. Kinetic enzymatic enantiomer resolution of 9-benzyl-9-azabicyclo[3.3.1]nonane-2,6-diol enabling access to gram quantities of both enantiomers was developed.
4. Two new bis-Ic monomers **52** and **53** based on 9-azabicyclo[3.3.1]nonane and monomer **56** based on bicyclo[3.3.1]nonane framework were synthesized. Their aggregation into nanotubular structures was investigated. Tubular assemblies are held together by orthogonal inter-tetramer H-bonding interface which is established after tautoleptic aggregation into tetrameric rings has taken place.
5. New bis-UPy monomers based on 9-azabicyclo[3.3.1]nonane framework were synthesized and their aggregation in nonpolar solvents investigated. In $CDCl_3$, this type of monomers were found to assemble into tetramers as the main species accompanied by lactim form aggregates. In toluene, unexpected aggregation into polymeric structures were observed which is the outcome of solvophobic effects and the absence of steric crowding near the H-bonding sites.

6. Self-assembled organic nanotube composed of eight identical monomers that incorporates Ic and UPy motifs in one molecule was designed. New H-bonding interface Ic-UPy which originates from 3H-bonding hetero-association of Ic-UPy motifs enables directional assembly of the two tetramers via orthogonal H-bonding interface, similar as in the case of tubular structures from bis-Ic monomers. It was demonstrated, that delicate balance in molecular structure, i.e. butyl urea substitution and decyl solubilizing side chains, are prerequisite for high integrity assembly into octameric tube.
7. The octameric tube was found to be guest responsive and to undergo extreme structural switch upon inclusion of C_{60} and C_{70} guests. The complexation events occur through short lived intermediate complexed octamer species $\mathbf{91_8@C_{60}}$ as evident from ^{1}H NMR, which subsequently undergoes rearrangement into cyclic tetramer $\mathbf{91_4@C_{60}}$. After the rearrangement, the binding fashion is switched from Ic-UPy hetero-association to homo-association of the UPy-UPy and Ic-Ic motifs.
8. Self-recognition fidelity and guest induced switch of the novel Ic-UPy monomer was tested in the presence of structurally similar bis-UPy monomers **62** and **68**. **91** and **68** form fully scrambled hetero aggregates $\mathbf{91_n68_{4-n}}$ in $CDCl_3$, which can be transferred into toluene solution and forced to self-sort to homoaggregates upon C_{60} complexation.

8 EXPERIMENTAL PART

General. All chemicals were used as received from commercial suppliers. Compounds **2**, **3** , **55** [129], $^{15}N_1$ -guanidine hydrochloride[137] and **39** [84] were synthesized according to the published procedures. NMR spectra were recorded on Bruker Ascend 400 MHz NMR spectrometer equipped with a broadband observe probe. HMBC spectra were optimized for ^{n}J = 10 Hz and ^{1}J = 145 Hz. The ROESY spectra were performed with a spinlock time of 250 ms. DOSY spectra were recorded on Bruker Avance III 500 MHz spectrometer equipped with a broadband observe probe. The following parameters were used: Δ 100 ms, δ 6 ms, employing 2 % - 90 % of 53.5 Gauss cm^{-1} gradient strength, number of measured data points was 32. Chemical shifts are given in ppm relative to TMS using the residual solvent peaks at δ = 7.26 ppm (^{1}H NMR) and 77.00 ppm (^{13}C NMR) in $CDCl_3$. Resonance multiplicities are denoted s, d, t, m and br for singlet, doublet, triplet, multiplet and broad, respectively. HRMS was recorded in positive mode on Bruker Daltonics microTOF-II spectrometer equipped with ESI ion source. IR spectra recorded on Perkin Elmer Spectrum BX FT-IR System. Optical rotations were measured on a KRÜSS P3001RS automatic digital polarimeter at 589 nm; $[\alpha]_{20}$ values are given in 10^{-1} deg cm^2 g^{-1}, and concentrations are given in units of g/100 cm^3. Melting points were recorded with a Gallenkamp melting apparatus and are not corrected. Column chromatography was performed using Merck Silica gel 60 (0.040 - 0.063 mm) unless otherwise specified. Yields refer to isolated material judged to be ≥95% pure by ^{1}H NMR spectroscopy. Conversion of the enzymatic reaction was determined by GC using RESTEK Rtx-1701 column (30 m x 0.25 mm) increasing temperature to 260 ºC. Enantiomeric excesses determined on CHIRALPAK IB-3 (250 mm x 4.6 mm) analytical HPLC column. TGA was performed on TGA Q50 thermogravimetric analyzer using ramp rate of 10 ºC/min. DSC scans were obtained using a TA DSC Q2000 model. To obtain DSC traces three cycles were carried out for each sample at ramp rate 10 ºC/min

under nitrogen atmosphere. Viscosity was measured on AMVn Automated Micro Viscosimeter (Antor Paar) using 2.5 mm diameter gold coated ball.

***(5S,6R,11S,12R)*-2,8-diamino-5,11-bis(3,5-bis(decyloxy)benzyl)-5,6,11,12-tetrahydro-6,12-methanocycloocta[1,2-d:5,6-d']dipyrimidine-4,10(*1H*,*9H*)-dione ^{15}N-2**

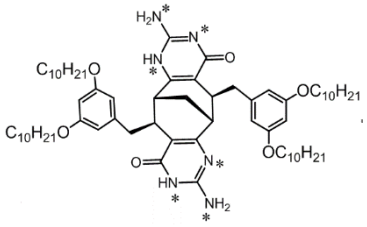

β-keto ester **3** (50 mg, 0.0465 mmol, 1 eq.), KOBu^t (26 mg, 0.233 mmol, 5 eq.) and $^{15}N_1$-guanidine hydrochloride (23 mg, 0.233 mmol, 5 eq.) in 1 ml MeOH was stirred at 100 ºC in a pressurized vial for 12 hours. Reaction mixture was then diluted with water and extracted with DCM. Column chromatography on silica gel using gradient eluent system MeOH/DCM 1 : 20/ 1 : 10 afforded 35 mg (69 %) of the singly randomly ^{15}N labeled compound **^{15}N-2**. ^{1}H NMR (500 MHz, $CDCl_3$) δ 14.3 (s, d, *J* = 88 Hz, 1H), 11.9 (s, d, *J* = 88 Hz, 1H), 7.6 (br, 2H, NH), 6.5 (s, 2H, NH), 6.3 (s, 3H), 6.2 (s, 1H), 4.8 (t, *J* = 88 Hz, 2H), 4.0 (t, *J* = 6.5 Hz, 4H), 3.7 (t, *J* = 6.3 Hz, 4H), 3.3 (d, *J* = 12 Hz, 1H), 3.12 - 2.92 (m, 2H), 2.90 – 2.79 (m, 1H), 2.76 (s, 1H), 2.68 – 2.52 (m, 2H), 2.4 (t, *J* = 13.5 Hz, 1H), 2.15 – 1.90 (m, 2H), 1.89 – 1.72 (m, 4H), 1.70 – 1.55 (m, 4H), 1.54 – 1.43 (m, 4H), 1.43 – 1.12 (m, 52 H), 0,95 – 0.80 (m, 12 H); ^{15}N NMR (50 MHz, $CDCl_3$) δ 201, 196, 151, 147, 78, 67; HRMS (ESI) calc. for $C_{67}H_{106}{}^{14}N_4{}^{15}N_2O_6+H^+$ 1093.8313, found $C_{67}H_{106}{}^{14}N_4{}^{15}N_2O_6+H^+$ 1093.8207.

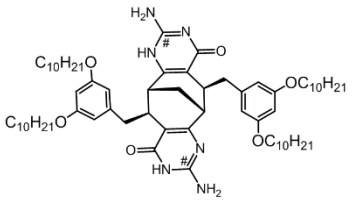

^{13}C-2. 30 mg (0.028 mmol, 1 eq.) of compound **3** was reacted with 8.2 mg (0.084 mmol, 3 eq.) ^{13}C enriched guanidinium chloride and 9.4 mg (0.084 mmol, 3 eq.) of KOBu^t and was purified in the same manner as **^{15}N-2**. Yield: 20 mg (65 %) of a off-white- powder. ^{13}C NMR (100 MHz, CS_2) δ 155.8, 155.7, 154.2, 153.4, 152.3 (only ^{13}C enriched carbon atoms are given); HRMS (ESI) calc. for $^{12}C_{65}{}^{13}C_2H_{106}N_6O_6+H^+$ 1093.8314, found 1093.8312.

3,5-bis-(3,5-bis(decyloxy)benzyloxy)benzaldehyde 36

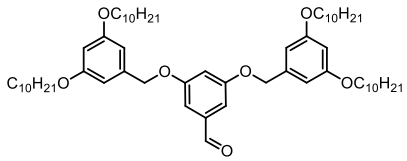

To the solution of 1.825 g (1.93 mmol, 1 eq.) of 3,5-bis(3,5-bis(decyloxy)benzyloxy)benzoic acid methyl ester in 40 ml dry CH_2Cl_2 624 mg of solid PCC was added in portions. The color of reaction mixture changed from orange to black immediately. Reaction mixture was stirred at rt overnight. Then, 100 ml of diethyl ether was poured to the reaction which caused the precipitation of chromium salts. Solution was decanted from black residues and evaporated under reduced pressure. Column chromatography (1 : 20 petroleum ether/EtOAc) of crude material gave 1.674 g (92 %) of a white fatty solid. mp 33 ºC; FTIR (neat, cm^{-1}): 2919, 2850, 1702, 1595, 1169; ^{1}H NMR (400 MHz, $CDCl_3$) δ 9.89 (s, 1H, CHO), 7.09 (d, *J* =2.3 Hz, 2H, CH (arom.)), 6.85 (t, *J* =2.3 Hz, 1H (arom.)), 6.55 (d, *J* =2.1 Hz, 4H (arom.)), 6.41 (t, *J* =2.1 Hz, 2H (arom.)), 5.00 (s, 4H, CH_2 (benzylic)), 3.94 (t, *J* =6.5 Hz, 8H, OCH_2), 1.77 (p, *J* =7.0 Hz, 8H, CH_2), 1.18-1.51 (m, 56H, CH_2), 0.88 (t, *J* =7.0 Hz, 12H, CH_3); ^{13}C NMR (100 MHz, $CDCl_3$) δ 191.9, 160.6, 160.4, 138.4, 138.3, 108.7, 108.3, 105.7, 100.9, 70.4, 68.1, 31.9, 29.6, 29.5, 29.4, 29.3, 29.2, 26.1, 22.7, 14.1; HRMS (ESI) calc. for $C_{61}H_{99}O_7$ ($M+H^+$):943.7385, found 943.7377; Elemental analysis: calc. $C_{61}H_{98}O_7$: C 77.66, H 10.47, found C 77.85, H 10.35.

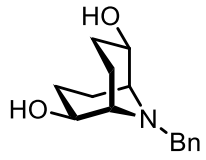

Kinetic enzymatic resolution of 9-benzyl-9-azabicyclo[3.3.1]nonane-2,6-diol 39. 3 g of 9-azabicyclo[3.3.1]nonane-2,6-diol ***rac*-39** was dissolved in 150 ml of freshly distilled vinyl acetate. The solution was thermostated at 20 °C. 600 mg of *Candida Rugosa* lipase was added and the mixture was stirred for 2.5 h at this temperature. The reaction was quenched by filtering off the enzyme through a pad of Celite®. After evaporation of vinyl acetate the mixture of the unreacted diol and the monoacetate was separated by column chromatography eluting with EtOAc/PE (1 : 2). The diol fraction (1,448 g, 84 %ee) was crystallized from

hexane/$CHCl_3$ (1 : 1) mixture in an open Erlenmeyer flask by bringing the solution to simmer and adding a new portion of solvent mixture until the white solid has completely dissolved. Crystallization yielded 820 mg (27 % yield) of **(+)-39** as transparent crystals that were 99 %ee. The combined monoacetate **(-)-44** and diacetate **(-)-45** fraction was first hydrolyzed to the diol (1,268 g, 74 %ee) and then crystallized as above to give 700 mg (23 % yield) 99 %ee of **(-)-39**. 1.4 g of material left in mother liqueurs after crystallizations is nearly racemic diol **39**.

(+)-(*1S,2S,5S,6S*)-39 $[\alpha]^{20}_D$ = +30 ° (c 0.1 in $CHCl_3$), mp 142 - 144 °C;

(-)-(*1R,2R,5R,6R*)-39 $[\alpha]^{20}_D$ = -30 ° (c 0.1 in $CHCl_3$), mp 142 - 144 °C.

9-benzyl-9-azabicyclo[3.3.1]nonane-2,6-diyl diacetate 45.

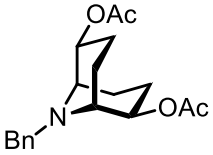

1 eq. of diol **24** (or monoacetate **29**) was dissolved in minimum amount of DCM. To this solution, 5 eq. of Ac_2O and 2 mol% of DMAP was added. Reaction mixture was stirred at room temperature overnight, then neutralized with sat. $NaHCO_3$ solution and the product was extracted with DCM. Column chromatography of the residue gave **45** as a colorless oil in 95% yield suitable for HPLC analysis.

Hydrolysis of 44 and 45. To 1 eq. of the diacetate **45** (or the monoacetate **44**) dissolved in a minimum amount of methanol, 2 eq. of solid K_2CO_3 was added. Reaction mixture was stirred for 3 hours at room temperature, then diluted with water and the product extracted with DCM. The purity of so obtained **39** is suitable for further synthesis. Column chromatography using EtOAc/PE (1 : 2) mixture as eluent gave the diol **39** in 96 % yield.

***(1R,5R)*-9-tert-butyl 3,7-diethyl 2,6-dihydroxy-9-azabicyclo[3.3.1]nona-2,6-diene-3,7,9-tricarboxylate 47**

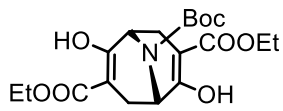

The solution of 1.588 g (6.26 mmol, 1 eq.) of **46** in 20 ml of THF is added dropwise to the solution of 15.6 ml (15.6 mmol, 1 M, 2.5 eq.) of LiHMDS in 60 ml THF at -78 °C. The formation of dienolate resulted in viscous solution with some precipitates. To complete the enolization, the mixture was allowed to warm to -40 °C and then brought back to -78 °C. 2.71 ml (15.6 mmol, 2.5 eq.) of HMPA was then added followed by 1.54 ml (15.6 mmol, 2.5 eq.) of ethyl cyanoformate. Reaction mixture was stirred for 15 min at -78° and quenched by pouring cool reaction mixture into water. Crude product was extracted with DCM (3 x 10 ml), dried over Na_2SO_4 and concentrated under reduced pressure. Column chromatography on silica gel (35 g) eluting with EtOAc/PE (1 : 50, 1 : 30) gradient solvent system afforded 1.726 g (69 %) of a colorless liquid. $[\alpha]\ ^{20}{}_D$ = +20 ° (c 1.0 in $CHCl_3$); FTIR (neat, cm^{-1}): 2981, 2933, 1701, 1662, 1284, 1208; ^{1}H NMR (400 MHz, $CDCl_3$) δ 12.14 (s, 1H, OH), 12.08 (s, 1H, OH), 4.83 (d, *J* = 5.6 Hz, 1H, CH), 4.66 (d, *J* = 5.6 Hz, 1H, CH), 4.21 (q, *J* = 7.2 Hz, 4H, CH_2(Et)), 2.67 (m, 2H, CH_2), 2.55 (dd, *J* = 16 Hz, *J* = 7.3 Hz, 2H, CH_2), 1.46 (s, 9H, CH_3), 1.30 (t, *J* = 7.2 Hz, 6H, CH_3); ^{13}C NMR (100 MHz, $CDCl_3$) δ 172.1, 171.9, 169.8, 169.0, 152.8, 95.7, 95.7, 95.2, 80.9, 60.8, 49.9, 48.3, 28.3, 26.6, 26.3, 14.2; HRMS (ESI) calc. for $C_{19}H_{28}NO_8$ ($M+H^+$): 398.1809, Found: 398.1814.

***(1R,5R)*-diethyl-9-(3,5-bis(decyloxy)benzyl)-2,6-dihydroxy-9-azabicyclo[3.3.1]nona-2,6-diene-3,7-dicarboxylate 48**

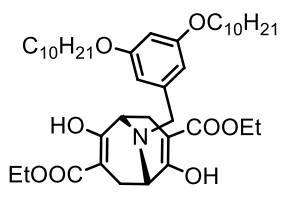

678 mg (1.706 mmol, 1 eq.) of **47** and 3.5 ml TFA were stirred in 8 ml CH_2Cl_2 at rt for 3 h. The reaction mixture was concentrated to dryness and dissolved in 20 ml of dry CH_2Cl_2. 0.3 ml (2.218 mmol, 1.3 eq.) of TEA, 928 mg (2.218 mmol, 1.3 eq.) of 3,5-bis(decyloxy)benzaldehyde **50** and 940 mg (4.436 mmol, 2.6 eq.) of $Na(OAc)_3BH$ were added subsequently. Reaction mixture was

stirred at rt for 2 days. The residue was concentrated under reduced pressure and chromatographed on silica gel to afford 919 mg (77 %) of **48** as a colorless liquid. $[\alpha]\ ^{20}_{D}$ = +104 ° (c 1.04 in $CHCl_3$); FTIR (neat, cm^{-1}): 2925, 2855, 1660, 1596, 1277, 1206, 1162, 1016, 819; ^{1}H NMR (400 MHz, $CDCl_3$) δ 12.03 (s, 2H, OH), 6.36 (s, 1H, CH (arom.)), 6.49 (s, 2H, CH (arom.)), 6.36 (s, 1H, CH), 6.49 (s, 2H), 4.22 (q, *J* = 7.1 Hz, 4H, OCH_2), 3.92 (t, *J* = 6.5 Hz, 4H, CH_2(Et)), 3.63 (dd, *J* = 35 Hz, *J* = 12 Hz, 2H, CH_2 (benzylic)), 3.46 (s, 2H, CH), 2.69 (d, *J* = 14 Hz, 2H, CH_2), 2.44 (d, *J* = 14 Hz, 2H, CH_2), 1.76 (p, *J* =6.6 Hz, 4H, CH_2), 1.12-1.50 (m, 34H, CH_2 and CH_3(Et)), 0.88 (t, *J* = 6.5 Hz, 6H, CH_3); ^{13}C NMR (100 MHz, $CDCl_3$) δ 172.1, 170.52, 160.4, 139.9, 107.0, 100.3, 94.8, 68.1, 60.6, 56.1, 54.0, 31.9, 29.6, 29.5, 29.4, 29.3, 26.1, 24.8, 22.7, 14.2, 14.1; HRMS (ESI) calc. for $C_{41}H_{66}NO_8$ ($M+H^+$):700.4783; Found: 700.4790.

***(1R,5R)*-diethyl-9-(3,5-bis((3,5-bis(decyloxy)benzyl)oxy)benzyl)-2,6-dihydroxy-9-azabicyclo[3.3.1]nona-2,6-diene-3,7-dicarboxylate 49**

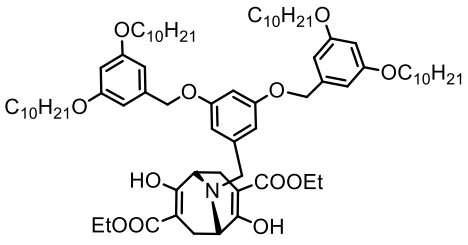

To the solution of 500 mg (1.258 mmol, 1 eq.) of **47** in 20 ml of DCM 5 ml (50 eq.) of TFA was added. The mixture was stirred at rt for 3h and then evaporated to dryness. The solid residue was dissolved in 20 ml of dry DCM followed by addition of 1.780 g (1.887 mmol, 1.5 eq.) of aldehyde **51**, 0.27 ml (1.887 mmol, 1.5 eq.) of TEA and 800 mg (3.77 mmol, 3 eq.) of Na $(OAc)_3BH$. The reaction mixture was stirred at rt for 3 days until TLC (EtOAc) shows consumption of the deprotected **47** TFA salt. Reaction mixture was then evaporated to dryness and purified by column chromatography on silica gel (PE/EtOAc 35 : 1) to afford 1.254 g (81 %) of **49** as a yellowish solid. $[\alpha]\ ^{20}_{D}$ = +65 ° (c 1.51 in $CHCl_3$); FTIR (neat, cm^{-1}): 2924, 2854, 1660, 1596, 1207, 1164; ^{1}H NMR (400 MHz, $CDCl_3$) δ 12.03 (s, 2H, OH), 6.61 (d, *J* = 2.2 Hz, 2H, CH (arom.)), 6.55 (d, *J* = 2.2 Hz, 4H, CH (arom.)), 6.52 (t, *J* = 2.2 Hz, 1H, CH (arom.)), 6.4 (t, *J* = 2.2 Hz, 2H, CH (arom.)), 4.93 (s, 2H, CH_2 (benzylic)), 4.22

(q, J = 7.1 Hz, 4H, OCH_2), 3.93 (t, J = 6.6 Hz, 8H, CH_2), 3.64 (ABq, $\Delta\delta_{AB}$ = 0.08, J = 13.5 Hz, 2H, CH (benzylic)), 3.43 (d, J = 5.9 Hz, 2H, CH), 2.64 (dd, J = 16.0 Hz, J = 7.0 Hz, 2H, CH_2), 2.41 (d, J = 16 Hz, 2H, CH_2), 1.76 (p, J =6.6 Hz, 8H, CH_2), 1.18-1.50 (m, 60H, CH_2 and CH_3(Et)), 0.88 (t, J = 6.6 Hz, 12H, CH_3); ^{13}C NMR (100 MHz, $CDCl_3$) δ 172.2, 170.5, 160.96, 160.5, 160.1, 140.2, 139.0, 107.6, 105.8, 101.0, 100.9, 94.8, 70.2, 68.1, 60.6, 56.0, 54.0, 31.9, 29.6, 29.5, 29.4, 29.3, 29.2, 26.1, 24.8, 22.7, 14.2, 14.1; HRMS (ESI) calc. for $C_{75}H_{118}NO_2$ ($M+H^+$): 1224.8649; Found: 1224.8654.

(6S,12S)-2,8-diamino-13-(3,5-bis(decyloxy)benzyl)-5,6,11,12-tetrahydro-6,12-epiminocycloocta[1,2-d:5,6-d']dipyrimidine-4,10(*1H,7H*)-dione 52

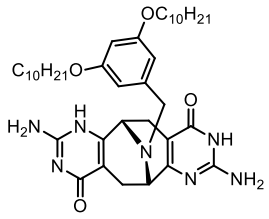

300 mg (0.428 mmol, 1 eq.) of **48**, 155 mg (1.714 mmol, 4 eq.) of guanidinium carbonate and 237 mg (1.714 mmol, 4eq.) of K_2CO_3 was refluxed in 10 ml of EtOH for 5 hr. After the reaction mixture was cooled down, 10 ml of 1 M HCl was added to the reaction flask. The precipitate was filtered and washed thoroughly with distilled water, MeOH and acetone which yielded 225 mg (76 %) of **52** as a yellowish powder. [α] $^{20}_D$ = +102 ° (c 0.1 in $CHCl_3$); mp (enantiopure) >260 °C (decomp.); FTIR (neat, cm^{-1}): 3138, 2924, 2853, 1686, 1596, 1164; ^{1}H NMR (400 MHz, $CDCl_3$/TFA) δ 10.92 (s, NH), 8.19 (br, 4H, NH_2), 6.57 (s, 1H, CH (arom.)), 6.50 (s, 2H, CH (aromatic)), 5.02 (s, 2H, CH), 4.16 – 4.61 (m, 2H, CH_2(benzylic)), 3.89 (s, 4H, CH_2 (OCH_2)), 2.42 (dd, J^1 = 8.0 Hz, J^2 = 15.0 Hz, 4H, CH_2), 1.73 (s, 4H, CH_2), 1.07-1.54 (m, 28H, CH_2), 0.8 (t, J = 6.5 Hz, 6H, CH_3); ^{13}C NMR (100 MHz, $CDCl_3$) δ could not be acquired due to line broadening; HRMS (ESI) calc. for $C_{39}H_{60}N_7O_4$ ($M+H^+$):690.4701; Found: 690.4710.

(*6S,12S*)-2,8-diamino-13-(3,5-bis((3,5-bis(decyloxy)benzyl)oxy)benzyl)-5,6,11,12-tetrahydro-6,12-epiminocycloocta[1,2-d:5,6-d']dipyrimidine-4,10(*1H,7H*)-dione 53

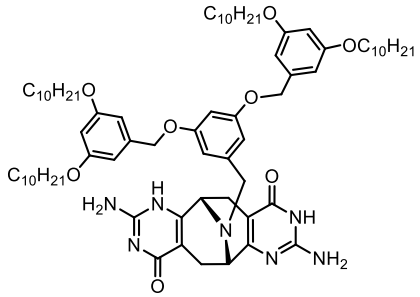

1.156 g (0.923 mmol, 1 eq.) of β-keto ester **49** was heated overnight with 442 mg (4.613 mmol, 5 eq.) of guanidine carbonate and 442 mg (4.613 mmol, 5 eq.) of K_2CO_3. Reaction mixture was cooled down, diluted with water and extracted with CH_2Cl_2 (3 x 5 ml). Combined organic phases were dried over Na_2SO_4 and concentrated under reduced pressure. Crude material was dissolved in minimum amount $CHCl_3$, precipitated with MeOH and filtered. Filter cake was washed with MeOH to give 906 mg (81 %) of **53** as off-white powder. $[\alpha]\ ^{20}_D$ = +15 ° (c 0.1 in $CHCl_3$); mp (enantiopure) > 230 °C (decomp.), (rac) > 280 °C (decomp.); FTIR (neat, cm^{-1}): 3329, 3152, 2924, 2853, 16547, 1596, 1458, 1166, 1054; ^{1}H NMR (400 MHz, $CDCl_3$/TFA) δ 11.14 (s, NH), 6.75 (s, 1H, CH (arom.)), 6.61 (s, 6H, CH (arom.)), 6.54 (s, 2H, CH (arom.)), 5.19 (br, 2H, CH_2), 4.49 (d, *J* =13.0 Hz, 1H, CH), 4.36 (d, *J* =13.0 Hz, 1H, CH), 4.03 (t, *J* =7.0 Hz, 8H, CH_2), 3.34 (d, *J* =18.0 Hz, 2H, CH_2), 3.12 (d, *J* =18.0 Hz, 2H, CH_2), 1.78 (t, *J* =7.0 Hz, 8H, CH_2), 1.16-1.50 (m, 56 H, CH_2), 1.87 (t, *J* =7.0 Hz, 12H, CH_3); ^{13}C NMR (50 MHz, $CDCl_3$) δ 162.8, 162.3, 161.9, 161.5, 160.8, 160.2, 159.7, 152.1, 144.4, 138.1, 127.86, 118.5, 115.7, 112.9, 110.0, 107.5, 106.54, 104.3, 102.6, 70.5, 57.6, 51.5, 31.9, 29.6, 29.3, 28.9, 25.8, 22.7, 13.9; HRMS (ESI) calc. for $C_{73}H_{112}N_7O_8$ ($M+H^+$): 1214.8567; Found: 1214.8582.

(*1S,4R,5S,8R*)-dimethyl-4,8-didecyl-2,6-dihydroxybicyclo[3.3.1]nona-2,6-diene-3,7-dicarboxylate 55

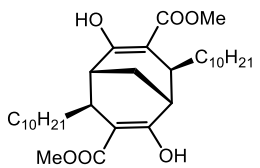

Formation of Grignard reagent. 100 ml two neck RBF was heated in 160 °C oven and cooled under vacuum. The flask equipped with stirring bar, reflux condenser with nitrogen inlet and septum was purged with argon gas and kept under stream of

argon during the course of the reaction. 500 mg (20.8 mmol, 1 eq.) Mg tunings were added and suspended in 2 ml of dry THF. A crystal of I_2 was added to activate Mg. Brown color of iodine faded away after stirring at rt for several minutes. 4.32 ml (20.8 mmol, 1 eq.) of decyl bromide in 10 ml THF was added dropwise over 15 min at rt. Reaction mixture was gently refluxed for 30 min. after which only small amount of Mg is left undissolved. Reaction mixture was diluted up to 40 ml of total amount of THF to afford approximately 0.5 M decyl magnesium bromide solution.

Michael addition to enone 54. 400 mg (4.468 mmol, 4.2 eq) of CuCN is weighted to 50 ml RBF and flushed with argon gas. 3 ml of dry THF was added to suspend CuCN and the reaction flask was cooled to -30 °C. 9.5 ml (4.25 mmol, 4 eq.) of 0.5 M decyl magnesium bromide solution was added dropwise causing CuCN to dissolve. Reaction mixture was stirred for 10 min at -30 °C whereupon color changed to yellow and eventually to brown. Reaction mixture is cooled to -78 °C and solution of 300 mg (1.064 mmol, 1 eq.) of dienone **54**[65] in 3 ml of THF is added dropwise. After stirring for 10 min enone **54** is completely consumed. Reaction mixture is quenched while cold with saturated NH_4Cl solution or ammonia solution, allowed to warm to rt and stirred overnight. Next day the blue mixture is extracted with DCM, dried over Na_2SO_4 and chromatographed on silica gel (35 g) eluting with EtOAc/PE (1 : 100) solvent mixture to afford 423 mg (72 %) of **55** as colorless oil. $[\alpha]\ ^{20}_D$ = +120 ° (c 0.2 in $CHCl_3$); FTIR (neat, cm^{-1}): 2924, 2854, 1651, 1440, 1210, 1200 ^{1}H NMR (400 MHz, $CDCl_3$) δ 12.28 (s, 2H, OH), 2.74 (s, 6H, OCH_3), 2.60 (d, 2H, CH), 2.44 – 2.49 (m, 2H, CH), 1.79 (t, *J* = 3.0 Hz, 2H, CH_2), 1.49 – 1.71 (m, 4H, CH_2), 1.16 – 1.49 (m, 32H, CH_2), 0.88 (t, *J* = 6.5 Hz, 6H, CH_3); ^{13}C NMR (100 MHz, $CDCl_3$) δ 174.1, 173.3, 100.8, 51.4, 37.4, 35.9, 33.6, 31.9, 29.7, 29.65, 29.6, 29.5, 29.4, 27.9, 22.7, 18.1, 14.1; HRMS (ESI) calc. for $C_{33}H_{56}O_6Na$ ($M+Na^+$): 571.3969, Found: 571.3962.

(*5S,6R,11S,12R*)-2,8-diamino-5,11-didecyl-5,6,11,12-tetrahydro-6,12-methanocycloocta[1,2-d:5,6-d']dipyrimidine-4,10(*1H,9H*)-dione 56

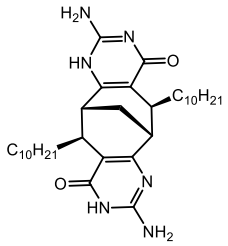

820 mg (1.494 mmol 1 eq.) of **55**, 713 mg (7.47 mmol, 5 eq.) of KOBu^t and 936 mg (7.47 mmol, 5 eq.) of guanidinium chloride and 5 ml of MeOH was added to a sealable vial with a magnetic stir bar. The vial was sealed and stirred overnight at 100 ºC. Reaction mixture was cooled down, diluted with 10 ml of 1 M HCl and the white precipitate filtered using glass frit filter. The white solid was washed thoroughly with water followed by small wash with MeOH. After drying under vacuum 700 mg (82.6 %) of **56** was obtained as a white powder. [α] $^{20}_D$ = +602 ° (c 0.1 in $CHCl_3$); mp (enantiopure) >300 ºC (decomp.), mp (rac) >300 ºC (decomp.); FTIR (neat, cm^{-1}): 2921, 2851, 1645, 1495, 1467, 1373; ^{1}H NMR (400 MHz, acetone-*d*$_6$/DMSO-*d*$_6$ (1:1, v/v)) δ 10.89 (br, 2H, NH_2), 6.45 (s, 4H, NH_2), 1.82 (s, 2H, CH), 1.69 (t, *J* = 12.0 Hz, 2H, CH), 1.47 (br, 2H, CH_2), 1.10 – 1.40 (m, 36H, CH_2), 0.86 (t, *J* = 7.0 Hz, 6H, CH_3); ^{13}C NMR (100 MHz, acetone-*d*$_6$/DMSO-*d*$_6$ (1:1, v/v)) could not be acquired due to line broadening; HRMS (ESI) calc. for $C_{33}H_{55}N_6O_2$ (M+H$^+$): 567.4381, Found: 567.4376.

1,1'-((*6S,12S*)-13-(3,5-bis(decyloxy)benzyl)-4,10-dioxo-1,4,5,6,7,10,11,12-octahydro-6,12-epiminocycloocta[1,2-d:5,6-d']dipyrimidine-2,8-diyl)bis(3-butylurea) 57

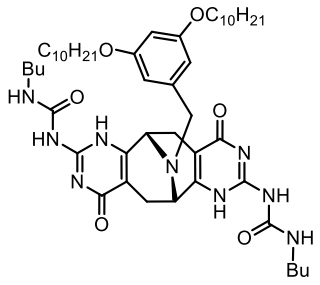

To the solution of 50 mg (0.0724 mmol, 1 eq.) of **52** and in 1 ml of dry pyridine 65 µl (0.580 mmol, 8 eq.) of BuNCO was added under inert atmosphere. The reaction mixture was stirred at 80 °C for 2 hrs. After cooling down, 10 ml of 1 M HCl t was added . The yellowish solid formed was filtered. The crude material was dissolved in $CHCl_3$, dried over Na_2SO_4 and filtered. After concentrating to minimum amount, precipitating with MeOH and filtering using glass frit filter

gave 30 mg (46.6 %) of **57** as a white powder. [α] $^{20}_{D}$ = +40 ° (c 0.1 in $CHCl_3$); mp (enantiopure) >260 °C (decomp.); FTIR (neat, cm^{-1}): 3329, 3233, 2926, 1643, 1560, 1221; ^{1}H NMR (400 MHz, $CDCl_3$/TFA) δ 13.07 (s, 1H, NH), 11.96 (s, 1H, NH), 9.88 (s, 2H, NH), 6.42 – 6.58 (m, 2H, CH (arom.)), 6.38 (s, 1H, CH (arom.)), 3.86 – 4.06 (m, 4H, CH_2), 3.82 (s, 2H, CH), 3.54 – 3.76 (m, 2H, CH), 3.10 – 3.41 (m, 4H, CH_2), 2.93 (d, *J* = 16.0 Hz, 2H, CH), 2.54 (d, *J* = 16.0 Hz, 2H, CH), 1.70 – 1.87 (m, 4H, CH_2), 1.51 - 1.68 (m, 4H, CH_2), 1.12-1.50 (m, 32H, CH_2), 0.94 (t, *J* = 7 Hz, 6H, CH_3), 0.88 (t, *J* = 7 Hz, 6H, CH_3); ^{13}C NMR (100 MHz, $CDCl_3$/TFA) δ 109.2, 68.8, 40.8, 31.9, 30.8, 29.7, 29.5, 29.3, 28.9, 25.7, 22.6, 19.7, 14.0, 13.3; HRMS (ESI) calc. for $C_{49}H_{78}N_9O_6$ ($M+H^+$):888.6067; Found: 888.6061.

1,1'-((*6S,12S*)-13-(3,5-bis(decyloxy)benzyl)-4,10-dioxo-1,4,5,6,7,10,11,12-octahydro-6,12-epiminocycloocta[1,2-d:5,6-d']dipyrimidine-2,8-diyl)bis(3-(3-(1,3-dioxoisoindolin-2-yl)propyl)urea) 58

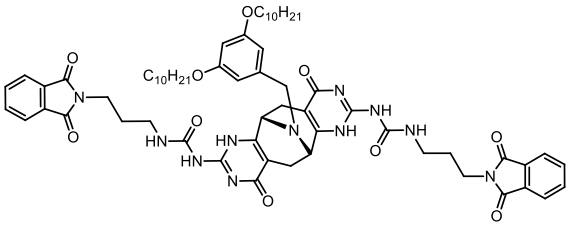

50 mg (0.0724 mmol, 1 eq.) of **52** and 133 mg (0.580 mmol, 8 eq.) of freshly prepared 4-(1,3-dioxoisoindolin-2-yl)propane isocyanate **65** was added as solid to a MW vial. The reaction mixture was flushed with nitrogen and 0.5 ml of dry pyridine was added. The mixture was heated in MW reactor for 10 min at 120 ºC. Reaction mixture was cooled down and 0.5 ml of MeOH was added to quench the excess of the isocyanate. Then the mixture was diluted with 5 ml 1M HCl and extracted with DCM. After drying over Na_2SO_4 and filtering off the crude reaction mixture was concentrated until most of DCM is removed. The product was successfully separated from isocyanate dimerization byproduct by precipitation with MeOH and filtering through glass frit filter. Drying under vacuum gave 52 mg (62.6 %) of **58** as off-white powder. [α] $^{20}_{D}$ = +145 ° (c 0.1 in $CHCl_3$); mp (enantiopure) >260 °C (decomp.); FTIR (neat, cm^{-1}):3329, 3225, 2925, 2853, 1716, 1647, 1546, 1396, 719; ^{1}H NMR (400

MHz, $CDCl_3$/TFA) δ 10.79 (s, NH), 7.81 – 7.89 (m, 4H, CH (Pht)), 7.73 – 7.81 (m, 4H, CH (Pht)), 6.49 (s, 2H, CH (arom.)), 6.33 (s, 1H, CH (arom.)), 5.12 (s, 2H, CH), 4.49 (d, *J* = 13 Hz, 1H, CH_2 (benzylic)), 4.31 (d, *J* = 13.0 Hz, 1H, CH_2(benzylic)), 3.66 – 3.91 (m, 8H, CH_2 (OCH_2 and Pr)), 3.14 – 3.54 (m, 8H, CH_2), 1.93 (s, 4H, CH_2 (Pr)), 1.67 (s, 4H, CH_2), 1.11-1.50 (m, 28H, CH_2), 0.87 (t, *J* = 7.0 Hz, 6H, CH_3); ^{13}C NMR (100 MHz, $CDCl_3$) δ 169.8, 160.9 (TFA), 134.9, 131.3, 123.9, 118.5, 115.7, 112.9, 110.05, 108.7, 68.5, 37.3, 34.8, 31.9, 29.5, 29.33, 29.3, 28.9, 27.8, 25.8, 22.7, 14.1; HRMS (ESI) calc. for $C_{63}H_{80}N_{11}O_{10}$ ($M+H^+$):1150.6084; Found: 1150.6077.

1,1'-((*6R,12R*)-13-(3,5-bis((3,5-bis(decyloxy)benzyl)oxy)benzyl)-4,10-dioxo-1,4,5,6,7,10,11,12-octahydro-6,12-epiminocycloocta[1,2-d:5,6-d']dipyrimidine-2,8-diyl)bis(3-butylurea) 59

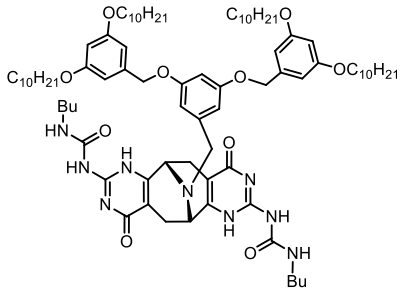

10 ml RBF with a stirring bar was charged with 54 mg (0.0461 mmol, 1 eq.) of **53** and flushed with nitrogen. 1 ml of dry pyridine was added through syringe, the mixture was stirred until solid dissolved followed by addition of 42 µL (0.369 mmol, 1 eq.) of BuNCO. Reaction mixture was stirred for 1 hour at 80 ºC. After cooling down to rt, the reaction mixture was transferred into 50 ml Erlenmeyer flask and 20 ml of 1M HCl was added to neutralize pyridine. The mixture was extracted with $CHCl_3$ (3 x 5 ml), dried over Na_2SO_4, filtered, concentrated to minimum amount and precipitated with MeOH. Filtering through glass frit gave 42 mg (64 %) of a off-white powder. mp (enantiopure) 180 ºC (decomp.); $[\alpha]\ ^{20}_{D}$ = +130 º (c = 0.1 in $CHCl_3$); FTIR (neat, cm^{-1}): 2921, 2852, 1589, 1549, 1156, 1050; ^{1}H NMR (400 MHz, $CDCl_3$) δ 11.55 (s, 2H, NH), 9.35 (s, 2H, NH), 7.02 (br, 2H, NH_2), 6.55 (s, 2H, CH (arom.)), 6.45 (s, 5H, CH (arom.)), 6.28 (s, 2H, CH (arom.)), 4.86 (s, 4H, CH_2 (Bu)), 3.78 – 3.93 (m, 8H, CH_2), 3.70 (d, *J* = 15.0 Hz, 2H, CH_2), 3.62 (s, 2H, CH_2 (benzylic)), 3.55 (d, *J* = 15.0 Hz, 2H, CH_2), 3.12 (s, 4H, CH_2), 2.72 (d, *J* = 15.0 Hz, 2H, CH), 1.56 – 1.78

(m, 8H, CH_2), 1.32 – 1.50 (m, 12H, CH_2), 1.04 – 1.32 (m, 56H, CH_2), 0.81 (m, 18H, CH_3); ^{13}C NMR could not be acquired due to line broadening; HRMS (ESI) calc. for $C_{83}H_{129}N_9O_{10}$ ($M+H^+$): 1412.9941, Found: 1412.9906.

1,1'-((*6R,12R*)-13-(3,5-bis((3,5-bis(decyloxy)benzyl)oxy)benzyl)-4,10-dioxo-1,4,5,6,7,10,11,12-octahydro-6,12-epiminocycloocta[1,2-d:5,6-d']dipyrimidine-2,8-diyl)bis(3-(3-(1,3-dioxoisoindolin-2-yl)propyl)urea) 60

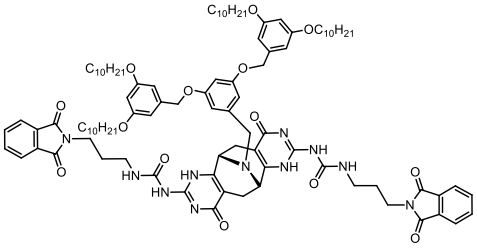

159 mg (0.132 mmol, 1 eq.) of compound **53** and 242 mg (1.055 mmol, 8 eq.) of freshly synthesized 4-(1,3-dioxoisoindolin-2-yl)propane isocyanate **65** in 1 ml dry pyridine were heated at 120 ºC in MW reactor for 10 min. Reaction mixture was cooled down, diluted with 1 M HCl. White precipitate was filtered and washed with water. The crude material was dissolved in minimum amount of $CHCl_3$, dried over Na_2SO_4 and filtered. The solution was concentrated, precipitated with MeOH and filtered through glass frit filter to give 221 mg (80 %) of **60** as a off-white powder. mp (rac) 260 ºC (decomp.); FTIR (neat, cm^{-1}): 3225, 2925, 2853, 1715, 1595, 1166, 719; ^1H NMR (400 MHz, DMSO-d_6): 10.94 (br, 2H, NH), 8.89 (br, 2H, NH), 7.18 – 7.30 (m, 4H, CH (Pht)), 7.08 – 7.18 (m, 4H, CH (Pht)), 7.03 (br, 2H, NH), 6.08 (s, 2H, CH (arom.)), 5.91 (s, 4H, CH (arom.)), 5.82 (s, 1H, CH (arom.)), 5.78 (s, 2H, CH (arom.), 4.26 (s, 4H, CH_2 (benzylic)), 3.32 (s, 8H, OCH_2), 3.01 – 3.24 (m, 6H, CH_2 (benzylic) and CH_2 (Pr)), 2.64 (s, 4H, CH_2 (Pr)), 2.32 (d, J = 17.0 Hz, 2H, CH_2), 2.11 (d, J = 17.0 Hz, 2H, CH_2), 2.02 (s, 2H, CH), 1.28 (s, 4H, CH_2 (Pr)), 0.85 (s, 8H, CH_2), 0.58 – 0.80 (m, 48H, CH_2), 0.30 (s, 12H, CH_3); ^{13}C NMR (100 MHz, DMSO- d_6) could not be acquired due to line broadening; HRMS (ESI) calc. for $C_{97}H_{132}N_{11}O_{14}$ ($M+H^+$): 1674.9950; Found: 1674.9931.

61,1'-((*5S,6R,11S,12R*)-5,11-didecyl-4,10-dioxo-1,4,5,6,7,10,11,12-octahydro-6,12-methanocycloocta[1,2-d:5,6-d']dipyrimidine-2,8-diyl)bis(3-butylurea) 62

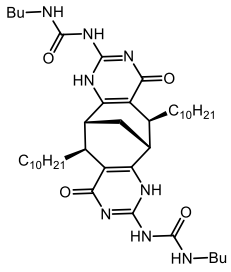

For synthesis, see compound **91**. [α] $^{20}_{D}$ = -10 ° (c 0.1 in $CHCl_3$); mp 250 ºC; FTIR (neat, cm^{-1}): 3219, 2957, 2925, 2854, 1663, 1593, 1465, 1253; ^{1}H NMR (400 MHz, $CDCl_3$) δ 12.80 (s, 2H, NH), 12.01 (s, 2H, NH), 9.72 (s, 2H, NH), 3.2 – 3.3 (s, 2H, CH_2 (Bu)), 3.1 – 3.2 (s, 2H, CH_2 (Bu)), 2.76 (s, 2H, CH), 2.72 (d, *J* = 10.0 Hz, 2H, CH), 2.06 – 2.21 (m, 2H, CH_2), 2.00 (s, 2H, CH_2), 1.49 – 1.73 (m, 8H, CH_2), 1.11 – 1.49 (m, 36H, CH_2), 0.76 – 1.03 (m, 12H, CH_3); ^{13}C NMR (100 MHz, $CDCl_3$) δ 171.7, 156.5, 153.6, 147.1, 116.2, 39.6, 38.4, 33.6, 31.9, 31.2, 31.0, 29.8, 29.7, 29.6, 29.4, 28.0, 22.7, 20.2, 14.1, 13.8; HRMS (ESI) calc. for $C_{43}H_{73}N_8O_4$ ($M+H^+$): 765.5749, Found: 765.5750.

Dibenzyl-2,2'-(((((*5S,6R,11S,12R*)-5,11-didecyl-4,10-dioxo-1,4,5,6,7,10,11,12-octahydro-6,12-methanocycloocta[1,2-d:5,6-d']dipyrimidine-2,8-diyl)bis(azanediyl))bis(carbonyl))bis(azanediyl))diacetate 63

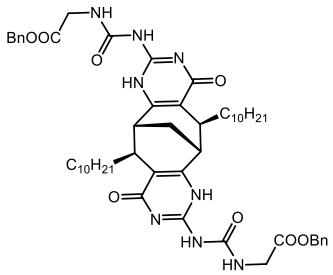

300 mg (0.529 mmol, 1 eq.) of **56**, 549 mg (2.11 mmol, 4 eq.) of Im(CO)NH-CH_2COOBn and 0.3 ml of TEA in 20 ml THF were stirred in a closed vial overnight at 100 °C. After cooling down, the reaction mixture was transferred to a 50 ml RBF and THF evaporated under reduced pressure. Crude mixture was purified by column chromatography on silica gel eluting with gradient mixture DCM/MeOH (60 : 1, 50 : 1, 20 : 1, v/v)to afford 242 mg (48 %) of **63** and 41 mg (10 %) of **98** as a white powder. [α] $^{20}_{D}$ = +26 ° (c 0.1 in $CHCl_3$); mp (enantiopure) 207 ºC; FTIR (neat, cm^{-1}): 2921, 2851, 1532, 1173, 694; ^{1}H NMR (400 MHz, $CDCl_3$) δ 12.6 (s, 2H, NH), 11.27 (s, 2H, NH), 10.38 (s, 2H, NH), 7.27 – 7.38 (m, 10H, CH, (arom.)), 5.16 (ABq, $\Delta\delta_{AB}$ = 0.03, J_{AB} = 12.0 Hz, 2H, CH (benzylic)), 4.21 (dd, *J* = 17.0 Hz,

J = 5.0 Hz, 2H, CH_2), 3.84 (dd, *J* = 17.0 Hz, *J* = 5.0 Hz, 2H, CH_2), 2.77 (s, 2H, CH), 2.66 (d, *J* = 11.0 Hz, 2H, CH), 2.12 – 2.01 (m, 2H, CH_2), 1.99 (m, 2H, CH_2), 1.42 – 1.53 (m, 4H, CH_2), 1.06 – 1.43 (m, 32H, CH_2), 0.85 (t, *J* = 7.0 Hz, 6H, CH_3); ^{13}C NMR (100 MHz, $CDCl_3$) δ 169.7, 128.5, 128.2, 128.1, 66.8, 31.9, 29.73, 29.66, 29.55, 29.45, 29.4, 22.7, 14.1; HRMS (ESI) calc. for $C_{53}H_{73}N_8O_8$ ($M+H^+$): 949.5546, Found: 949.5534.

1,1'-((*5S,6R,11S,12R*)-5,11-didecyl-4,10-dioxo-1,4,5,6,7,10,11,12-octahydro-6,12-methanocycloocta[1,2-d:5,6-d']dipyrimidine-2,8-diyl)bis(3-(3-(1,3-dioxoisoindolin-2-yl)propyl)urea) 64

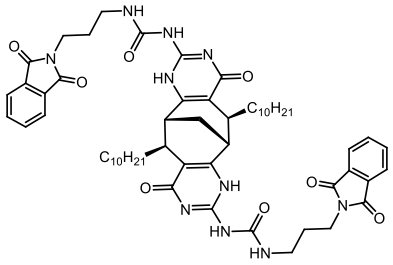

31 mg (0.0543 mmol, 1 eq.) of compound **56** and 100 mg (0.434 mmol, 8 eq.) of freshly synthesized 4-(1,3-dioxoisoindolin-2-yl)propane isocyanate **65** in 1 ml of dry pyridine was stirred at 80 ºC overnight. Reaction mixture was cooled down and diluted with 1M HCl. White precipitate was filtered and washed with water. Crude material was dissolved in $CHCl_3$, dried over Na_2SO_4 and filtered. After concentrating the solution, precipitating the product with MeOH and filtering through glass frit filter gave 30 mg (54 %) of **64** as a white powder. mp (enantiopure) 245 ºC; $[\alpha]\ ^{20}_D$ = +10 º (0.1 in $CHCl_3$); FTIR (neat, cm^{-1}): 3218, 2924, 2853, 1716; ^{1}H NMR (400 MHz, $CDCl_3$) δ 12.73 (s, 2H, NH), 11.91 (s, 2H, NH), 9.88 (ABq, $\Delta\delta_{AB}$ = 0.01, J_{AB} = 6.0 Hz, 2H, NH), 7.73 – 7.84 (m, 4H, CH (arom.)), 7.62 – 7.72 (m, 4H, CH (arom.)), 3.76 (dp, *J* = 16.0 Hz, *J* = 7 Hz, 4H, CH_2 (Pr)), 3.51 (sextet, *J* = 7.0 Hz, 2H, CH_2 (Pr)), 3.09 – 3.23 (m, 2H, CH_2 (Pr)), 2.73 (s, 2H, CH), 2.63 (d, *J* = 1.0 Hz, 2H, CH_2), 2.03 – 2.18 (m, 2H, CH_2), 1.83 – 2.03 (m, 6H, 2*CH_2 (Pr) and CH_2), 1.40 – 1.57 (m, 4H, CH_2), 0.86 – 1.40 (m, 32H, CH_2), 0.86 (t, *J* = 7.0 Hz, 6H, CH_3); ^{13}C NMR (100 MHz, $CDCl_3$) δ 171.6, 168.0, 156.5, 153.4, 147.0, 133.7, 132.52, 123.1, 116.3, 38.5, 37.5, 36.1, 33.6, 31.9, 30.9, 29.73, 29.7, 29.6, 28.1, 28.0, 22.7, 14.1; HRMS (ESI) calc. for $C_{57}H_{75}N_{10}O_8$ ($M+H^+$): 1027.5764, Found: 1027.5755.

4-(1,3-dioxoisoindolin-2-yl)propane isocyanate 65

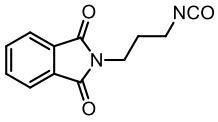

The mixture of 300 mg (1.286 mmol, 1 eq.) 4-(1,3-dioxoisoindolin-2-yl)butanoic acid, 0.3 ml (1.415 mmol, 1.1 eq.) of DPPA and 0.2 ml (1.415 mmol, 1.1 eq.) TEA was stirred at 100 ºC for 1h under inert atmosphere. Nitrogen gas evolves during the first 20 minutes of the reaction time. Reaction mixture was cooled down and evaporated under reduced pressure. The residue was purified by column chromatography (7 g of silica gel, 1 : 2 EtOAc/petroleum) giving 237 mg (80 %) of **65** as a white solid. mp 34 °C; FTIR (neat, cm^{-1}): 3281, 2551, 1933, 1478, 853; ^{1}H NMR (400 MHz, $CDCl_3$) δ 7.85 – 7.87 (m, 2H, CH (Pht), 7.72 – 7.74 (m, 2H, CH (Pht)), 3.40 (t, *J* = 6.6 Hz, 2H, CH_2), 3.80 (t, *J* = 6.6 Hz, 2H, CH_2), 1.98 (p, *J* = 6.6 Hz, 2H, CH_2); ^{13}C NMR (100 MHz, $CDCl_3$) δ 168.3, 134.1, 132.0, 123.4, 40.6, 35.1, 30.1; HRMS (ESI) calc. for $C_{12}H_{11}N_2O_3$ ($M+H^+$): 231.0692; Found: 231.0689;

1-((*5S,6R,11S,12R*)-8-amino-5,11-didecyl-4,10-dioxo-1,4,5,6,7,8,9,10,11,12-decahydro-6,12-methanocycloocta[1,2-d:5,6-d']dipyrimidin-2-yl)-3-butylurea 91

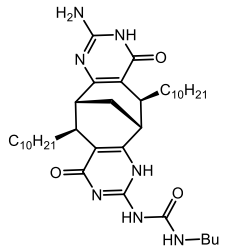

To the well stirred solution of 200 mg (0.352 mmol, 1 eq.) of **56** in 3 ml of dry pyridine, 40 µl (0.352 mmol, 1 eq.) of neat BuNCO was added dropwise under inert atmosphere. The reaction mixture was then stirred at 80 ºC for 1h. Reaction mixture was cooled down and diluted with 10 ml 1M HCl. The white solid obtained was filtered and washed with distilled water followed by MeOH. The resulting mixture of **62**, **91** and unreacted starting material **56** was separated on silica gel eluting with gradient eluent system ($CHCl_3$/MeOH 50 : 1, 30 : 1, 20 : 1, 10 : 1). The products were obtained as white powders in the order of polarity: 150 mg (55.6 %) of **62**, 56 mg (24 %) of **91** and 29 mg (14.5 mg) of **56**. [α] $^{20}_{D}$ = +65 ° (c 0.1 in $CHCl_3$); mp (enantiopure) 245 ºC, mp (rac)

>300 ºC (decomp.); FTIR (neat, cm^{-1}): 3096, 2925, 2853, 1654, 1592, 1465, 1258; ^{1}H NMR (400 MHz, $CDCl_3$) δ 14.10 (s, 1H, NH), 12.74 (s, 1H, NH), 11.40 (s, 1H, NH), 8.62 (s, 1H, NH_2), 8.25 (s, 1H, NH_2), 5.53 (t, *J* = 5.0 Hz, 1H, NH), 3.40 (m, 2H, CH_2 (Bu)), 3.23 (m, 2H, CH_2 (Bu)), 2.94 (s, 1H, CH), 2.48 – 2.85 (m, 4H, CH_2), 2.40 (s, 1H, CH), 1.78 – 2.14 (m, 4H, CH_2), 1.79 (s, 2H, CH_2), 1.46 – 1.63 (m, 4H, CH_2), 0.99 – 1.46 (m, 34H, CH_2), 0.95 (t, *J* = 6.5 Hz, 3H, CH_3), 0.75 – 0.92 (m, 6H, CH_3); ^{13}C NMR (100 MHz, $CDCl_3$) δ 169.8, 167.2, 165.9, 156.52, 155.5, 155.4, 153.1, 151.9, 145.8, 130.0, 118.9, 108.8, 39.4, 38.6, 38.0, 36.5, 35.9, 38.9, 32.1, 32.0, 31.9, 30.1, 30.0, 29.9, 29.7, 29.6, 29.4, 29.3, 28.4, 27.2, 27.1, 25.5, 22.7, 22.6, 20.2, 20.0, 19.9, 18.1, 14.3, 14.1, 13.7; HRMS (ESI) calc. for $C_{38}H_{64}N_7O_3$ ($M+H^+$): 666.5065, Found: 666.5073.

1-((*5S,6R,11S,12R*)-8-amino-5,11-bis(3,5-bis(decyloxy)benzyl)-4,10-dioxo-1,4,5,6,7,10,11,12-octahydro-6,12-methanocycloocta[1,2-d:5,6-d']dipyrimidin-2-yl)-3-butylurea 92

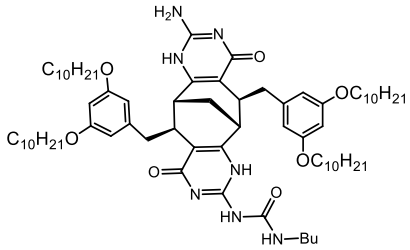

To the well stirred solution of 200 mg (0.183 mmol, 1 eq.) of compound **2** in 3 ml of dry pyridine, 20 µL (0.183 mmol. 1 eq.) of BuNCO was added dropwise. The reaction mixture was stirred at 80 °C for 1h and then cooled down to rt. 1 M HCl was added causing white solid to precipitate. After filtering and washing thoroughly with distilled water the material was dissolved in $CHCl_3$ and dried over Na_2SO_4. The crude mixture of **67**, **92** and unreacted **2** was separated by column chromatography using gradient eluent system ($CHCl_3$, ($CHCl_3$/MeOH 50 : 1, 15 : 1). The medium polarity product **92** was collected, concentrated to minimum amount of solvent and converted into white powder by diluting with MeOH. The white precipitate was filtered yielding 55 mg (25 %) of **92**. $[\alpha]\ ^{20}_{D}$ = -80 º (c 0.1 in $CHCl_3$); mp (enantiopure) 160 ºC; FTIR (neat, cm^{-1}): 2921, 2851, 1585, 1456, 1251, 1058,1161, 826; ^{1}H NMR (400 MHz, $CDCl_3$/DMSO-d_6 40 %v/v) δ 11.30 (br, 1H, NH), 10.51 (s, 1H, NH), 9.14 (br,

1H, NH), 7.24 (br, 1H, NH), 6.40 (s, 4H (arom.)), 6.24 (s, 2H, CH (arom.)), 6.06 (s, 2H, NH_2), 3.89 (s, 8H, OCH_2), 2.98 – 3.18 (m, 3H, 2*CH (benzylic), CH), 2.77 – 2.98 (m, 3H, 2*CH (benzylic), CH (Bu)), 2.67 (s, 1H, CH), 2.25 – 2.40 (m, 2H, CH), 2.11 (s, 2H, CH_2), 2.08 (s, 1H, CH), 1.70 (s, 8H, CH_2), 1.01 – 1.55 (m, 63H, CH_2, CH_3), 0.83 (s, 12H, CH_3); ^{13}C NMR (100 MHz, $CDCl_3$/ DMSO-d_6 40 %v/v) could not be acquired due to line broadening; HRMS (ESI) calc. for $C_{72}H_{116}N_7O_7$ ($M+H^+$): 1190.8936, Found: 1190.8931.

***(5S,6R,9S,10R)*-methyl-2-amino-5,9-didecyl-7-hydroxy-4-oxo-1,4,5,6,9,10-hexahydro-6,10-methanocycloocta[d]pyrimidine-8-carboxylate 93**

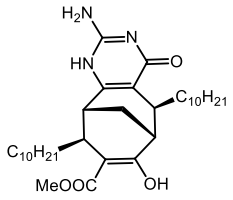

The mixture of 500 mg (0.911 mmol, 1 eq.) of compound **55** and 164 mg (1.822 mmol, 2 eq.) of guanidinium carbonate in 10 ml MeOH was stirred overnight in a sealed vial at 80 °C. Reaction mixture was cooled to rt, diluted with 1M HCl and extracted with $CHCl_3$. The crude statistical mixture of **55**, **93** and **56** was separated chromatographically on silica gel eluting with gradient solvent mixture ($CHCl_3$, $CHCl_3$/MeOH (50 : 1)). 127 mg (25 %) of **93** was obtained as a colorless oil. $[\alpha]^{20}_D$ = +190 ° (c 0.2 in $CHCl_3$); FTIR (neat, cm^{-1}): 2921, 2851, 1644, 1353, 1209, 821; ^{1}H NMR (400 MHz, $CDCl_3$) δ 12.25 (s, 1H, OH), 5.88 (br, 2H, NH_2), 3.69 (s, 3H, CH_3 (OCH_3)), 2.72 (s, 1H, CH), 2.61 (s, 1H, CH), 2.57 (s, 1H, CH), 2.49 (s, 1H, CH), 1.73 – 2.01 (m, 2H, CH_2), 0.99 – 1.72 (m, 36H, CH_2), 0.81 – 0.92 (m, 6H, CH_3); ^{13}C NMR (100 MHz, $CDCl_3$) δ 174.2, 173.3, 172.8, 153.8, 111.6, 100.7, 51.3, 38.8, 37.9, 35.6, 34.3, 31.9, 29.7, 29.4, 28.3, 28.1, 22.7, 18.4, 18.0, 14.1; HRMS (ESI) calc. for $C_{33}H_{56}N_3O_4$ ($M+H^+$): 558.4271, Found: 558.4265.

***(5S,6R,9S,10R)*-methyl-2-(3-butylureido)-5,9-didecyl-7-hydroxy-4-oxo-1,4,5,6,9,10-hexahydro-6,10-methanocycloocta[d]pyrimidine-8-carboxylate 94**

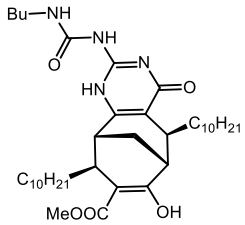

83 mg (0.149 mmol, 1 eq.) of compound **93** was dissolved in 2 ml of dry pyridine under inert atmosphere and heated to 80 °C. 20 µL (0.179 mmol, 1.2 eq.) of BuNCO was added and the reaction mixture was stirred for 1h at this temperature. After cooling the reaction mixture to rt, 20 ml of 1M HCl was added and crude product extracted with $CHCl_3$. The product was purified by column chromatography to give 88 mg (90 %) of **93** as a white solid. $[\alpha]\ ^{20}_D$ = +230 º (c 0.2 in $CHCl_3$); mp (enantiopure) 150 ºC, mp (rac) 160 ºC; FTIR (neat, cm^{-1}): 2920, 2852, 1584, 1439, 1252, 1215, 790; ^{1}H NMR (400 MHz, $CDCl_3$) δ 12.93 (s, 1H, OH), 12.26 (s, 1H, NH), 11.84 (s, 1H, NH), 10.15 (t, *J* = 5.0 Hz, 1H, NH), 3.71 (s, 3H, CH_3 (OCH_3)), 3.26 – 3.41 (m, 1H, CH_2 (Bu)), 2.83 (d, *J* = 9.9 Hz, 1H, CH), 2.62 (s, 2H, CH), 2.49 (d, *J* = 9.2 Hz, 1H, CH), 1.78 – 2.01 (m, 4H, CH_2), 1.68 (m, 2H, CH_2), 1.59 (m, 2H, CH_2 (Bu)), 1.12 – 1.53 (m, 38H, CH_2), 0.93 (t, *J* = 7.3 Hz, 3H, CH_3 (Bu)), 0.83 – 0.91 (m, 6H, CH_3); ^{13}C NMR (100 MHz, $CDCl_3$) δ 174.1, 172.8, 171.8, 156.8, 153.5, 147.2, 117.3, 99.7, 51.5, 39.7, 38.8, 37.1, 35.9, 33.9, 33.7, 31.9, 31.5, 31.2, 29.70, 29.69, 29.64, 29.54, 29.47, 29.4, 22.7, 20.2, 18.2, 14.1, 13.8; HRMS (ESI) calc. for $C_{38}H_{64}N_4O_5$ ($M+H^+$): 657.4949, Found: 657.4951.

Benzyl-2-(3-((*5S,6R,11S,12R*)-8-amino-5,11-didecyl-4,10-dioxo-1,4,5,6,7,10,11,12-octahydro-6,12-methanocycloocta[1,2-d:5,6-d']dipyrimidin-2-yl)ureido)acetate 98

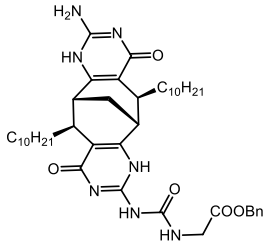

For synthesis, see compound **63**. $[\alpha]\ ^{20}_D$ = +100 º (c 0.1 in $CDCl_3$); mp (enantiopure) >200 ºC (decomp.); FTIR (neat, cm^{-1}): 2921, 2851, 1239, 1051, 695; ^{1}H NMR (400 MHz, $CDCl_3$ + 20% DMSO-d_6) δ 14.64 (s, 1H, NH), 14.64 (s, 1H, NH), 11. 04 (br, 1H, NH), 9.92 (s, 1H, NH), 9.57 (s, 1H,

NH), 8.16 (s, 1H, NH), 7.18 – 7.37 (m, 5H, CH (arom.)), 5.00 – 5.20 (m, 2H, CH_2 (benzylic)), 4.32 (s, 1H, CH), 4.01 (s, 1H, CH), 3.67 (s, 1H, CH), 2.72 (s, 2H, CH), 2.66 (s, 1H, CH), 1.66 – 2.00 (m, 4H, CH_2), 0.70 – 0.87 (m, 6H, CH_3); ^{13}C NMR (100 MHz, $CDCl_3$) δ 135.2, 135.1, 128.6, 128.4, 128.14, 128.1, 67.0, 31.9, 31.8, 29.95, 29.8, 29.8, 29.7, 29.6, 29.5, 29.4, 29.3, 22.6, 14.3, 14.1; HRMS (ESI) calc. for $C_{43}H_{64}N_7O_5$ ($M+H^+$): 758.4963, Found: 758.4968.

9 PUBLICATIONS

1. Vidmantas Bieliūnas, Dovilė Račkauskaitė, Edvinas Orentas, and Sigitas Stončius, Synthesis, Enantiomer Separation, and Absolute Configuration of 2,6-Oxygenated 9-Azabicyclo[3.3.1]nonanes, *J. Org. Chem.*, **2013**, 78 (11), 5339–5348;

2. Dovilė Račkauskaitė, Karl-Erik Bergquist, Qixun Shi, Anders Sundin, Eugenijus Butkus, Kenneth Wärnmark and Edvinas Orentas, A Remarkably Complex Supramolecular Hydrogen-Bonded Decameric Capsule Formed from an Enantiopure C2-Symmetric Monomer by Solvent-Responsive Aggregation, *J. Am. Chem. Soc*., **2015**, 137 (33), 10536–10546;

3. Dovilė Račkauskaite, Rokas Gegevičius, Yutaka Matsuo, Kenneth Wärnmark, and Edvinas Orentas, An Enantiopure Hydrogen-Bonded Octameric Tube: Self-Sorting and Guest-Induced Rearrangement, *Angew. Chem. Int. Ed.*, **2016**, 55, 208 –212.

Conference material:

1. Račkauskaitė D., Bieliūnas V., Stončius S., Orentas E., *Candida Rugosa* Lipase-catalyzed Kinetic Resolution of 2.6-deoxygenated 9-azabicyclo[3.3.1]nonanes; Conference „Lietuvos mokslas ir pramonė“, section „Organinė Chemija”, 24 April, 2013, KTU, Kaunas, Lithuania. Book of abstracts, p. 57;

2. Račkauskaitė D., Elucidation of the structure and the hydrogen bond pattern of cyclic self-assembled pentamer, The 27th Organic Chemistry Winter Meeting, OKV 2012, 12-15 January, 2012. Lillehammer, Norway. Book of abstracts, p. 44;

3. D. Račkauskaitė D, Bieliūnas V., Stončius S., Orentas E., Construction of a highly stable tubular hydrogen bonded oligomer. The 29 th Organic Chemistry Winter Meeting OKV29, 9-12 January 2014, Lillehammer, Norway. Book of abstracts, p.91.

10 REFERENCES

[1] J.-F. Xu, L. Chen, X. Zhang, *Chem Eur J* **2015**, *21*, 11938-11946.
[2] a) C. T. Seto, G. M. Whitesides, *J Am Chem Soc* **1993**, *115*, 905-916;b) J. M. McGrath, M. D. Pluth, *J Org Chem* **2014**, *79*, 711-719.
[3] T. J. Murray, S. C. Zimmerman, *J Am Chem Soc* **1992**, *114*, 4010-4011.
[4] J. D. Badjić, A. Nelson, S. J. Cantrill, W. B. Turnbull, J. F. Stoddart, *Acc Chem Res* **2005**, *38*, 723-732.
[5] B. Moulton, M. J. Zaworotko, *Chem Rev* **2001**, *101*, 1629-1658.
[6] A. G. Phillips, P. H. Beton, N. R. Champness, in *Supramolecular Chemistry*, John Wiley & Sons, Ltd, **2012**.
[7] M. M. Conn, J. Rebek, *Chem Rev* **1997**, *97*, 1647-1668.
[8] M.-J. Brienne, J. Gabard, M. Leclercq, J.-M. Lehn, M. Cesario, C. Pascard, M. Chevé, G. Dutruc-Rosset, *Tetrahedron Lett* **1994**, *35*, 8157-8160.
[9] S. K. Yang, S. C. Zimmerman, *Isr J Chem* **2013**, *53*, 511-520.
[10] D. C. Sherrington, K. A. Taskinen, *Chem Soc Rev* **2001**, *30*, 83-93.
[11] M. Dračínský, P. Jansa, K. Ahonen, M. Buděšínský, *Eur J Org Chem* **2011**, *2011*, 1544-1551.
[12] A. Kaito, Hatano, M., Ueda, T., Shibuya, S., *B Chem Soc Jpn* **1980**, *53*, 3073-3078.
[13] L. M. Toledo, K. Musa, J. W. Lauher, F. W. Fowler, *Chem Mater* **1995**, *7*, 1639-1647.
[14] S. G. Stepanian, E. D. Radchenko, G. G. Sheina, Y. P. Blagoi, *J Mol Struct* **1990**, *216*, 77-90.
[15] A. Patel, W. Lewis, M. S. Searle, M. F. G. Stevens, C. J. Moody, *Tetrahedron* **2015**, *71*, 7339-7343.
[16] H. Abe, M. Takase, Y. Doi, S. Matsumoto, M. Furusyo, M. Inouye, *Eur J Org Chem* **2005**, *2005*, 2931-2940.
[17] C. Montoro-García, J. Camacho-García, A. M. López-Pérez, M. J. Mayoral, N. Bilbao, D. González-Rodríguez, *Angew Chem Int Ed* **2016**, *55*, 223-227.
[18] P. Thordarson, *Chem Soc Rev* **2011**, *40*, 1305-1323.
[19] R. B. Martin, *Chem Rev* **1996**, *96*, 3043-3064.
[20] G. Ercolani, *J Am Chem Soc* **2003**, *125*, 16097-16103.
[21] G. Ercolani, L. Schiaffino, *Angew Chem Int Ed* **2011**, *50*, 1762-1768.
[22] C. A. Hunter, H. L. Anderson, *Angew Chem Int Ed* **2009**, *48*, 7488-7499.
[23] S. V. Kolotuchin, S. C. Zimmerman, *J Am Chem Soc* **1998**, *120*, 9092-9093.
[24] J. T. Davis, G. P. Spada, *Chem Soc Rev* **2007**, *36*, 296-313.
[25] H. M. Keizer, J. J. González, M. Segura, P. Prados, R. P. Sijbesma, E. W. Meijer, J. de Mendoza, *Chem Eur J* **2005**, *11*, 4602-4608.
[26] P. Baillargeon, Y. L. Dory, *J Am Chem Soc* **2008**, *130*, 5640-5641.
[27] C. K. Marco A. Balbo Block, Anzar Khan, Stefan Hecht, **2005**.
[28] E. Mattia, S. Otto, *Nat Nano* **2015**, *10*, 111-119.
[29] M. S. P. Sansom, R. J. Law, *Current Biology*, *11*, R71-R73.
[30] L. Echegoyen, *Nature* **1994**, *369*, 276-277.
[31] A. Lin Chun, J. G. Moralez, T. J. Webster, H. Fenniri, *Biomaterials* **2005**, *26*, 7304-7309.
[32] Zhan-Ting Li, Li-Zhu Wu, **2015**.
[33] D. T. Bong, T. D. Clark, J. R. Granja, M. R. Ghadiri, *Angew Chem Int Ed* **2001**, *40*, 988-1011.
[34] R. J. Brea, C. Reiriz, J. R. Granja, *Chem Soc Rev* **2010**, *39*, 1448-1456.
[35] B. Gong, Z. Shao, *Acc Chem Res* **2013**, *46*, 2856-2866.
[36] D. Zhao, J. S. Moore, *Chem Commun* **2003**, 807-818.

[37] E. E. Simanek, S. Qiao, I. S. Choi, G. M. Whitesides, *J Org Chem* **1997**, *62*, 2619-2621.
[38] I. S. Choi, X. Li, E. E. Simanek, R. Akaba, G. M. Whitesides, *Chem Mater* **1999**, *11*, 684-690.
[39] a) H.-A. Klok, K. A. Jolliffe, C. L. Schauer, L. J. Prins, J. P. Spatz, M. Möller, P. Timmerman, D. N. Reinhoudt, *J Am Chem Soc* **1999**, *121*, 7154-7155;b) N. Kimizuka, T. Kawasaki, K. Hirata, T. Kunitake, *J Am Chem Soc* **1995**, *117*, 6360-6361.
[40] H. Fenniri, P. Mathivanan, K. L. Vidale, D. M. Sherman, K. Hallenga, K. V. Wood, J. G. Stowell, *J Am Chem Soc* **2001**, *123*, 3854-3855.
[41] J. G. Moralez, J. Raez, T. Yamazaki, R. K. Motkuri, A. Kovalenko, H. Fenniri, *J Am Chem Soc* **2005**, *127*, 8307-8309.
[42] H. Fenniri, B.-L. Deng, A. E. Ribbe, K. Hallenga, J. Jacob, P. Thiyagarajan, *P Natl Acad Sci* **2002**, *99*, 6487-6492.
[43] N. Sakai, Y. Kamikawa, M. Nishii, T. Matsuoka, T. Kato, S. Matile, *J Am Chem Soc* **2006**, *128*, 2218-2219.
[44] G. Gottarelli, S. Masiero, E. Mezzina, S. Pieraccini, J. P. Rabe, P. Samorí, G. P. Spada, *Chem Eur J* **2000**, *6*, 3242-3248.
[45] G. Gottarelli, G. P. Spada, *The Chemical Record* **2004**, *4*, 39-49.
[46] Y. Wang, Z. Huang, Y. Kim, Y. He, M. Lee, *J Am Chem Soc* **2014**, *136*, 16152-16155.
[47] N. C. Burgess, T. H. Sharp, F. Thomas, C. W. Wood, A. R. Thomson, N. R. Zaccai, R. L. Brady, L. C. Serpell, D. N. Woolfson, *J Am Chem Soc* **2015**, *137*, 10554-10562.
[48] E. H. Egelman, C. Xu, F. DiMaio, E. Magnotti, C. Modlin, X. Yu, E. Wright, D. Baker, V. P. Conticello, *Structure*, *23*, 280-289.
[49] N. Nandi, **2011**.
[50] F. Hof, S. L. Craig, C. Nuckolls, J. J. Rebek, *Angew Chem Int Ed* **2002**, *41*, 1488-1508.
[51] R. G. Chapman, J. C. Sherman, *J Am Chem Soc* **1998**, *120*, 9818-9826.
[52] K. Kobayashi, T. Shirasaka, K. Yamaguchi, S. Sakamoto, E. Horn, N. Furukawa, *Chem Commun* **2000**, 41-42.
[53] B. C. Hamann, K. D. Shimizu, J. Rebek, *Angew Chem Int Ed Eng* **1996**, *35*, 1326-1329.
[54] K.-D. Zhang, D. Ajami, J. Rebek, *J Am Chem Soc* **2013**, *135*, 18064-18066.
[55] K. Kobayashi, K. Ishii, S. Sakamoto, T. Shirasaka, K. Yamaguchi, *J Am Chem Soc* **2003**, *125*, 10615-10624.
[56] D. Yuan, M. Wu, B. Wu, Y. Xu, F. Jiang, M. Hong, *Cryst Growth Des* **2006**, *6*, 514-518.
[57] D. Ajami, J. Rebek, *J Org Chem* **2009**, *74*, 6584-6591.
[58] W. Jiang, J. Rebek, *J Am Chem Soc* **2012**, *134*, 17498-17501.
[59] R. Wyler, J. de Mendoza, J. Rebek, *Angew Chem Int Ed Eng* **1993**, *32*, 1699-1701.
[60] C. A. Schalley, J. M. Rivera, T. Martín, J. Santamaría, G. Siuzdak, J. Rebek, *Eur J Org Chem* **1999**, *1999*, 1325-1331.
[61] J. M. Rivera, S. L. Craig, T. Martín, J. J. Rebek, *Angew Chem Int Ed* **2000**, *39*, 2130-2132.
[62] E. S. Barrett, T. J. Dale, J. Rebek, *J Am Chem Soc* **2008**, *130*, 2344-2350.
[63] J. L. Atwood, L. J. Barbour, A. Jerga, *Chem Commun* **2001**, 2376-2377.
[64] M. R. Ams, D. Ajami, S. L. Craig, J.-S. Yang, J. Rebek, *J Am Chem Soc* **2009**, *131*, 13190-13191.
[65] E. Orentas, C.-J. Wallentin, K.-E. Bergquist, M. Lund, E. Butkus, K. Wärnmark, *Angew Chem Int Ed* **2011**, *50*, 2071-2074.
[66] C. J. Wallentin, E. Orentas, E. Butkus, K. Wärnmark, *Synthesis* **2009**, *2009*, 864-867.
[67] A. J. Dingley, L. Nisius, F. Cordier, S. Grzesiek, *Nat. Protocols* **2008**, *3*, 242-248.
[68] S. H. M. Söntjens, M. H. P. van Genderen, R. P. Sijbesma, *J Org Chem* **2003**, *68*, 9070-9075.
[69] B. Gözler, M. S. Lantz, M. Shamma, *J Nat Prod* **1983**, *46*, 293-309.
[70] S. E. Lewis, *Tetrahedron* **2006**, *62*, 8655-8681.
[71] N. Ward, D. A. Jones, V. W. Jacewicz, *WO9730049 (A1)* **1997**.

[72] a) J. L. Haller, I. Panyutin, A. Chaudhry, C. B. Zeng, R. H. Mach, J. A. Frank, *Mol Imaging Biol* **2012**, *14*, 325-335;b) N. Zaveri, F. Jiang, C. Olsen, W. Polgar, L. Toll, *J Med Chem* **2010**, *53*, 8187-8191.
[73] M. Shibuya, M. Tomizawa, Y. Sasano, Y. Iwabuchi, *J Org Chem* **2009**, *74*, 4619-4622.
[74] a) K. Sidorowicz, R. Lazny, A. Nodzewska, K. Wolosewicz, A. Ratkiewicz, Z. Urbanczyk-Lipkowska, P. Kalicki, *Tetrahedron* **2015**, *71*, 5148-5158;b) R. Lazny, A. Ratkiewicz, A. Nodzewska, A. Wynimko, L. Siergiejczyk, *Tetrahedron* **2012**, *68*, 6158-6163;c) J. R. Wiseman, H. O. Krabbenhoft, R. E. Lee, *J Org Chem* **1977**, *42*, 629-632.
[75] N. S. Zefirov, V. A. Palyulin, in *Topics in Stereochemistry*, John Wiley & Sons, Inc., **2007**, pp. 171-230.
[76] R. H. Mach, R. R. Leudtke, C. D. Unsworth, V. A. Boundy, P. A. Nowak, J. G. Scripko, S. T. Elder, J. R. Jackson, P. L. Hoffman, *J Med Chem* **1993**, *36*, 3707-3720.
[77] K. Orito, Y. Satoh, H. Nishizawa, R. Harada, M. Tokuda, *Org Lett* **2000**, *2*, 2535-2537.
[78] A. C. D. Cope, H. L.; Howell, C. F., *Organic Syntheses* **1955**, *Coll.Vol. 4*, 816-819.
[79] S. Singh, *Chem Rev* **2000**, *100*, 925-1024.
[80] Z. Chen, S. Izenwasser, J. L. Katz, N. Zhu, C. L. Klein, M. L. Trudell, *J Med Chem* **1996**, *39*, 4744-4749.
[81] M. L. Trudell, J. M. Cook, *J Am Chem Soc* **1989**, *111*, 7504-7507.
[82] R. E. Portmann, C. Ganter, *Helv Chim Acta* **1973**, *56*, 1991-2007.
[83] R. Aráoz, J. Molgó, N. Tandeau de Marsac, *Toxicon* **2010**, *56*, 813-828.
[84] P. Michel, A. Rassat, *J Org Chem* **2000**, *65*, 2572-2573.
[85] I. S. Cloudsdale, A. F. Kluge, N. L. McClure, *J Org Chem* **1982**, *47*, 919-928.
[86] G. Haufe, U. Rolle, E. Kleinpeter, J. Kivikoski, K. Rissanen, *J Org Chem* **1993**, *58*, 7084-7088.
[87] W.-H. Ham, K.-S. Kim, Y.-H. Jung, T.-H. Cho, S.-H. Cho, H. Park, *Arch Pharmacal Res*, *19*, 432-434.
[88] J. Barluenga, J. Pérez-Prieto, A. M. Bayón, G. Asensio, *Tetrahedron* **1984**, *40*, 1199-1204.
[89] R. M. Lagidze, N. K. Iremadze, M. S. Vashakidze, B. V. Rozynov, *Chem Nat Compd* **1973**, *9*, 183-187.
[90] A. P. Vartak, L. P. Dwoskin, P. A. Crooks, *Tetrahedron Lett* **2008**, *49*, 6330-6333.
[91] F. A. Davis, N. Theddu, P. M. Gaspari, *Org Lett* **2009**, *11*, 1647-1650.
[92] M. J. Munchhof, A. I. Meyers, *J Org Chem* **1996**, *61*, 4607-4610.
[93] R. K. Hill, L. A. Renbaum, *Tetrahedron* **1982**, *38*, 1959-1963.
[94] a) O. Muraoka, B.-Z. Zheng, K. Okumura, G. Tanabe, T. Momose, C. H. Eugster, *J Chem Soc Perkin Trans 1* **1996**, 1567-1575;b) T. Momose, N. Toyooka, Y. Hirai, *Chem Lett* **1990**, *19*, 1319-1322.
[95] O. Muraoka, K. Okumura, T. Maeda, G. Tanabe, T. Momose, *Tetrahedron: Asymmetry* **1994**, *5*, 317-320.
[96] R. Lazny, K. Wolosewicz, P. Zielinska, Z. Urbanczyk-Lipkowska, P. Kalicki, *Tetrahedron* **2011**, *67*, 9433-9439.
[97] E. Santaniello, P. Ferraboschi, P. Grisenti, A. Manzocchi, *Chem Rev* **1992**, *92*, 1071-1140.
[98] G. Carrea, S. Riva, *Angew Chem Int Ed* **2000**, *39*, 2226-2254.
[99] R. D. Schmid, R. Verger, *Angew Chem Int Ed* **1998**, *37*, 1608-1633.
[100] K. Naemura, T. Matsumura, M. Komatsu, Y. Hirose, H. Chikamatsu, *J Chem Soc, Chem Commun* **1988**, 239-241.
[101] K. Naemura, M. Murata, R. Tanaka, M. Yano, K. Hirose, Y. Tobe, *Tetrahedron: Asymmetry* **1996**, *7*, 1581-1584.
[102] K. Naemura, H. Ida, R. Fukuda, *B Chem Soc Jpn* **1993**, *66*, 573-577.
[103] R. J. Kazlauskas, A. N. E. Weissfloch, A. T. Rappaport, L. A. Cuccia, *J Org Chem* **1991**, *56*, 2656-2665.
[104] T. Momose, N. Toyooka, M. Jin, *Tetrahedron Lett* **1992**, *33*, 5389-5390.
[105] T. Momose, N. Toyooka, M. Jin, *J Chem Soc Perkin Trans 1* **1997**, 2005-2014.

[106] K. Hegemann, H. Schimanski, U. Höweler, G. Haufe, *Tetrahedron Lett* **2003**, *44*, 2225-2229.
[107] K. Naemura, T. Matsumura, M. Komatsu, Y. Hirose, H. Chikamatsu, *B Chem Soc Jpn* **1989**, *62*, 3523-3530.
[108] a) T. Aida, E. W. Meijer, S. I. Stupp, *Science* **2012**, *335*, 813-817;b) A. W. Bosman, R. P. Sijbesma, E. W. Meijer, *Mater Today* **2004**, *7*, 34-39.
[109] A. Tessa ten Cate, R. P. Sijbesma, *Macromol Rapid Comm* **2002**, *23*, 1094-1112.
[110] L. Brunsveld, B. J. B. Folmer, E. W. Meijer, R. P. Sijbesma, *Chem Rev* **2001**, *101*, 4071-4098.
[111] F. H. Beijer, R. P. Sijbesma, H. Kooijman, A. L. Spek, E. W. Meijer, *J Am Chem Soc* **1998**, *120*, 6761-6769.
[112] S. H. M. Söntjens, R. P. Sijbesma, M. H. P. van Genderen, E. W. Meijer, *J Am Chem Soc* **2000**, *122*, 7487-7493.
[113] R. P. Sijbesma, F. H. Beijer, L. Brunsveld, B. J. B. Folmer, J. H. K. K. Hirschberg, R. F. M. Lange, J. K. L. Lowe, E. W. Meijer, *Science* **1997**, *278*, 1601-1604.
[114] G. B. W. L. Ligthart, H. Ohkawa, R. P. Sijbesma, E. W. Meijer, *J Am Chem Soc* **2005**, *127*, 810-811.
[115] O. A. Scherman, G. B. W. L. Ligthart, R. P. Sijbesma, E. W. Meijer, *Angew Chem Int Ed* **2006**, *45*, 2072-2076.
[116] M. C. Stuparu, A. Khan, C. J. Hawker, *Polymer Chemistry* **2012**, *3*, 3033-3044.
[117] S. K. Yang, A. V. Ambade, M. Weck, *J Am Chem Soc* **2010**, *132*, 1637-1645.
[118] T. Park, S. C. Zimmerman, *J Am Chem Soc* **2006**, *128*, 11582-11590.
[119] M. V. Biyani, E. J. Foster, C. Weder, *ACS Macro Letters* **2013**, *2*, 236-240.
[120] C. Rest, R. Kandanelli, G. Fernandez, *Chem Soc Rev* **2015**, *44*, 2543-2572.
[121] A. P. H. J. Schenning, P. Jonkheijm, E. Peeters, E. W. Meijer, *J Am Chem Soc* **2001**, *123*, 409-416.
[122] F. J. M. Hoeben, L. M. Herz, C. Daniel, P. Jonkheijm, A. P. H. J. Schenning, C. Silva, S. C. J. Meskers, D. Beljonne, R. T. Phillips, R. H. Friend, E. W. Meijer, *Angew Chem Int Ed* **2004**, *43*, 1976-1979.
[123] a) H. Fenniri, B.-L. Deng, A. E. Ribbe, *J Am Chem Soc* **2002**, *124*, 11064-11072;b) T. Seki, A. Asano, S. Seki, Y. Kikkawa, H. Murayama, T. Karatsu, A. Kitamura, S. Yagai, *Chem Eur J* **2011**, *17*, 3598-3608.
[124] A. F. Abdel-Magid, K. G. Carson, B. D. Harris, C. A. Maryanoff, R. D. Shah, *J Org Chem* **1996**, *61*, 3849-3862.
[125] B. J. B. Folmer, R. P. Sijbesma, E. W. Meijer, *J Am Chem Soc* **2001**, *123*, 2093-2094.
[126] S. Abed, S. Boileau, L. Bouteiller, *Macromolecules* **2000**, *33*, 8479-8487.
[127] J. F. McConnell, B. D. Sharma, R. E. Marsh, *Nature* **1964**, *203*, 399-400.
[128] S. Stončius, E. Orentas, E. Butkus, L. Öhrström, O. F. Wendt, K. Wärnmark, *J Am Chem Soc* **2006**, *128*, 8272-8285.
[129] Q. Shi, K.-E. Bergquist, R. Huo, J. Li, M. Lund, R. Vácha, A. Sundin, E. Butkus, E. Orentas, K. Wärnmark, *J Am Chem Soc* **2013**, *135*, 15263-15268.
[130] V. G. H. Lafitte, A. E. Aliev, H. C. Hailes, K. Bala, P. Golding, *J Org Chem* **2005**, *70*, 2701-2707.
[131] M. M. Safont-Sempere, G. Fernández, F. Würthner, *Chem Rev* **2011**, *111*, 5784-5814.
[132] A. Wu, L. Isaacs, *J Am Chem Soc* **2003**, *125*, 4831-4835.
[133] B. H. Northrop, Y.-R. Zheng, K.-W. Chi, P. J. Stang, *Acc Chem Res* **2009**, *42*, 1554-1563.
[134] P. Mukhopadhyay, A. Wu, L. Isaacs, *J Org Chem* **2004**, *69*, 6157-6164.
[135] Y. Ma, S. V. Kolotuchin, S. C. Zimmerman, *J Am Chem Soc* **2002**, *124*, 13757-13769.
[136] M. L. Pellizzaro, K. A. Houton, A. J. Wilson, *Chem Sci* **2013**, *4*, 1825-1829.
[137] S. J. Benkovic, D. Sammons, W. L. F. Armarego, P. Waring, R. Inners, *J Am Chem Soc* **1985**, *107*, 3706-3712.